School of Civil and Mechanical Engineering

Cracking of Concrete, its Healing and Simultaneous Monitoring

Nimratpal Kaur

0000-0003-4337-2472

This thesis is presented for the Degree of

Doctor of Philosophy

of

Curtin University

February 2022

Author's Declaration

To the best of knowledge and belief this thesis contains no material previously published by any other person except where due acknowledgement has been made.

This thesis contains no material which has been accepted for the award of any other degree or diploma in any university.

Nimratpal Kaur

22nd February 2022

Abstract

Cracks in reinforced concrete structures are inevitable and they are one of the inherent weaknesses of concrete that adversely affect its structural integrity and durability. Cracks within the prescribed limit may not hamper immediate structures serviceability or safety, but they provide pathways for diffusion of fluids and aggressive chemicals that may trigger corrosion of embedded steel reinforcement; thus, making structures prone to imminent failure. Therefore, it is essential to heal cracks at an early stage to enhance the durability and increase service life of concrete structures.

Success of healing is influenced by three aspects: the healing material for filling the cracks; the delivery system for transporting healing material inside the crack; and the monitoring technique to ensure successful healing. An efficient repair method coupled with a reliable evaluation technique is of paramount importance to ensure proper healing of cracks.

This thesis explores healing of cracks in concrete coupled with non-destructive techniques to ensure progression of healing. Conventional and bacterial healing systems have been used to heal cracks of different widths. Ultrasonic signals have been captured through steel bar as well as concrete surrounding the bar. An attempt has been made to explore the efficacy of healing in impeding reinforcement corrosion.

The thesis is presented in a publication-based format. It consists of two published chapters (chapter 3 and chapter4) and two submitted chapters (chapter5 and chapter 6) in journal. The overall objective of this thesis is to illustrate the ability of the ultrasonic technique in monitoring the progression of healing.

Acknowledgements

First and foremost, I would like to express my gratitude to God for showering me with blessings throughout my research journey.

I would like to thank Australian Government and Curtin University for allowing me to pursue my PhD.

I would like to thank my supervisor, Professor Abhijit Mukherjee for his supervision during the course of my PhD degree. Your guidance and expert advice has been invaluable throughout all stages of the research.

Thank you to my Co-supervisor, Dr. Navdeep Dhami, for your time, help, and valuable suggestions throughout the research study.

I'd like to express my gratitude to Dr. Ranjan, my PhD chairperson, for his invaluable advice, support, and encouragement throughout my studies.

I'd like to thank Ms. Chery Cheng in particular for her assistance with all administrative tasks. You've always been a wonderful companion.

Thank you very much to all Curtin Lab Technicians for helping me sail through my research smoothly.

Special thanks to my fellow post-graduates Jay, Subhra, Asha, Sakshi, Sukrit, Yikuan, Anant, Raja and Abhijit Mistri for the wonderful time we spent together in lab and out. Your laughter, encouragement, and thoughtful assistance have made my studies and life a joy.

I owe my parents a debt of gratitude for their unwavering love, prayers, and encouragement in keeping me motivated and confident. Because they believed in me, I was able to achieve great success. My siblings, who keep me grounded, remind

me of what is important in life, and are always supportive of my adventures, deserve my gratitude. I appreciate it. In addition, I owe my in-laws a debt of gratitude for their assistance. You are all wonderful!

Finally, I owe my deepest gratitude to my loving, caring and supporting husband Amrit. Without your inspiration and cooperation, this PhD would not have been possible. Your support is greatly appreciated, both in good and bad times. Thank you for being there for me every step of the way. I also thank new addition to my family "my daughter" (born Jan 2022) for her patience. I feel blessed to have you both in my life.

Dedication

This thesis is dedicated to my husband Amrit for his unwavering love, support, kindness and encouragement.

Table of Contents

Author's Declaration i
Abstract ii
Acknowledgements iii
Dedication v
List of Figures x
Attributes xiii
Attribution statement for Chapter 3 xiii
Attribution statement for Chapter 5 xvi
Attribution statement for Chapter 6 xvii
Chapter 1 Introduction 1
1.1 Motivation 1
1.2 Thesis outline 2
Chapter 2 Literature review 5
1. Introduction 5
2. Healing of concrete 5
3. Healing materials for crack repair 6
3.1 Conventional healing materials 6
3.2 Microbial based healing system 8
3.3 Microbial Induced Calcite Precipitation (MICP) as a crack healing agent for concrete 8
3.4 Impact of calcium sources on MICP 11
4. Techniques for crack healing 12
4.1 Healing via encapsulation 13
4.2 Healing via vascular system 14
5. Evaluation techniques for crack healing 15
5.1 Ultrasonic technique for monitoring damage and healing 16
6. Research Gaps 20
7. Scope of work 20
References 21
Chapter 3 Healing and Simultaneous Ultrasonic Monitoring of Cracks in Concrete 33
1. Introduction 34
2. Numerical model 38
2.1 Healing and monitoring of the concrete 39

3. Experimental program 40
3.1 Specimen preparation 40
3.2 Inducing cracks 41
3.2.1 Tensile cracks 41
3.2.2 Corrosion cracks 42
3.3. Ultrasonic investigations 42
3.4. Healing of specimens 44
4. Results and discussion 45
4.1 Numerical results 45
4.1.2 Progressive healing 48
4.1.3 Partially filled cracks 51
4.2 Experimental results 55
4.2.1 Transducer configuration 55
4.2.2 Treatment of tensile cracks 58
4.2.3 Treatment of corrosion cracks 59
4.2.4 Progressive healing 61
5. Conclusions 62
REFERENCES 64
Chapter 4 Healing Fine Cracks in Concrete with Bacterial Cement for an Advanced Non-destructive Monitoring 72
Abstract 72
1. Introduction 73
2. Experimental program 77
2.1 Preparation of test specimens and damage introduction 77
2.2 Bacteria-based healing treatment for cracks 78
2.3 Ultrasonic investigation 79
2.4 Watertightness Test 80
2.5 Microstructural analysis 81
3. Results and discussion 81
3.1 Visual monitoring 81
3.2 Chemical monitoring 83
3.3 Microstructural study 84
3.4 Ultrasonic tests 85
3.4.1 Waveform analysis 85
3.4.2 Time-Frequency Analysis 90

3.5 Water tightness tests 92
4. Conclusions 94
References 96
Chapter 5 Performance of Different Calcium Sources on Bacterial Healing of Concrete 103
Abstract 103
1. Introduction 104
2. Materials and Methods 107
2.1 Preparation of reinforced concrete specimen and cracking 107
2.2 Microorganism and culture medium 108
2.3 Preparation of cementing fluids 108
2.4 Healing Treatment 108
2.5 Watertightness test 109
2.6 Ultrasonic measurements 109
2.6.1 Ultrasonic measurements through concrete 109
..... 110
2.6.2 Ultrasonic measurements through steel bar 110
2.7 Electrochemical measurements 111
2.7.1 Half-cell measurements 111
2.7.2 Linear Polarisation Resistance (LPR) measurements 112
2.8 Mass loss and tensile strength of rebars 113
3. Results and Discussion 114
3.1 Monitoring healing 114
3.1.1 Visual monitoring 114
3.1.2 Chemical monitoring 115
3.1.3 Watertightness tests 117
3.1.4 Ultrasonic monitoring through concrete 119
3.2 Monitoring of corrosion 122
3.2.1 Electrochemical Measurements 122
3.2.2 Ultrasonic guided wave measurements 125
3.7 Destructive tests 128
4. Conclusions 129
Acknowledgements 130
Conflicts of Interest 130
References 131

Chapter 6 Long Term Corrosion Monitoring of Bacterially Healed Concrete Using Electrochemical and Ultrasonic Techniques 134
Abstract 134
1. Introduction 135
2. Experimental Program 139
2.1 Preparation of test specimens and cracking 139
2.2 Preparation of healing fluids and treatment 140
2.3 Corrosion monitoring and exposure regime 141
2.4 Half-cell measurements 141
2.5 Linear Polarisation Resistance (LPR) measurements 142
2.6 Guided wave inspection of reinforced bar 143
2.7 Mass loss and tensile strength of rebars 144
3. Results And Discussion 144
3.1 Half-cell Potential Measurements 144
3.2 LPR Measurements 146
3.3 Guided wave inspection of reinforced bar 149
3.4 Mass loss and tensile strength of rebars 155
Conclusions 157
Data Availability Statement 159
Acknowledgements 159
References 159
Chapter 7 Conclusions and recommendations 165
7.1 Recommendations for future research 167

List of Figures

Figure 2.1: Conventional healing materials [19] 7
Figure 2.2:Simplified representation of the events occurring during the ureolytic induced carbonate precipitation. 10
Figure 2.3: Methods of applying healing agents in concrete 13
Figure 2.4: Healing via capsule-based [37].....14
Figure 2.5: Healing via vascular system [37] 14
Figure 2.6: Wave velocity for different damage content [92].....17
Figure 2.7: Amplitude and energy for different damage content [92] 17
Figure 2.8: Arrival time and attenuation for different cracks [17].....18
Figure 3.1: The self-healing Loop.....35
Figure 3.2: Schematic diagram of the numerically modelled experiment 38
Figure 3.3: Reinforced concrete specimen design 41
Figure 3.4: Specimen with tensile crack. 42
Figure 3.5: Specimen with corrosion crack.....42
Figure 3.6: Experimental setup for ultrasonic data acquisition in transmission mode. 44
Figure 3.7: Wave propagation through (a) pristine specimen (b) fully cracked specimen (c) soft material in the cracked region. [Stress wave form: Gaussian].....46
Figure 3.8: Reflection analysis at location R2 for the specimen with dimension of (a) 500 mm x 300 mm and (b) 500 mm x 150 mm 48
Figure 3.9: Wave propagation for different acoustic impedances (a) 0.04 η (b) 0.25 η 49
Figure 3.10: (a) v_x vs propagation time plot showing time history of the transmitted wave (b) Variation of arrival time of first peak and attenuation in the third peak 50
Figure 3.11: Wave propagation through partially filled cracks [Stress wave form: Gaussian].....51
Figure 3.12: Transmitted signal received with (a) S-R1 and (b) S'-R1'.....52
Figure 3.13:(a) arrival time and (b) attenuation variation in the observed peak for different healed lengths for bottom (S and R1) and top (S' and R1') positions of source and receiver. 54
Figure 3.14:Ultrasonic signals using (a) reflection approach (b) transmission mode for uncracked, tensile crack and corrosion crack specimens. 56
Figure 3.15:Bar graph showing variation of arrival time (largest peak) and attenuation for signals in transmission mode.....57
Figure 3.16: Tensile cracked specimen: before cracking (uncracked), after cracking (cracked) and after the grout treatment (treated).....58
Figure 3.17:Ultrasonic transmission through corrosion cracked specimen: before cracking (uncracked), after cracking (corrosion crack) and after treatment (treated). 59
Figure 3.18: Velocity and attenuation variations for tensile and corrosion crack before and after treating.....61

Figure 3.19: Healing stages of corrosion cracked specimen at different time intervals. 62
Figure 4.1: The healing-monitoring loop 73
Figure 4.2: Methods of applying healing material 75
Figure 4.3: Layout of experimental plan (front view).....77
Figure 4.4: Set-up for ultrasonic data acquisition 79
Figure 4.5: Specimen showing placement of transducers at different locations.....80
Figure 4.6: Visible calcite deposition seen on the surface post healing.....81
Figure 4.7: Visual observations of the crack at different stages of deposition (Note: these are the close-up images of the portion of the crack marked red in Figure 4.6b) 83
Figure 4.8: Rise in volume of calcium carbonate and reduction in healing fluid with healing progression. 84
Figure 4.9: (a) SEM images of the precipitates after healing treatment (b) EDS analysis of the crystals. 85
Figure 4.10: Recorded waveforms at different healing stages 88
Figure 4.11: Velocity and amplitude ratio for point 1 measured at different healing percentage.....89
Figure 4.12: Amplitude ratios at different stages of healing.....90
Figure 4.13: (a) Typical time-frequency spectra of the received signal for point 1 (b) spectral contour corresponding to the window (marked in red).....91
Figure 4.14: Plot of values corresponding to spectral contour at different healing stages 92
Figure 4.15: Locations and set-up for water flow test. 93
Figure 4.16: Water flow through different locations of the crack.....93
Figure 5.1: Set-up for ultrasonic data acquisition 110
Figure 5.2: Specimen showing different locations of transducers 110
Figure 5.3: Set-up for ultrasonic measurements through steel bar.....111
Figure 5.4: Half-cell Potential set-up 112
Figure 5.5: Potentiostat set-up.....113
Figure 5.6: Stages of crack healing for CL specimen 115
Figure 5.7: Stages of crack healing for CA specimen.....115
Figure 5.8: Rise in volume of calcium carbonate and reduction in fluid intake with progression of healing. 116
Figure 5.9: Water flow test set-up.....117
Figure 5.10: Water flow through different locations of the crack for (a) specimen CL and (b) specimen AC.....118
Figure 5.11: Amplitudes for points 1-6 for CL specimen at different stages of healing. 120
Figure 5.12: Amplitudes for CA specimen at different stages of healing.....122
Figure 5.13: Electrochemical readings for specimens during healing. (a) Half-cell vs CSE values; (b) Current vs time; (c) Potential vs time 124
Figure 5.14: Transmission index for specimens CL and CA during healing progression for 300 kHz frequency.....126
Figure 5.15: Transmission index for different frequencies for specimens CA and CL 128

Figure 5.16: Visual inspection of rebar 128
Figure 5.17: Stress-strain curves 129
Figure 6.1. Specimen exposure to salt water 141
Figure 6.2. Half-cell Potential set-up 142
Figure 6.3. Potentiostat set-up 143
Figure 6.4. Set-up for ultrasonic data acquisition 144
Figure 6.5. Half-cell measurements with time for (a) UD and D specimen (b) DHC and DHA specimen 146
Figure 6.6. Linear polarisation measurements 149
Figure 6.7. Time domain signals for (a) UD and (b) D specimens for day 0 and day 120. 151
Figure 6.8. Transmission index for UD & D specimens 152
Figure 6.9. Transmission index the healed DHC and DHA specimens 154
Figure 6.10. Visual inspection of rebar 155
Figure 6.11. Fracture morphology for all specimens after tensile testing 156
Figure 6.12. Stress-strain curves of the bars 157

Attributes

This thesis contains two published and two submitted for publication chapters. The co-authors of these chapters are hereby acknowledged for their contribution. The signed attribution statements have been included as follows:

Attribution statement for Chapter 3

STATEMENT OF AUTHORSHIP

Title	Healing and simultaneous ultrasonic monitoring of cracks in concrete
Status	✓ Published Accepted by the Journal Submitted in a Journal Unsubmitted work in manuscript style
Publication details	Kaur, N.P., Shah, J.K., Majhi, S., Mukherjee, A., *Healing and Simultaneous Ultrasonic Monitoring of Cracks in Concrete*. Materials Today Communications, 2019. 18: p. 87-99.

Principal Author

Name (candidate)	Nimrat Pal Kaur
Contribution	This co-author has carried out the experiments, analysis and prepared the figures and wrote the manuscript for publication.
Certification	This paper reports on original research I conducted during the period of my HDR candidature and is not subjected to any obligations or contractual agreement with a third party that would constrain its inclusion in this thesis. I am the primary author of this paper.

Signature & date	30/09/2021

Co-authorship agreement

By signing the statement of authorship agreement, each author agrees that their contribution stated by the principal author is accurate and they grant permission to the candidate to include this work in his/ her thesis.

Name of Co-Author 1	Jay Kumar Shah
Contribution	This co-author performed the numerical simulations and prepared the corresponding portion of the manuscript.
Signature & date	30/09/2021

Name of Co-Author 2	Subhra Majhi
Contribution	This co-author helped in performing the experiments with ultrasonics
Signature & date	30-09-2021

Name of Co-Author 3	Abhijit Mukherjee
Contribution	This co-author is the supervisor of the candidate and provided key advice on the analysis and direction of the investigation and helped in giving the manuscript the final shape.
Signature & date	30/09/2021

Attribution statement for Chapter 4

STATEMENT OF AUTHORSHIP

Title	Healing fine cracks in concrete with bacterial cement for an advanced non-destructive monitoring	
Status	✓	Published

		Accepted by the Journal
		Submitted in a Journal
		Unsubmitted work in manuscript style
Publication details	Kaur, N.P., Majhi, S., Dhami, N.K., Mukherjee, A., *Healing fine cracks in concrete with bacterial cement for an advanced non-destructive monitoring.* Construction and Building Materials, 2020. 242: p. 118151.	

Principal Author

Name (candidate)	Nimrat Pal Kaur
Contribution	This co-author has carried out the experiments, analysis, prepared figures and wrote the manuscript for publication.
Certification	This paper reports on original research I conducted during the period of my HDR candidature and is not subjected to any obligations or contractual agreement with a third party that would constrain its inclusion in this thesis. I am the primary author of this paper.
Signature & date	30/09/2021

Co-authorship agreement

By signing the statement of authorship agreement, each author agrees that their contribution stated by the principal author is accurate and they grant permission to the candidate to include this work in his/ her thesis.

Name of Co-Author 1	Subhra Majhi
Contribution	This co-author helped with analysing the time-frequency part of the manuscript.

Signature & date	30-09-2021

Name of Co-Author 2	Navdeep Kaur Dhami
Contribution	This co-author provided key advice on bacterial treatment
Signature & date	29-09-21

Name of Co-Author 3	Abhijit Mukherjee
Contribution	This co-author is the supervisor of the candidate and provided key advice on the analysis and direction of the investigation and helped in giving the manuscript the final shape.
Signature & date	30/09/2021

Attribution statement for Chapter 5

STATEMENT OF AUTHORSHIP

Title	Performance of Different Calcium Sources on Bacterial Healing of Concrete
Status	☐ Published ☐ Accepted by the Journal ☑ Submitted in a Journal ☐ Unsubmitted work in manuscript style
Publication details	Nimrat Pal Kaur, Navdeep Kaur Dhami and Abhijit Mukherjee, *Performance of Different Calcium Sources on Bacterial Healing of Concrete.*

Principal Author

Name (candidate)	Nimrat Pal Kaur
Contribution	This co-author has carried out the experiments, analysis and prepared the figures and wrote the manuscript for publication.
Certification	This paper reports on original research I conducted during the period of my HDR candidature and is not subjected to any obligations or contractual agreement with a third party that would constrain its inclusion in this thesis. I am the primary author of this paper.
Signature & date	12/01/2022

Co-authorship agreement

By signing the statement of authorship agreement, each author agrees that their contribution stated by the principal author is accurate and they grant permission to the candidate to include this work in his/ her thesis.

Name of Co-Author 1	Navdeep Kaur Dhami
Contribution	This co-author provided key advice on bacterial treatment
Signature & date	12 – 01 - 2022

Name of Co-Author 2	Abhijit Mukherjee
Contribution	This co-author is the supervisor of the candidate and provided key advice on the analysis and direction of the investigation and helped in giving the manuscript the final shape.
Signature & date	12/01/2022

Attribution statement for Chapter 6

STATEMENT OF AUTHORSHIP

Title	Long Term Corrosion Monitoring of Bacterially Healed Concrete Using Electrochemical and Ultrasonic Techniques
Status	☐ Published ☐ Accepted by the Journal ✓ Submitted in a Journal ☐ Unsubmitted work in manuscript style
Publication details	Nimrat Pal Kaur, Yikuan Wang, Navdeep Kaur Dhami and Abhijit Mukherjee, *Long Term Corrosion Monitoring of Bacterially Healed Concrete Using Electrochemical and Ultrasonic Techniques.*

Principal Author

Name (candidate)	Nimrat Pal Kaur
Contribution	This co-author has carried out the experiments, analysis, prepared figures and wrote the manuscript for publication.
Certification	This paper reports on original research I conducted during the period of my HDR candidature and is not subjected to any obligations or contractual agreement with a third party that would constrain its inclusion in this thesis. I am the primary author of this paper.
Signature & date	12/01/2022

Co-authorship agreement

By signing the statement of authorship agreement, each author agrees that their contribution stated by the principal author is accurate and they grant permission to the candidate to include this work in his/ her thesis.

Name of Co-Author 1	Yikuan Wang
Contribution	This co-author helped with analysing the guided wave rebar results.
Signature & date	12-Jan-2022

Name of Co-Author 2	Navdeep Kaur Dhami
Contribution	This co-author provided key advice on bacterial treatment
Signature & date	12 – 01 - 2022

Name of Co-Author 3	Abhijit Mukherjee
Contribution	This co-author is the supervisor of the candidate and provided key advice on the analysis and direction of the investigation and helped in giving the manuscript the final shape.
Signature & date	12/01/2022

Chapter 1 Introduction

1.1 Motivation

Reinforced concrete is the key component of civil infrastructure construction all over the world. However, keeping concrete structures from deteriorating prematurely is proving to be a difficult task. The creation of micro-cracks in concrete structures at an early age has a significant impact on their serviceability and is a prevalent durability-related occurrence in many concrete structures.

Cracks in reinforced concrete structures are inevitable and can occur due to thermal stresses, creep, drying shrinkage, or general loading under serviceability conditions [1]. Cracks provide an easy pathway for ingress of moisture or harmful substances, leading to premature matrix degradation and corrosion of embedded steel reinforcement [2, 3]. To address this problem, many treatments and maintenance procedures are used after construction to assure the structure's long-term endurance. Although crack formation is not a new phenomenon, its repair and maintenance have been a major source of concern.

The deterioration of concrete structures over the last few decades necessitates the development of appropriate healing and monitoring systems for assessing and maintaining their condition. As a result, apart from conventional materials such as cementitious grout, epoxy, resins or polymers, microbial healing techniques have been developed which have shown promising results for civil infrastructure [4-6]. Various non-destructive testing (NDT) methodologies for monitoring civil infrastructures have been developed [7]. NDT technologies are proven to be more practical for assessing and evaluating the state of RC structures. However, few studies have focused their

scope into simultaneous monitoring of healing using advanced non-destructive techniques.

Keeping this in view, it is essential to heal the cracks at an early stage and simultaneously monitor them, to enhance the durability and increase service life of structures.

1.2 Thesis outline

The thesis is presented in a publication-based format. It consists of two published chapters (chapter 3 and chapter4) and two submitted chapters (chapter5 and chapter 6) in journal. The overall objective of this thesis is to illustrate the ability of ultrasonic techniques in monitoring the progression of healing. The contents of the thesis are discussed in detail below.

Chapter 1: Introduction describes the motivation behind the work and presents the overall contents of the thesis.

Chapter 2: Literature Review presents the background and significance of the research.

Chapter 3: is a published work in the journal as *'Kaur, et al., Healing and Simultaneous Ultrasonic Monitoring of Cracks in Concrete. Material Today Communications, 2018'* https://doi.org/10.1016/j.mtcomm.2018.10.022. This chapter investigates the healing of cracks of different widths in concrete and illustrates the ability of the ultrasonic techniques to monitor the progression of healing. A numerical technique based on two-dimensional finite difference time domain (FDTD) has also been used to determine the potential of ultrasonic stress waves in monitoring healing.

It has been reported that the ultrasonic technique is able to discern the progressive healing process. Signal attenuation was found to be most suitable for monitoring healing.

Chapter 4 is a published work in the journal as *'Kaur, et al., Healing Fine Cracks in Concrete with Bacterial Cement for an Advanced Non-destructive Monitoring. Construction and Building Materials, 2020'* *https://doi.org/10.1016/j.conbuildmat.2020.118151*. This chapter investigates the healing of fine cracks using the bacterial based healing technique. The evidence and efficiency of bacterial healing is investigated using advanced monitoring techniques. The ultrasonic signal has been processed further using an advanced STFT technique to obtain a nuanced observation of the crack healing process. The evidence of bacterial healing was confirmed through visual inspection, scanning electron microscopy and X-ray dispersion spectrum and water tightness tests.

Chapter 5 reports the efficacy of using various calcium sources for microbially induced crack healing of concrete. The evidence of healing is investigated using advanced monitoring techniques. Simultaneously, an attempt has been made to monitor rebar through electrochemical measurements and guided wave technique to study the efficacy of healing in impeding corrosion.

Chapter 6 reports the long-term performance of healed samples subjected to chloride induced reinforcement corrosion. The healed samples were subjected to salt water ponding for 120 days. They were monitored through various electrochemical and ultrasonic guided wave techniques. After ponding, the samples were broken to visually

examine the rebar condition. Mass loss tests were carried out to get insights of rebar condition.

Chapter 7 provides key conclusions from the findings and reveals the directions for future research.

Chapter 2 Literature review

1. Introduction

Cement and steel are the two most widely used materials in the construction industry. Reinforced concrete is the most widely used and versatile materials for building structures. However, one of the major durability problems in reinforced concrete is its cracking. Cracks can occur due to thermal stresses, creep, drying shrinkage, general loading under serviceability conditions or corrosion of embedded steel. Eurocode 2 [1] permits crack widths up to 0.3 mm. These cracks do not affect the strength of structure, but durability and service life of structures is greatly affected by cracking of concrete; as cracks provide pathways for water and other aggressive agents such as chloride, sulphates or carbon dioxide inside concrete. These deleterious ions can lead to reinforcement corrosion and if left untreated, may ultimately lead to catastrophic structural failure [2]. It is therefore essential to heal the cracks at an early stage to enhance the durability and increase service life of the infrastructure. However, while healing is being undertaken, it is important to simultaneously have a measure of the achieved healing. With this background, the aim of current research is to explore the essential components of the healing system such as healing agent, delivery system and monitoring mechanism to ensure successful healing.

2. Healing of concrete

Crack healing is a phenomenon in which chemical or physical processes result in formation of solid products inside the crack, thereby blocking the pathway for ingress of aggressive agents and reducing permeability. Width of the crack and solidification process of the healing agent are significant for the success of healing [3]. The viscosity of the healing agent influences efficiency of its penetration within the crack. A high viscosity healing agent doesn't flow well and fill the micro-cracks. On the contrary, a

low viscosity healing agent may not remain in the crack and seep out of it instead [4]. An ideal healing material should be compatible with the concrete and volumetrically stable, so that cracks become sealed and reduce permeability, thus preventing reinforced steel corrosion.

In general, concrete is observed to have a natural ability to autogenously heal cracks of a certain extent, around ~50μm width [5, 6] by chemical or physical mechanisms such as hydration of unhydrated cement particles in the presence of water [7, 8]. Calcium carbonate precipitation has been recorded to occur in the presence of water, however the precipitation depends on the width of the crack as well as the amount of water present [9, 10]. The limitation for autogenous healing is the crack width. There are cracks in concrete constructions that are significantly broader than ~50μm. As a result, the development of engineering methods is crucial and external assistance for healing is warranted.

3. Healing materials for crack repair

Following section presents a review on conventional and bacterial healing materials and highlights their advantages and limitations for crack repair.

3.1 Conventional healing materials

A variety of healing agents are available in the construction industry. Healing agent should not only be compatible with concrete substrates but should possess properties such as adequate viscosity, cure right on time and place, stable and durable, environment friendly and low cost. Amongst various materials, cement grout and epoxy resin have been extensively used for remediation of cracks [4, 11-15]. Superplasticizers are added to improve the rheological properties of grout, so that it is

able to flow into the crack [15]. In case of epoxy (two-part), resin and hardener is first mixed and then injected to the cracked surface [4, 16]. Although these agents contribute to healing, the extent of healing not only depends on crack width which dictates the capillary forces, but also on the viscosity of the healing agent which influences efficiency of its penetration within the crack [17, 18].

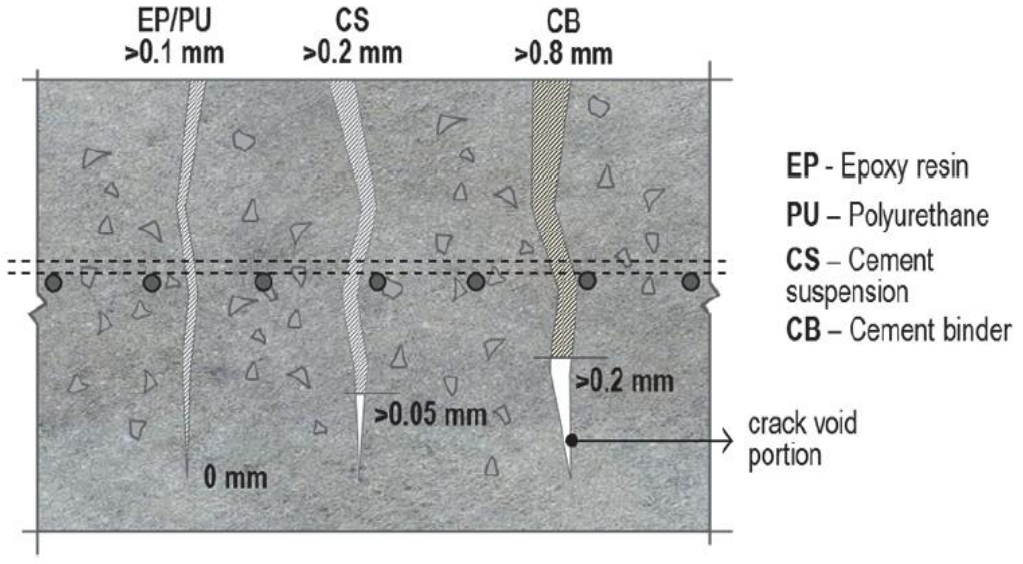

Figure 2.1: Conventional healing materials [19]

Panasyuk et al. [19] reported the use of different healing materials (Figure 2.1) and observed that voids remain unfilled using cement suspension or cement binder. Kaur et al. [20] used cementitious grout for healing cracks of different widths. It was reported that the grout was unable to penetrate thin cracks. Tittleboom et al. [18] compared grout and epoxy for filling cracks and observed that epoxy was able to fill deep cracks while no filling of crack was observed with grout. It is noted that in conventional systems, the ingredients are premixed before pumping into the cracks. As a result, the reaction starts before the ingredients have reached the site of healing, therefore voids remain unfilled [19, 20]. Also, these materials tend to degrade over time and require repeatable maintenance. To overcome the limitations of these

conventional systems, researchers in the past few decades have proposed microbial based healing systems for civil engineering applications.

3.2 Microbial based healing system

Microbial/Bacterial-based technology for civil engineering applications, is an emerging technology that has gained popularity in recent years. The use of microbially induced carbonate precipitation to protect and rehabilitate building structures and materials has proven to be a success [21, 22]. MICP is a process in which naturally occurring microorganisms such as bacteria, through their metabolic activity are able to precipitate calcium carbonate in ambient conditions [23]. Many carbonate rocks have been cemented by precipitation of carbonates driven by microbes, so using bacteria to remediate building materials is a natural process. As an innovative and environmentally acceptable approach to safeguard and restore decayed construction materials, this technology has been effectively employed for durability enhancement of construction materials. De Belie and Wang discussed the possible use of MICP in crack repair [3]. Dhami et al. [24] reported the potential of using MICP in different engineering applications. Muynck et al. [25] discussed the importance of MICP in construction materials.

3.3 Microbial Induced Calcite Precipitation (MICP) as a crack healing agent for concrete

In recent years, a bacterial based system also known as Microbially Induced Calcite Precipitation or Biocementation has gained widespread attention for healing of cracks. Several types of bacterial metabolic pathways for healing have been investigated in the last decade. Aerobic respiration of bacteria is among the first to be applied in crack self-healing. In this method spores and nutrients are added in concrete and

precipitation can be induced by bacterial oxidation of organic matters [26]. Other pathway known as enzymatic urea hydrolysis, has been used in concrete other than self-healing. In this method, urea is catalysed into ammonium and carbonate by urease that is produced by bacteria resulting in increase of pH, and precipitation [27]. Carbon dioxide sequestration with carbonic anhydrase pathway has also been explored [28]. Recently, denitrification via bacteria was proposed as another pathway in which precipitation can be induced by biological nitrate reduction with additional corrosion inhibiting effect [29, 30]. In terms of the concrete healing, ureolytic pathway is preferred because of its high precipitation rate [31, 32]. Ramachandran et al. [33] and Bang et al. [34] were amongst the first to investigate the use of bacteria to repair cracks in concrete.

Calcium carbonate precipitation depends upon four key factors which include: pH of the surrounding environment, concentration of dissolved inorganic carbon, concentration of calcium ion, and the presence of nucleation site. Figure 2.2 represents the events occurring during the ureolytic induced carbonate precipitation. Researchers all over the world have been developing techniques using bacteria for crack repair [3] as well as self-healing concrete [35, 36].

Several bacterial species are known to precipitate calcium carbonate through different metabolic routes [31, 37, 38]. Owing to the high alkalinity of concrete, alkaliphilic strains of Bacillus group are expected to function in a concrete environment. *Bacillus/Sporosarcina pasteurii*, *Bacillus sphaericus*, *Bacillus megaterium* and *Bacillus subtilis* belong to this group. These have been widely used by various research groups [18, 33, 38, 39]. Recently, this technique is widely used for self-healing of concrete [3, 4, 38]. De Belie & De Muynck [25] used *S. sphaericus* bacteria for the repair of cracks in concrete.

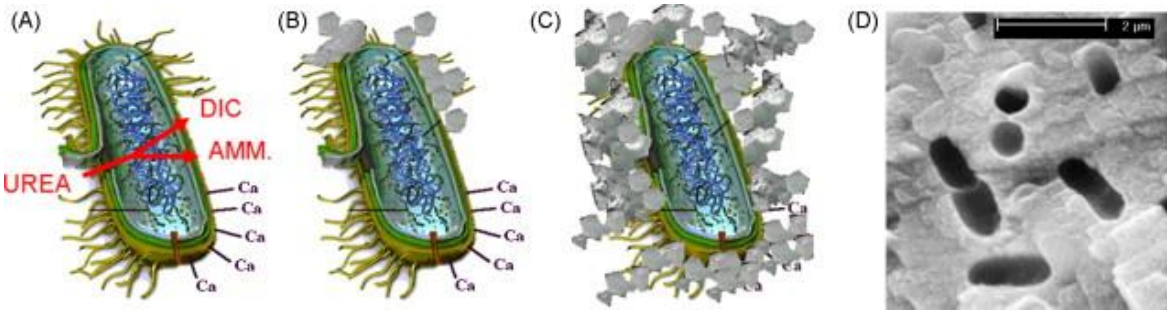

Figure 2.2:Simplified representation of the events occurring during the ureolytic induced carbonate precipitation.

Calcium ions in the solution are attracted to the bacterial cell wall due to the negative charge of the latter. Upon addition of urea to the bacteria, dissolved inorganic carbon (DIC) and ammonium (AMM) are released in the micro-environment of the bacteria (A). In the presence of calcium ions, this can result in a local supersaturation and hence heterogeneous precipitation of calcium carbonate on the bacterial cell wall (B). After a while, the whole cell becomes encapsulated (C), limiting nutrient transfer, resulting in cell death. Image (D) shows the imprints of bacterial cells involved in carbonate precipitation. A more in-depth representation can be found in Hammes and Verstraete [23].

For crack remediation enzymatic hydrolysis of urea is popular because of its high urease activity. In the urea hydrolysis process, bacteria produce an enzyme, urease, which catalyses the hydrolysis of urea into ammonium (NH_4^+) and carbonate ions (CO_3^{2-}). At this point, when calcium ions are added, calcium carbonate is formed [40, 41].

The process of calcium carbonate formation is given by the following equations:

$$CO(NH_2)_2 + 2H_2O \ \ Bacterial\ urease \rightarrow 2NH_4^+ + CO_3^{2-} \quad (2.1)$$

$$Ca^{2+} + CO_3^{2-} \rightarrow CaCO_3 \quad (2.2)$$

From a chemical point of view, calcium and carbonate concentrations directly determine the amount of calcium carbonate deposition. Porter et al. [42] investigated the consumption of urea and calcium throughout the MICP process at a concentration of 500 mM. It was noticed that equal amounts of urea and calcium were utilised to

precipitate calcium carbonate. Wang et al. [43] demonstrated that the optimum concentration of urea and calcium ions was 500 mM. It was observed that the ideal Ca2+ and urea dose is dependent not only on the type of bacteria but also on their concentration.

3.4 Impact of calcium sources on MICP

Although MICP has shown promising results in healing of cracks [18, 33, 38, 44, 45] most important concern with regard to reinforced concrete structures is the effect of calcium chloride cementation fluids on steel corrosion. Chlorides are a threat to steel reinforcement. Therefore, research is necessary to develop bacterial fluids that would inhibit steel corrosion.

Following section reviews the calcium source used for biocementation of concrete.

The precipitation of calcium carbonates is governed by a soluble calcium source. Various calcium sources are available such as calcium chloride, calcium lactate, calcium glutamate, calcium acetate and calcium nitrate [46]. Generally, calcium chloride is used as a calcium source, but there have been concerns that presence of chloride ions in the healing may have an undesirable effect of inducing corrosion in steel. Onset of corrosion accelerate deterioration of concrete as formation of rust which occupies volume 6 -10 times the volume of original steel. This in turn produces internal stresses and leads to widening of cracks, resulting in accelerated deterioration of concrete. Therefore, its optimisation and alternate sources are necessary.

Very few studies have been done using alternate calcium sources. Van Tittleboom et al. [18] used calcium chloride, calcium acetate and calcium nitrate to repair cracks. They observed equal reduction in water permeability using these calcium sources. Zhang et al. [47] used three different calcium sources namely calcium chloride,

calcium acetate and calcium nitrate and observed different types of crystals namely calcite, vaterite and aragonite. De Muynck [25] discovered that the nutrient composition had a significant impact on the crystal shape. When calcium chloride was utilised as the calcium source, the calcium carbonate crystal was rhombohedral, but spheroidal when calcium acetate was used. The mineralogical composition, which was primarily calcite, was, nevertheless, same. Although different calcium sources have been used but the healing technique and evaluation is mainly based on mechanical tests as well as SEM/XRD.

4. Techniques for crack healing

One of the most critical aspects that affect the development of an efficient healing mechanism is the selection of a delivery conduit. There are several methods of application of the healing material (Figure 2.3). It can be applied manually on the crack [48, 49] or it can be positioned inside concrete by self-healing using capsules or vascular system [37, 50]. Pre-existing cracks necessitate manual repair but in case of self- healing, the healing system must be placed inside concrete at the time of construction. The most extensively used practice to deliver the healing agent to the cracked location is injecting through the crack opening [12, 14]. Panasyuk et al. [19] reported the use of different healing materials by injecting. In case of capsules, healing agent is first encapsulated and then added to concrete matrix. Once cracks occur, the capsules are broken and healing agent is released to the crack [13]. In recent years, healing of cracks by providing capillaries or hollow channels in concrete structures for the distribution and replenishment of active fluids has also been reported [37, 51, 52].

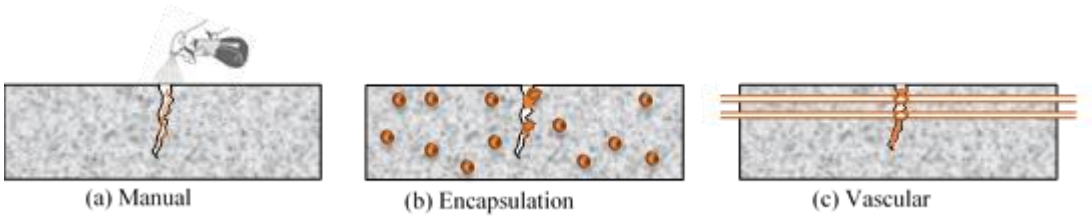

Figure 2.3: Methods of applying healing agents in concrete

4.1 Healing via encapsulation

In capsule-based self-healing, the healing agent can be dispersed in the concrete matrix in capsules. When cracking occurs, the capsules break, and the healing agent is released into the cracked zone by capillary action. Both chemical and bacterial healing agents can be encapsulated to extend their longevity while also managing their release into the matrix. Various materials such as Polyurethane or silica gel [53, 54], hydrogel [55], and expanded clay [6] have been used for encapsulation. However, the probability of breakage of capsules (Figure 2.4) in the cracked zone is uncertain as the capsules are randomly dispersed in concrete matrix [37]. The fundamental issue, however, is its long-term repeatability as well as the limit of capsules in concrete matrix. Concrete structures are subjected to multiple damage cycles throughout their service lives, and microcapsules can only contain a limited amount of repair agent, most of the healing agent is depleted after a single loading cycle, making long-term healing uncertain. As a result, more research into the repeatability of capsule-based systems is required in the future.

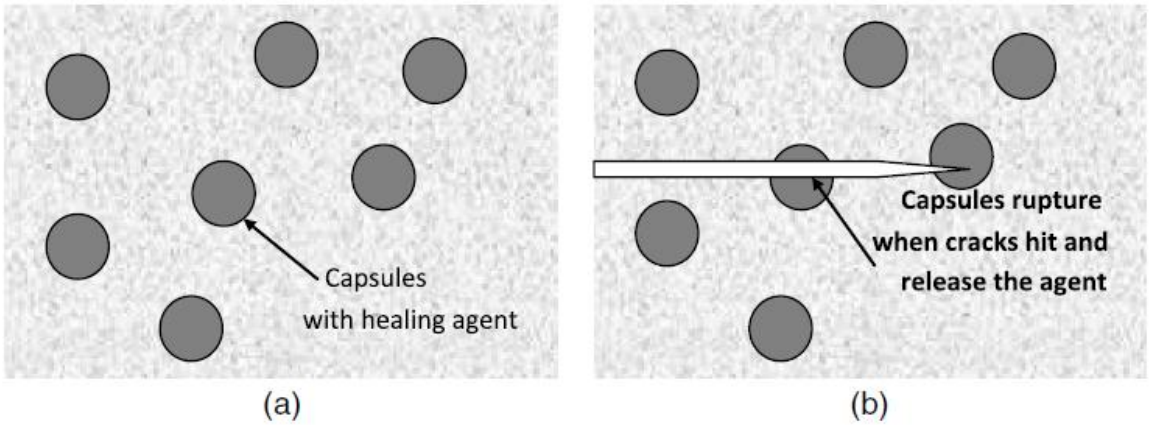

Figure 2.4: Healing via capsule-based [37]

4.2 Healing via vascular system

In vascular system, the healing agent is delivered at the point of damage by providing capillaries or hollow channels in the concrete matrix (Figure 2.5) [37, 51, 52]. It is important to consider various parameters such as dimensions, sizes, geometry, type and placement of vascular channels in concrete so that the strength of concrete is not affected [4]. Blaiszik et al. [56] suggested that through vascular systems large volume of healing agent can be supplied even for multiple damage events. The main limitation of this method is its difficulty in casting of concrete on site with network of pipes and tubes. Research is underway of using such technique for concrete structures. Therefore, in addition to healing agent, the medium of transporting also needs to be studied to ensure successful healing of cracks.

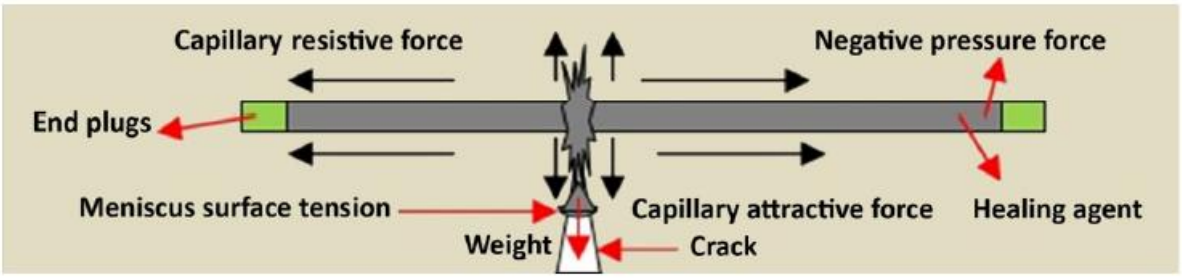

Figure 2.5: Healing via vascular system [37]

5. Evaluation techniques for crack healing

With the continued development of concrete healing technologies, there is a rising need to create methodologies for reliably evaluating the performance of these technologies [26–29]. An account of the evaluation techniques is available in [57] and [58].]. Visual evaluations such as Microstructural analysis have been widely used through Scanning Electron Microscopy (SEM), Energy Dispersive Spectroscopy (EDS), X-ray diffraction [3, 13, 18, 33, 37, 38, 59, 60] or X-ray computed tomography [61, 62] for qualitative and quantitative elemental analysis. The durability properties can be examined by sorptivity [63-65], water permeability tests [3, 60, 66], or air permeability tests [67]. The mechanical properties for healing can be analysed through strength tests [68-71]. Current evaluations of healing are primarily limited to lab-scale experiments. Furthermore, no standardised test procedures for evaluating the efficacy of healing have been established. Non-destructive test methods for healing are necessary in construction industry so that assessment chores do not disrupt the operation of structures.

Over the last few years, non-destructive techniques have been used to assess healing. Two such techniques are acoustic emission [72-76] and ultrasonic waves [58]. While acoustic emission technique may be able to detect the damage it is not capable of monitoring healing. Ultrasonic technique has both these capabilities. The monitoring can be performed by measuring a number of ultrasonic parameters. Ultrasonic pulse velocity (UPV) measurement is based on the time of flight and the simplest one to measure [51, 77]. However, UPV is not found to be very sensitive to cracks. In our work, ultrasonic pulse attenuation was found to be more effective in monitoring healing [78]. However, pulse amplitude can vary with other parameters such as the extent of coupling achieved. The frequency content of the signal can be analysed to

obtain deeper insights. Waveform analysis in various flavours such as surface-wave transmission [79]; ultrasound diffusivity [80]; non-linear ultrasonics [76]; coda wave interferometry [62, 81, 82] and more recently, direct wave interferometry [83] have been reported. A more recent technique based on Short Time Fourier Transform (STFT) retains both time and frequency information [84]. This technique has not been applied hitherto in monitoring of concrete.

5.1 Ultrasonic technique for monitoring damage and healing

Ultrasonic techniques is a non-destructive technique, which is capable of monitoring the quality of the concrete without destroying it [85]. Non-destructive evaluation (NDE) techniques have thus offered significant and often vital information for the safe operation of the most complicated systems in many fields of modern engineering. Significant developments in data acquisition systems and communication tools have greatly increased the utility of such tools [86, 87].

In concrete technology, ultrasonic technique as a method of assessing the strength, homogeneity, durability, and other qualities has gained popularity in the last few decades [72-76, 88] [58]. This is usually achieved through piezoelectric transducers which can be placed on concrete surface for detecting damage or can be used as waveguides for steel bars. The monitoring can be performed by measuring a number of ultrasonic parameters. Ultrasonic pulse velocity (UPV) measurement is based on the time of flight and the simplest one to measure [51, 77]. As of now, only ultrasonic pulse velocity method is relied on for studying concrete properties [51, 89, 90]. Standard test methods for measuring ultrasonic pulse velocity (UPV) are specified in ACI 228.2R [86] and ASTM C597 [91]. By measuring the transit time of the signal, and knowing the path length, pulse velocity is calculated. Shiotani and Aggelis [92] created 1%, 5% and 10% damage in the mortar matrix and studied the propagation of

ultrasonic waves. They reported that pulse velocity (Figure 2.6) had very slight difference, however the amplitude and energy of waveform varied significantly with different damage percentages (Figure 2.7). Kaur et al [20] created damage in the form of cracks of different widths and observed slight change in arrival time, but significant change in attenuation was observed (Figure 2.8).

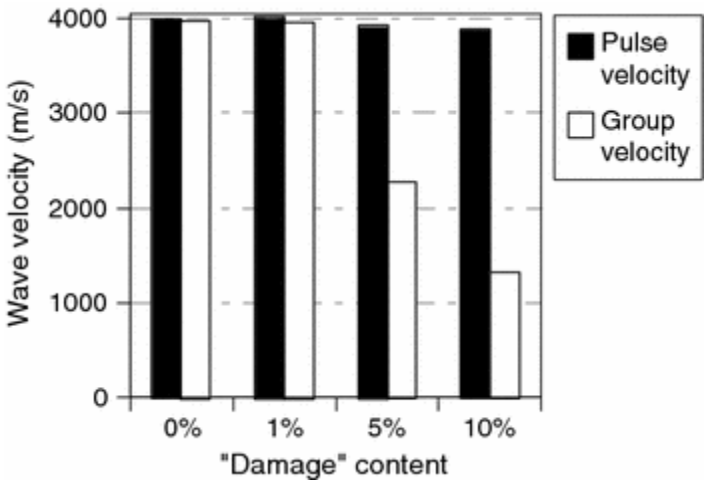

Figure 2.6: Wave velocity for different damage content [92]

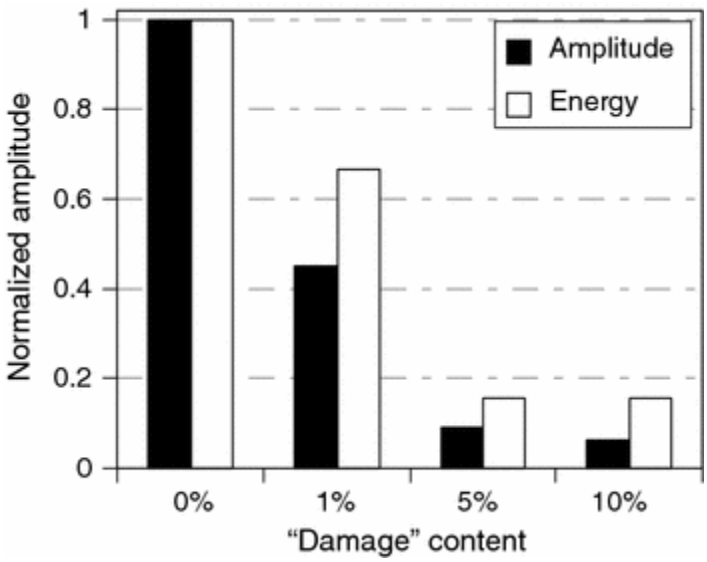

Figure 2.7: Amplitude and energy for different damage content [92]

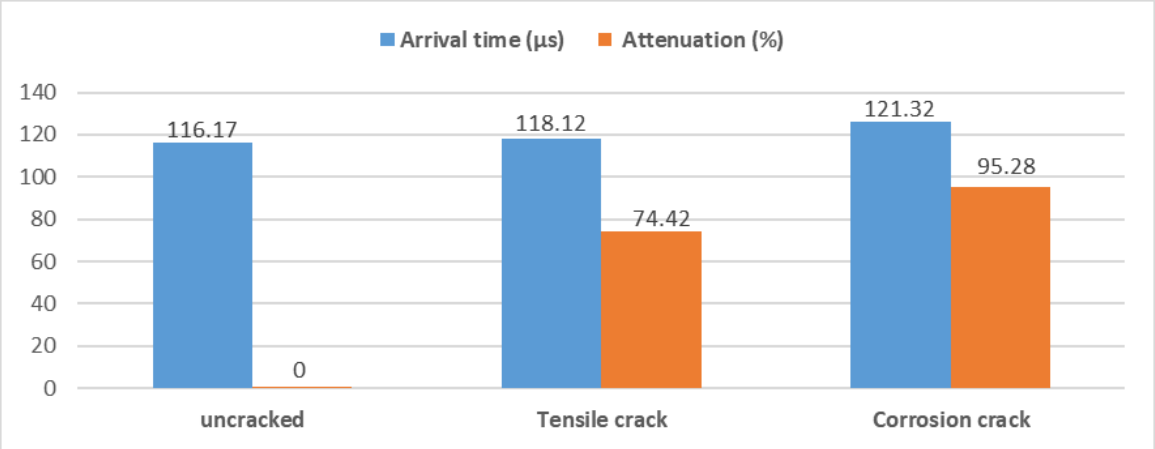

Figure 2.8: Arrival time and attenuation for different cracks [17]

Recently, various researchers have explored the ultrasonic waveform as it traverses through the damage in concrete. Sharma and Mukherjee [93] monitored the solidification process of freshly poured concrete using the rebar as a wave guide. The technique was also demonstrated for monitoring rebar corrosion [94, 95]. Using specific core and surface seeking wave modes, they were able to discern even the type of corrosion [96, 97]. Aggelis and Shiotani [79] investigated a combination of Rayleigh and longitudinal waves to study the effectiveness of using epoxy for filling the cracked bridge decks. Another group of investigators have been developing techniques for healing of concrete using chemical injections [14, 44], or a more recent self-healing technique using calcifying bacteria [4, 58, 69, 98].

Various studies have been conducted to monitor healing by ultrasonic method. Huang et al. [51] compared self-healing effect using ultrasonic pulse velocity. However, pulse velocity and the time of flight remains largely unaffected due to cracking [79]. Moreover, several compressional and shear waves are generated when the pulse interacts with the cracks. Therefore, studying and analysing other parameters such as amplitude or time of flight of ultrasonic signals is also vital to extract information about various properties of concrete [99].

It has been reported that ultrasonic pulse attenuation is more effective (Figure 2.8) in monitoring healing [78]. However, pulse amplitude can vary with other parameters such as the extent of coupling achieved. The frequency content of the signal can be analysed to obtain deeper insights. Waveform analysis such as surface-wave transmission [79]; ultrasound diffusivity [80]; non-linear ultrasonics [76]; coda wave interferometry [62, 81, 82] and more recently, direct wave interferometry [83] have been reported. A more recent technique based on Short Time Fourier Transform (STFT) retains both time and frequency information [84]. This technique has not been applied hitherto in monitoring of concrete.

Effect of bacterial healing in impeding reinforcement corrosion

Corrosion caused by chloride transmission is one of the most common damage processes that causes reinforced concrete structures to deteriorate. Chlorides reaching the steel reinforcement can break the passive layer of steel, thus initiating corrosion. Although MICP promises to reduce permeability, the studies regarding its effectiveness in decreasing reinforcement corrosion are very rare. Belleghem et al., [100, 101] used encapsulated polyurethane for autonomous healing of cracks. The healed specimens were subjected to chloride solution to monitor their corrosion behaviour using wet and dry period. It was reported that pitting corrosion was observed on cracked specimens whereas healed specimens showed better corrosion behaviour by providing a barrier against chloride ingress.

Based on the above literature, our study focusses on combining wave-based ultrasonic technique with healing to obtain detailed information on healing process and to ensure that the cracks have been healed [58].

6. Research Gaps

Success of healing is influenced by three aspects: the healing material for filling the cracks; the delivery system for transporting healing material inside the crack; and the monitoring technique to ensure healing [51, 92].

Keeping this in view, the aim of the proposed research is to monitor the healing process through advanced ultrasonic techniques in order to obtain comprehensive information about the healing progress. In this study the efficacy of conventional and bacterial healing shall be investigated with emphasis on monitoring and ensuring successful healing. The efficacy of bacterial healing using different calcium sources shall be studied with an aim to prevent/reduce corrosion in concrete structures. The proposed research is of paramount importance for civil engineering structures as it will provide better understanding of healing of cracks in concrete. If cracks are successfully healed/repaired, concrete structures would certainly serve longer and be more durable.

7. Scope of work

Key objectives of this research are as follows:

- To investigate the efficacy of conventional healing techniques for crack repair and its simultaneous monitoring
- To investigate the potential of bacterial healing technique for crack repair and its simultaneous monitoring
- To investigate the impact of varying calcium sources on efficacy of bacterial healing
- Long term monitoring of efficiency of healing in impeding reinforcement corrosion

References

1. Walraven, J. *Eurocode 2: Design of concrete structures EN1992-1-1*. in *Symposium Eurocodes: Background and Applications, Brussels*. 2008.
2. Basheer, L., J. Kropp, and D.J. Cleland, *Assessment of the durability of concrete from its permeation properties: a review.* Construction and building materials, 2001. **15**(2-3): p. 93-103.
3. De Belie, N. and J. Wang, *Bacteria-based repair and self-healing of concrete.* Journal of Sustainable Cement-Based Materials, 2016. **5**(1-2): p. 35-56.
4. Sangadji, S. and E. Schlangen, *Self Healing of Concrete Structures-Novel approach using porous network concrete.* Journal of Advanced Concrete Technology, 2012. **10**(5): p. 185-194.
5. Edvardsen, C., *Water permeability and autogenous healing of cracks in concrete.* Materials Journal, 1999. **96**(4): p. 448-454.
6. Palin, D., V. Wiktor, and H.M. Jonkers, *Autogenous healing of marine exposed concrete: Characterization and quantification through visual crack closure.* Cement and Concrete Research, 2015. **73**: p. 17-24.
7. Hearn, N., *Self-sealing, autogenous healing and continued hydration: what is the difference?* Materials and structures, 1998. **31**(8): p. 563.
8. Suleiman, A. and M. Nehdi, *Effect of environmental exposure on autogenous self-healing of cracked cement-based materials.* Cement and Concrete Research, 2018.
9. Edvardsen, C., *Water permeability and autogenous healing of cracks in concrete*, in *Innovation in concrete structures: Design and construction*. 1999, Thomas Telford Publishing. p. 473-487.

10. Clear, C., *The effects of autogenous healing upon the leakage of water through cracks in concrete*. 1985.

11. Neville, A.M., *Properties of concrete*. Vol. 4. 1995: Longman London.

12. Thanoon, W.A., et al., *Repair and structural performance of initially cracked reinforced concrete slabs.* Construction and Building Materials, 2005. **19**(8): p. 595-603.

13. Van Breugel, K. *Is there a market for self-healing cement-based materials*. in *Proceedings of the First International Conference on Self-Healing Materials, Noordwijk, The Netherlands*. 2007.

14. Yokota, O. and A. Takeuchi. *Injection of repairing materials to cracks using ultrasonic rectangular diffraction method*. in *16th World conference on non destructive testing*. 2004.

15. Anagnostopoulos, C.A., *Effect of different superplasticisers on the physical and mechanical properties of cement grouts.* Construction and Building Materials, 2014. **50**: p. 162-168.

16. Issa, C.A. and P. Debs, *Experimental study of epoxy repairing of cracks in concrete*. Construction and Building Materials, 2007. **21**(1): p. 157-163.

17. Pal Kaur, N., et al., *Healing and simultaneous ultrasonic monitoring of cracks in concrete.* Materials Today Communications, 2019. **18**: p. 87-99.

18. Van Tittelboom, K., et al., *Use of bacteria to repair cracks in concrete.* Cement and Concrete Research, 2010. **40**(1): p. 157-166.

19. Panasyuk, V., V. Marukha, and V. Sylovanyuk, *Injection Technologies for the Repair of Damaged Concrete Structures*. 2014: Springer Netherlands.

20. Pal Kaur, N., et al., *Healing and Simultaneous Ultrasonic Monitoring of Cracks in Concrete.* Materials Today Communications, 2018.

21. Dhami, N.K., S.M. Reddy, and A. Mukherjee, *Biofilm and microbial applications in biomineralized concrete.* Advanced topics in Biomineralization, 2012: p. 137-164.

22. Reddy, M.S., *Biomineralization of calcium carbonates and their engineered applications: a review.* Frontiers in microbiology, 2013. **4**: p. 314.

23. Hammes, F. and W. Verstraete, *Key roles of pH and calcium metabolism in microbial carbonate precipitation.* Reviews in environmental science and biotechnology, 2002. **1**(1): p. 3-7.

24. Dhami, N.K., M.S. Reddy, and A. Mukherjee, *Biomineralization of calcium carbonates and their engineered applications: a review.* Frontiers in Microbiology, 2013. **4**: p. 314.

25. De Muynck, W., et al., *Bacterial carbonate precipitation improves the durability of cementitious materials.* Cement and concrete Research, 2008. **38**(7): p. 1005-1014.

26. Jonkers, H.M., et al., *Application of bacteria as self-healing agent for the development of sustainable concrete.* Ecological engineering, 2010. **36**(2): p. 230-235.

27. Stocks-Fischer, S., J.K. Galinat, and S.S. Bang, *Microbiological precipitation of CaCO3.* Soil Biology and Biochemistry, 1999. **31**(11): p. 1563-1571.

28. Qian, C., et al., *Self-healing of early age cracks in cement-based materials by mineralization of carbonic anhydrase microorganism.* Frontiers in microbiology, 2015. **6**: p. 1225.

29. Erşan, Y.Ç., et al., *Enhanced crack closure performance of microbial mortar through nitrate reduction.* Cement and concrete composites, 2016. **70**: p. 159-170.

30. Erşan, Y.Ç., et al., *Nitrate reducing CaCO3 precipitating bacteria survive in mortar and inhibit steel corrosion.* Cement and Concrete Research, 2016. **83**: p. 19-30.

31. Wang, J., et al., *Application of microorganisms in concrete: a promising sustainable strategy to improve concrete durability.* Applied microbiology and biotechnology, 2016. **100**(7): p. 2993-3007.

32. Dubey, A.A., et al., *Investigation on the Impact of Cementation Media Concentration on Properties of Biocement under Stimulation and Augmentation Approaches.* Journal of Hazardous, Toxic, and Radioactive Waste, 2022. **26**(1): p. 04021050.

33. Ramachandran, S.K., V. Ramakrishnan, and S.S. Bang, *Remediation of concrete using micro-organisms.* ACI Materials Journal-American Concrete Institute, 2001. **98**(1): p. 3-9.

34. Bang, S.S., J.K. Galinat, and V. Ramakrishnan, *Calcite precipitation induced by polyurethane-immobilized Bacillus pasteurii.* Enzyme and microbial technology, 2001. **28**(4-5): p. 404-409.

35. De Muynck, W., N. De Belie, and W. Verstraete, *Microbial carbonate precipitation in construction materials: A review.* Ecological Engineering, 2010. **36**(2): p. 118-136.

36. Jonkers, H.M., *Bacteria-based self-healing concrete.* In-Genium, 2021.

37. Souradeep, G. and H.W. Kua, *Encapsulation technology and techniques in self-healing concrete.* Journal of Materials in Civil Engineering, 2016. **28**(12): p. 04016165.

38. Joshi, S., et al., *Microbial healing of cracks in concrete: a review.* Journal of Industrial Microbiology & Biotechnology, 2017: p. 1-15.

39. Feng, J., et al., *Microbial induced calcium carbonate precipitation study using Bacillus subtilis with application to self-healing concrete preparation and characterization.* Construction and Building Materials, 2021. **280**: p. 122460.

40. Castanier, S., G. Le Métayer-Levrel, and J.-P. Perthuisot, *Ca-carbonates precipitation and limestone genesis—the microbiogeologist point of view.* Sedimentary geology, 1999. **126**(1-4): p. 9-23.

41. Xu, J., X. Wang, and B. Wang, *Biochemical process of ureolysis-based microbial CaCO 3 precipitation and its application in self-healing concrete.* Applied microbiology and biotechnology, 2018. **102**(7): p. 3121-3132.

42. Porter, H., N.K. Dhami, and A. Mukherjee, *Synergistic chemical and microbial cementation for stabilization of aggregates.* Cement and Concrete Composites, 2017. **83**: p. 160-170.

43. Wang, J., et al. *Potential of applying bacteria to heal cracks in concrete*. in *Proceedings of the second international conference on sustainable construction materials and technologies*. 2010.

44. Van Tittelboom, K., *Self-Healing Concrete through Incorporation of Encapsulated Bacteria-or Polymer-Based Healing Agents ('Zelfhelend beton door incorporatie van ingekapselde bacteri*. 2012, Ghent University.

45. Dhami, N.K., M.S. Reddy, and A. Mukherjee, *Application of calcifying bacteria for remediation of stones and cultural heritages.* Frontiers in microbiology, 2014. **5**.

46. Xu, J., et al., *Effects of Calcium Source on Biochemical Properties of Microbial CaCO3 Precipitation.* Frontiers in microbiology, 2015. **6**.

47. Zhang, Y., H. Guo, and X. Cheng, *Role of calcium sources in the strength and microstructure of microbial mortar*. Construction and Building Materials, 2015. **77**: p. 160-167.

48. Choi, S.-G., et al., *Mortar crack repair using microbial induced calcite precipitation method.* Cement and Concrete Composites, 2017. **83**: p. 209-221.

49. Wiktor, V. and H. Jonkers, *Field performance of bacteria-based repair system: Pilot study in a parking garage*. Case Studies in Construction Materials, 2015. **2**: p. 11-17.

50. Sánchez, M., et al. *Self-healing approaches for the preventive repair of concrete structures: SARCOS COST Action*. in *2nd International RILEM/COST Conference on Early Age Cracking and Serviceability in Cement-based Materials and Structures (EAC-02)*. 2017. RILEM Publications.

51. Huang, H., G. Ye, and Z. Shui, *Feasibility of self-healing in cementitious materials–By using capsules or a vascular system?* Construction and Building materials, 2014. **63**: p. 108-118.

52. Minnebo, P., et al., *A Novel Design of Autonomously Healed Concrete: Towards a Vascular Healing Network.* Materials, 2017. **10**(1): p. 49.

53. Wang, J., et al., *Use of silica gel or polyurethane immobilized bacteria for self-healing concrete.* Construction and Building Materials, 2012. **26**(1): p. 532-540.

54. Van Belleghem, B., et al., *Chloride induced reinforcement corrosion behavior in self-healing concrete with encapsulated polyurethane.* Cement and Concrete Research, 2018. **113**: p. 130-139.

55. Wang, J., et al., *Application of hydrogel encapsulated carbonate precipitating bacteria for approaching a realistic self-healing in concrete.* Construction and building materials, 2014. **68**: p. 110-119.

56. Blaiszik, B.J., et al., *Self-healing polymers and composites.* Annual review of materials research, 2010. **40**: p. 179-211.

57. Ferrara, L., et al., *Experimental characterization of the self-healing capacity of cement based materials and its effects on the material performance: A state of the art report by COST Action SARCOS WG2.* Construction and Building Materials, 2018. **167**: p. 115-142.

58. Ahn, E., et al., *Principles and Applications of Ultrasonic-Based Nondestructive Methods for Self-Healing in Cementitious Materials.* Materials, 2017. **10**(3): p. 278.

59. Khaliq, W. and M.B. Ehsan, *Crack healing in concrete using various bio influenced self-healing techniques.* Construction and Building Materials, 2016. **102**: p. 349-357.

60. Achal, V., A. Mukerjee, and M. Sudhakara Reddy, *Biogenic treatment improves the durability and remediates the cracks of concrete structures.* Construction and Building Materials, 2013. **48**(Supplement C): p. 1-5.

61. Wang, J., et al., *X-ray computed tomography proof of bacterial-based self-healing in concrete.* Cement and Concrete Composites, 2014. **53**: p. 289-304.

62. Hilloulin, B., et al., *Monitoring of autogenous crack healing in cementitious materials by the nonlinear modulation of ultrasonic coda waves, 3D microscopy and X-ray microtomography.* Construction and Building Materials, 2016. **123**: p. 143-152.

63. Alghamri, R., A. Kanellopoulos, and A. Al-Tabbaa, *Impregnation and encapsulation of lightweight aggregates for self-healing concrete.* Construction and Building Materials, 2016. **124**: p. 910-921.

64. Achal, V., A. Mukherjee, and M.S. Reddy, *Microbial concrete: way to enhance the durability of building structures.* Journal of materials in civil engineering, 2010. **23**(6): p. 730-734.

65. Maes, M., D. Snoeck, and N. De Belie, *Chloride penetration in cracked mortar and the influence of autogenous crack healing.* Construction and building materials, 2016. **115**: p. 114-124.

66. Gruyaert, E., et al., *Self-healing mortar with pH-sensitive superabsorbent polymers: testing of the sealing efficiency by water flow tests.* Smart Materials and Structures, 2016. **25**(8): p. 084007.

67. Kang, C. and M. Kunieda, *Evaluation and observation of autogenous healing ability of bond cracks along rebar.* Materials, 2014. **7**(4): p. 3136-3146.

68. Hilloulin, B., et al., *Mechanical regains due to self-healing in cementitious materials: Experimental measurements and micro-mechanical model.* Cement and Concrete Research, 2016. **80**: p. 21-32.

69. Zhong, W. and W. Yao, *Influence of damage degree on self-healing of concrete.* Construction and building materials, 2008. **22**(6): p. 1137-1142.

70. Wang, X., et al., *Experimental study on cementitious composites embedded with organic microcapsules.* Materials, 2013. **6**(9): p. 4064-4081.

71. Nishiwaki, T., et al., *Self-healing capability of fiber-reinforced cementitious composites for recovery of watertightness and mechanical properties.* Materials, 2014. **7**(3): p. 2141-2154.

72. Van Tittelboom, K., et al., *Acoustic emission analysis for the quantification of autonomous crack healing in concrete.* Construction and Building Materials, 2012. **28**(1): p. 333-341.

73. Tsangouri, E., et al., *Detecting the activation of a self-healing mechanism in concrete by acoustic emission and digital image correlation.* The Scientific World Journal, 2013. **2013**.

74. Van Den Abeele, K., et al., *Active and passive monitoring of the early hydration process in concrete using linear and nonlinear acoustics.* Cement and Concrete Research, 2009. **39**(5): p. 426-432.

75. Garnier, V., et al., *Acoustic techniques for concrete evaluation: Improvements, comparisons and consistency.* Construction and Building Materials, 2013. **43**: p. 598-613.

76. Ait Ouarabi, M., et al., *Ultrasonic Monitoring of the Interaction between Cement Matrix and Alkaline Silicate Solution in Self-Healing Systems.* Materials, 2017. **10**(1): p. 46.

77. Karaiskos, G., et al., *Monitoring of concrete structures using the ultrasonic pulse velocity method.* Smart Materials and Structures, 2015. **24**(11): p. 113001.

78. Kaur, N.P., et al., *Healing and Simultaneous Ultrasonic Monitoring of Cracks in Concrete.* Materials Today Communications, 2018.

79. Aggelis, D. and T. Shiotani, *Repair evaluation of concrete cracks using surface and through-transmission wave measurements.* Cement and Concrete Composites, 2007. **29**(9): p. 700-711.

80. In, C.-W., et al., *Monitoring and evaluation of self-healing in concrete using diffuse ultrasound.* NDT & E International, 2013. **57**: p. 36-44.

81. Liu, S., et al., *Evaluation of self-healing of internal cracks in biomimetic mortar using coda wave interferometry.* Cement and Concrete Research, 2016. **83**: p. 70-78.

82. Hilloulin, B., et al., *Small crack detection in cementitious materials using nonlinear coda wave modulation.* NDT & E International, 2014. **68**: p. 98-104.

83. Deraemaeker, A. and C. Dumoulin, *Embedding ultrasonic transducers in concrete: A lifelong monitoring technology.* Construction and Building Materials, 2019. **194**: p. 42-50.

84. Stockwell, R.G., L. Mansinha, and R. Lowe, *Localization of the complex spectrum: the S transform.* IEEE transactions on signal processing, 1996. **44**(4): p. 998-1001.

85. Suaris, W. and V. Fernando, *Detection of crack growth in concrete from ultrasonic intensity measurements.* Materials and Structures, 1987. **20**(3): p. 214-220.

86. Davis, A., et al., *Nondestructive test methods for evaluation of concrete in structures.* American Concrete Institute, ACI, 1998. **228**.

87. Shah, S.P., et al., *New directions in concrete health monitoring technology.* Journal of engineering mechanics, 2000. **126**(7): p. 754-760.

88. Popovics, S., J.L. Rose, and J.S. Popovics, *The behaviour of ultrasonic pulses in concrete.* Cement and Concrete Research, 1990. **20**(2): p. 259-270.

89. Lin, Y., C.-P. Lai, and T. Yen, *Prediction of ultrasonic pulse velocity (UPV) in concrete.* Materials Journal, 2003. **100**(1): p. 21-28.

90. Demirboğa, R., İ. Türkmen, and M.B. Karakoc, *Relationship between ultrasonic velocity and compressive strength for high-volume mineral-*

admixtured concrete. Cement and concrete research, 2004. **34**(12): p. 2329-2336.

91. ASTM, C., *597-83 (Reapproved 1991).* Test for Pulse Velocity Through Concrete, ASTM, USA, 1991.

92. Shiotani, T. and D.G. Aggelis, *Wave propagation in cementitious material containing artificial distributed damage.* Materials and Structures, 2009. **42**(3): p. 377-384.

93. Sharma, S. and A. Mukherjee, *Ultrasonic guided waves for monitoring the setting process of concretes with varying workabilities.* Construction and Building Materials, 2014. **72**: p. 358-366.

94. Sharma, A., et al., *Ultrasonic guided waves for monitoring corrosion of FRP wrapped concrete structures.* Construction and Building Materials, 2015. **96**: p. 690-702.

95. Sharma, S. and A. Mukherjee, *Monitoring corrosion in oxide and chloride environments using ultrasonic guided waves.* Journal of Materials in Civil Engineering, 2011. **23**(2): p. 207-211.

96. Sharma, S. and A. Mukherjee, *Nondestructive evaluation of corrosion in varying environments using guided waves.* Research in Nondestructive Evaluation, 2013. **24**(2): p. 63-88.

97. Sharma, S. and A. Mukherjee, *Ultrasonic guided waves for monitoring corrosion in submerged plates.* Structural Control and Health Monitoring, 2015. **22**(1): p. 19-35.

98. Huang, H., G. Ye, and Z. Shui, *Feasibility of self-healing in cementitious materials – By using capsules or a vascular system?* Construction and Building Materials, 2014. **63**: p. 108-118.

99. Fröjd, P. and P. Ulriksen, *Amplitude and phase measurements of continuous diffuse fields for structural health monitoring of concrete structures.* NDT & E International, 2016. **77**(Supplement C): p. 35-41.

100. Van Belleghem, B., P. Van den Heede, and N. De Belie. *Resistance to chloride penetration of self-healing concrete with encapsulated polyuretyhane*. in *4th International Conference on Sustainable Construction Materials and Technologies (SCMT4)*. 2016.

101. Van Belleghem, B., et al., *Quantification of the service life extension and environmental benefit of chloride exposed self-healing concrete.* Materials, 2017. **10**(1): p. 5.

Chapter 3 Healing and Simultaneous Ultrasonic Monitoring of Cracks in Concrete

Nimrat Pal Kaur, Jay Kumar Shah, Subhra Majhi, Abhijit Mukherjee

School of Civil and Mechanical Engineering, Curtin University, WA 6102, Australia

Abstract

Premature cracking is a prime cause for deterioration of concrete structures. Techniques, especially wave-based technologies, have been developed for monitoring deteriorations of such structures. Recently, techniques for healing of the deteriorations are emerging necessitating expansion of monitoring techniques to healing as well. This paper reports experimental results for healing of cracks of different widths in concrete and illustrates the ability of the ultrasonic techniques to monitor the progression of healing. A numerical technique based on two-dimensional finite difference time domain (FDTD) has been used to determine the potential of the ultrasonic stress waves in monitoring healing. Based on the theoretical results, an experimental study has been conducted on reinforced concrete samples by creating a fine tensile crack of width ~0.1 mm and a relatively wide corrosion crack of ~2 mm width. They were monitored ultrasonically after cement grout was injected in the cracks. It is found that the ultrasonic technique is able to discern the progressive healing process. Signal attenuation was found to be most suitable for monitoring healing.

Keywords: concrete, healing, finite difference in time domain, healing fluid, ultrasonic monitoring

1. Introduction

Cracks in reinforced concrete structures are inevitable and they are one of the inherent weaknesses of concrete that adversely affect its structural integrity and durability. Cracks provide pathways for water and other aggressive agents such as chlorides, sulphates or carbon dioxide ingress that can lead to reinforcement corrosion and often spalling of concrete. Therefore, it is essential to heal cracks at an early stage to enhance the durability and increase service life of concrete structures. An efficient repair method coupled with a reliable evaluation technique is of paramount importance to ensure proper healing of cracks. Traditionally, cracks are manually repaired by injecting cementitious or polymeric agents [1-3]. Recently, research on self-healing using the inorganic [4-6] and the bacterial healing fluid [7-9] have been reported.

Self-healing material would exhibit the ability to repair itself and to recover the functionality using the resources inherently available to it. Concrete is observed to heal thin cracks (~50μm wide) autogenously [10]. However, this is not enough for most damages and external assistance for healing is warranted [11]. The key aspects of the healing system are the healing fluid and the delivery mechanism [12-14]. Saturated calcium hydroxide has been used as the healing fluid used for experiments with concrete [15]. It is demonstrated that a more versatile healing could be achieved with comparable time and reliable quality using the bacterial route [16-19]. It is noted that self-healing extends life of RC by alleviating water permeability and impeding corrosion [20]. The healing material is delivered either directly at the time of mixing [18] or by encapsulation [21, 22]. Polyurethane shells [23] and porous expanded clay particles [17] have been used for encapsulation. A vascular system where the healing fluid is delivered at the point of damage through vesicles has also been reported [5].

In this method, it is possible to control the healing process by coupling an online non-destructive monitoring system in a loop with the healing system (Figure 3.1). The monitoring system discovers damage and informs the controller. The controller triggers the healing system while the monitoring system constantly estimates the progress of healing. When the monitoring system indicates that the target healing is achieved, the controller cuts the healing system off. Although the healing and monitoring components of this scheme have progressed separately, there is not integration of them hitherto [14].

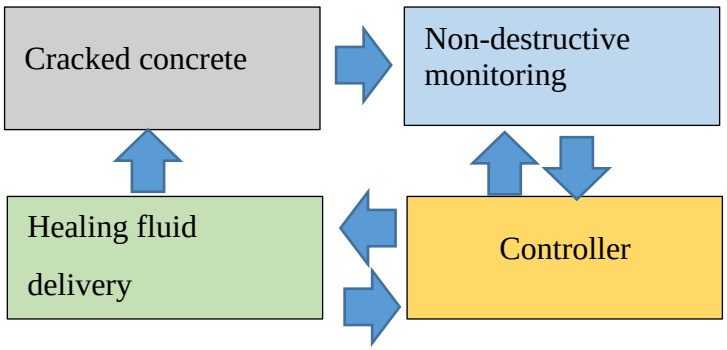

Figure 3.1: The self-healing Loop

The methods that have been applied so far in evaluation of healing have been reviewed by [24]. A significant number of these methods are microstructural evaluations such as Scanning Electron Microscopy and Energy Dispersive Spectroscopy [7, 25] or X-ray dispersion [26]. The macroscopic properties such as strength [27] and permeability [28] have also been reported. Although they are valuable for understanding the healing process these are destructive tests where the specimen needs to be fragmented and elaborate preparation is required in conducting them. Moreover, these tests are unsuitable for simultaneous monitoring of healing as it happens. Thus, an instant, non-intrusive monitoring technology is imperative. Some non-destructive evaluation techniques [29] have also been applied to assess and monitor self-healing capability

of concrete which include ultrasonic pulse velocity (UPV) measurements [5]; acoustic emission (AE) [30-34]; surface-wave transmission [35]; ultrasound diffusivity [36]; and coda wave interferometry [37-39] and non-linear ultrasonics [6, 34, 40, 41]. In these techniques, either the acoustic waves generated due to the damage in the structure is monitored [30, 31] or a stress pulse is applied to create a propagating wave within the structure [42]. Acoustic wave method is capable of capturing the events only during cracking/loading of concrete. Thus, the specimens can be evaluated only after healing through reloading and monitoring acoustic events in the healed samples [30, 31]. On the other hand, applied pulse method is a genuinely non-destructive technique and has the ability of evaluating the progression of healing constantly repeating the tests during the occurrence of damage and its healing [15, 34, 43]. Out of the stress pulse generation techniques, ultrasonic method is widely used due to their reliability and versatility.

In the ultrasonic method, the pulses are transmitted and received by a pair of transducers and the change in wave characteristics is monitored. The most common form of generating the waves is through piezoelectric transducers. These can either be located opposite to each other (known as transmission mode) or attached to the same surface of the specimen (known as reflection mode) [44]. In recent years, piezoelectric transducers embedded inside the concrete matrix, also known as smart aggregates have also been proposed [45]. However, their placement and functioning in concrete necessitates sophisticated designing and planning.

The state of the damage is evaluated by analysing the recorded waveform. Different wave characteristics such as velocity, attenuation and phase shift can be monitored. The simplest of them is pulse velocity, which has been reported by a number of investigators [5, 7, 46-48]. Based on the arrival time of the pulse over a known path

length, the pulse velocity is calculated. However, pulse velocity is not sensitive to the deteriorations such as cracking, as the damage is restricted to a limited area and the arrival time remains largely unaffected due to cracking [49, 50]. Thus, analysis based on velocity is not enough and other parameters such as pulse attenuation and phase shift may need to be explored for monitoring healing. Also, since concrete is a heterogeneous material with many scatterers, a high signal-to-noise ratio must be maintained to ensure a reliable monitoring.

Numerical models help in a better understanding of a phenomenon before performing experiments. There are numerical models in self-healing to predict mechanical characteristics such as fracture toughness and strength [27, 51, 52]. A fair amount of these works are devoted to modelling of self-healing mechanisms in encapsulated bacterial systems [53, 54]. Numerical models for evaluation of healing of fractured bones using ultrasonics have been attempted using a finite difference code [55]. Cracking and healing of concrete mortar has been modelled in 2D using a nonlinear scaling subtraction method by Gliozzi et al. [6]. However, a generic numerical model of damage and subsequent healing of concrete is yet to be reported.

In this paper, we report a numerical model to investigate the effect of generation and healing of cracks on the propagation of ultrasonic waves in concrete. A finite difference in time domain code has been developed to model wave propagation in cracked concrete as well as in different states of healing. Based on the numerical work, an experimental investigation has been performed to monitor healing. Corrosion and tensile cracks (thick and thin cracks) induced by dissimilar ways have been healed to report the ability of the ultrasonic technique in monitoring the healing process. Finally,

the potential use of this approach and future work has been proposed in the conclusions section.

2. Numerical model

A numerical model has been developed to provide an insight into the interaction of a stress wave with the healing cracked region. For this study, a plane of a 500 mm x 250 mm x 150 mm concrete slab is modelled as shown in Figure 3.2. Air on all the four sides of the slab and a vertical crack in the middle of the slab are modelled. S, R1 and R2 show the position of the ultrasonic wave source and receivers respectively.

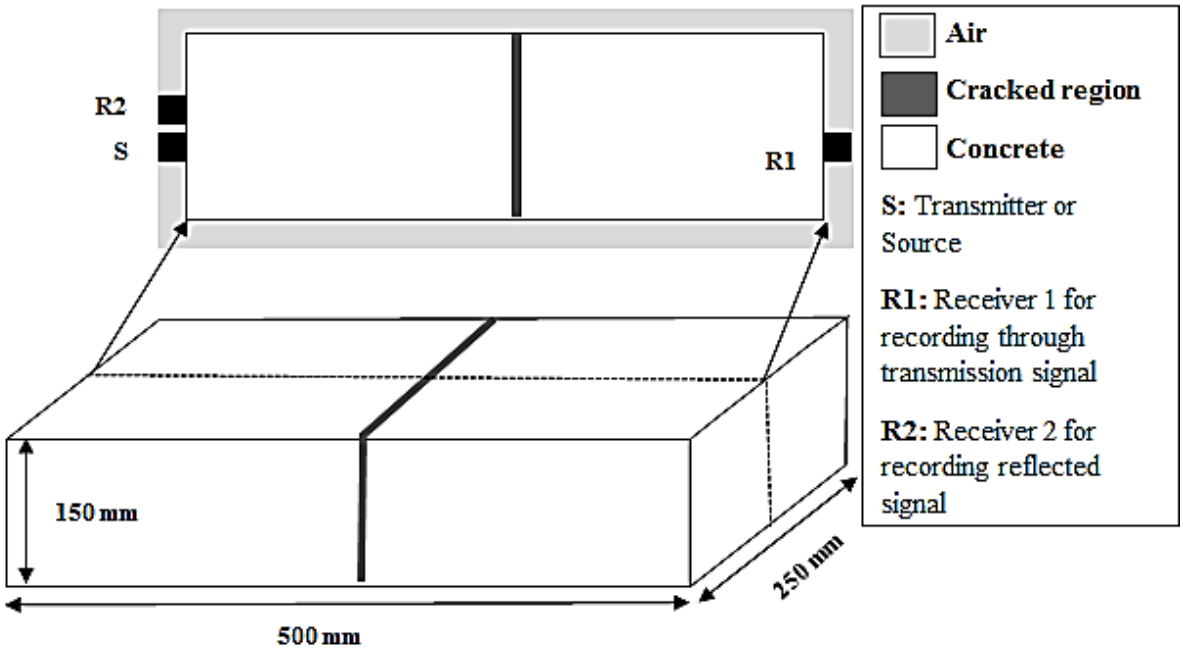

Figure 3.2: Schematic diagram of the numerically modelled experiment

To simulate the propagation of elastic waves, the governing stress-velocity relations, as in equations 3.1-3.3, have been solved using centred finite difference method [56].

$$\rho \frac{\partial v}{\partial t} = \boldsymbol{\nabla}.\boldsymbol{S} \; ; \boldsymbol{v} = \sum_{i=x,y,z} \boldsymbol{v_i}\, \hat{\boldsymbol{i}} \tag{3.1}$$

$$\frac{\partial \sigma_{ii}}{\partial t} = (\lambda + 2\mu)\frac{\partial v_i}{\partial i} + \lambda \sum_{j \neq i} \frac{\partial v_j}{\partial j} \quad (i, j = x, y, z) \tag{3.2}$$

$$\frac{\partial \tau_{ij}}{\partial t} = \mu \left(\frac{\partial v_i}{\partial j} + \frac{\partial v_j}{\partial i} \right) \quad (i, j = x, y, z \; and \; i \neq j) \tag{3.3}$$

In above relations,ρ and v represent the material density and particle velocities while ∇ stands for Nabla operator while S represents the stress tensor. λ and μ are Lamé parameters and σ, τ denote the normal and the shear stresses. Yee's grid model has been used to discretise the domain. Stress and velocity components are solved at definite locations in both space and time domain as in Schröder [56]. For stability of the numerical code, material properties at the air-concrete and crack-concrete interfaces are averaged [57].

2.1 Healing and monitoring of the concrete

Two cases of healing are considered in this numerical investigation. The first case models the progressive hardening of the healing fluid in the cracked region by choosing a varying elastic modulus (E) and density (ρ). Table 1 shows values for material and wave properties used in the model which are calculated using standard relations [58]. To model healing, the cracks are considered to be filled with a material that initially has only a small fraction of the wave velocities of concrete, but as healing progresses the velocities approaches that of concrete.

Table 1: Material and wave properties used for the simulation

Material	ρ (kg/m^3)	c_p (m/s) P-wave velocity	c_s (m/s) S-wave velocity	λ (kg/ms^2)	μ (kg/ms^2)
Air	1.21	330	0	1.31 x 10^5	0
Concrete	2.3 x 10^3	4400	2700	1.09 x 10^{10}	1.67 x 10^{10}

Stress waves excited at point S propagate through the specimen and interact with the cracked region. Pattern of these propagating waves is susceptible to change due to local acoustic impedance mismatch at the cracked region. Different stages of healing would be captured through the varying effect of the impedance mismatch between

concrete and the healing material. This wave-crack interaction information gets enciphered in the time history of the propagating wave which is recorded at receivers R1 and R2.

3. Experimental program

The experimental program was performed in the following steps:

1. Casting reinforced concrete slab specimens
2. Inducing cracks of different widths in slab specimens
3. Healing of cracked specimens with cementitious grout
4. Monitoring of progressive healing through ultrasonic measurements

3.1 Specimen preparation

Two set of specimens were casted in this investigation, one for inducing tensile crack and another for inducing corrosion crack. Concrete slab specimens of size 500mm (length) x 250mm (width) x 150mm (height) with an embedded steel bar were cast as shown in Figure 3.3. A standard plain mild steel reinforcing bar of 900mm length and 24 mm nominal diameter was used. Ordinary portland cement, sand and coarse aggregates (nominal size of 10 mm) were used in casting concrete. The ratio of cement: sand: coarse aggregate was 1: 1.62: 3.4. The water-to-cement ratio was 0.5 and the resulting compressive strength of concrete after 28 days was 43 MPa. The bar was protruded by 200mm on both sides for easy handling of the specimen. The specimens were demoulded after 24 hours from casting and moist cured for 28 days. The initial ultrasonic pulse transmission through all the specimens before cracking and corroding was measured as baseline reference.

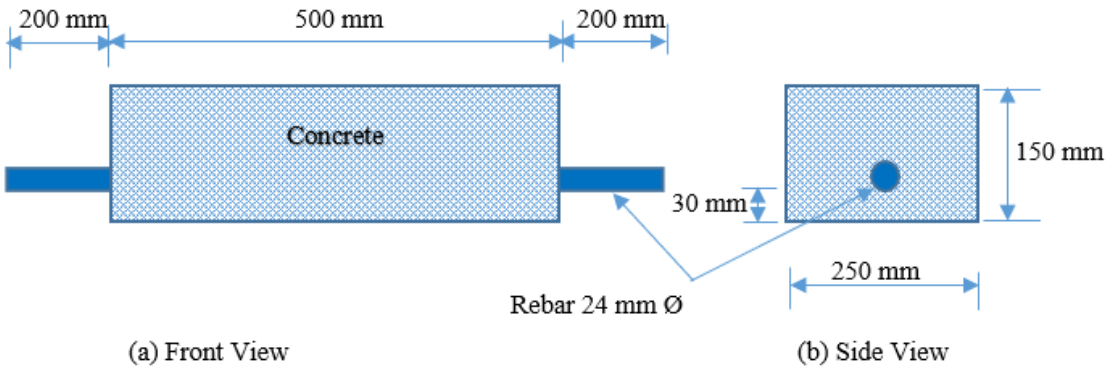

Figure 3.3: Reinforced concrete specimen design

3.2 Inducing cracks

In the present research, crack width was considered as a critical parameter to monitor the healing efficiency in the slab specimens. Thin crack in one set of specimens was generated through tensile cracking of concrete while the thick crack in the other set of specimens was obtained through anodic corrosion of the reinforcing bar.

3.2.1 Tensile cracks

For inducing the tensile cracks, the slab specimens were loaded to three-point bending configuration to induce tensile stresses, which forms a crack in the middle of the slab as shown in Figure 3.4. The stress in the reinforcement was within its yield limit. At a load of 72 KN, visible crack was seen, and the loading was terminated. Thus, due to the elastic recovery of the reinforcement after removing the load, the crack width was less than 0.1mm.

Figure 3.4:Specimen with tensile crack.

3.2.2 Corrosion cracks

For inducing corrosion cracks, the slab specimens were subjected a constant anodic current. A constant 25V voltage was continuously applied to the specimen for 28 days. The crack width and depth increased with the increase in exposure time. After 28 days, two wide cracks were observed along the length and width of the slab as shown in Figure 3.5. Crack width was measured, and it varied in the range of 1 and 3 mm.

Figure 3.5: Specimen with corrosion crack.

3.3. Ultrasonic investigations

A pair of GC200-D25 Ultran piezoelectric transducers with central frequency of 200 kHz and diameter of 25mm were used to generate compressional waves and record them. The choice of frequency is a trade-off between minimisation of scattering and

ability to detect the smallest crack. With 200 kHz, the wave length was around 20 mm, which is larger than the aggregates. Thus, scattering from the aggregates is minimal, also the wave length is smaller than the length of crack. The transducers were attached to a JSR DPR 300 pulse-receiver system. The ultrasonic data was digitized using Pico Scope 6 version 6.4.64.0 and a modular oscilloscope with gain of 40 dB. This sensitivity range of this instrument lies between ±20 mV to ±20 V, measured peak to peak. It has a vertical resolution of 8 bits. The surface of concrete was cleaned free of dust prior to attaching the transducers. A viscous coupling agent was used to securely attach the transducers to the surface of the concrete. All readings were taken by the same person and repeated at least three times for each signal. It was observed that the readings were consistent and repeatable.

Two techniques of ultrasonic measurement: (1) Pulse transmission, (2) Pulse reflection have been employed. In pulse transmission method, the transmitter and the receiver are placed on the opposite faces of the slab to measure the pulse transmitted through the crack as shown in Figure 3.6. In the reflection method, both the transmitter and the receiver are placed on the same surface of the slab next to each other to measure the pulse reflected from the crack. A periodic recording of the ultrasonic pulse is done throughout the healing process. The arrival time of the incident ultrasonic wave in the specimen is measured between the transmitting and receiving transducers. The distance between the two transducers was 500 mm. The arrival time of the first peak of the pulse for the pristine specimen is recorded between 112 and 115 µ-sec. The calculated velocity lies in the range 4300 m/s - 4400 m/s, which agrees with the theoretical value for concrete.

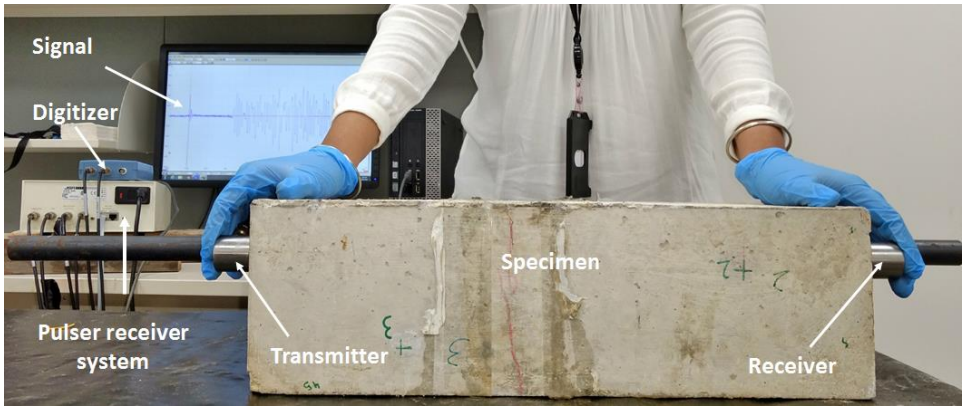

Figure 3.6: Experimental setup for ultrasonic data acquisition in transmission mode.

3.4. Healing of specimens

A cementitious grout mixture of ordinary portland cement with water to cement ratio 0.45 and a superplasticiser (1% of cement weight) was used as a healing agent. A similar healing fluid has been used in [59]. The viscosity of the healing agent influences efficiency of its penetration within the crack. A high viscosity healing agent doesn't flow well into the microcracks. On the contrary, a low viscosity healing agent may not remain in the crack and seep out of it instead. Thus, the viscosity of the cementitious grout was maintained between 15-20 centipoise. It is interesting to note that such a viscosity may not fill the tensile crack but would certainly fill the corrosion crack giving us the opportunity of monitoring the healing of the thin and thick cracks. The grout mixture was injected using a syringe to flow into the cracks under gravity and fill the crack. No additional effort was made to pump the mixture under pressure.

The healing characteristics of the cracked specimens were evaluated through periodic ultrasonic testing. In these tests, the efficacy of the healing process was determined by comparing the signal attenuation of intact specimens with that of the cracked specimens while they were being healed.

4. Results and discussion

4.1 Numerical results

A 200 kHz stress wave of Gaussian nature is applied at point S (Figure 3.7). The signals are recorded at points R1 and R2. R1 is situated on the opposite end of the source S. Thus, it records the signal that is transmitted through the crack. R2 and S are located on the same side of the specimen. Thus, it records the reflected waves from the cracked region.

Figure 3.7a shows the wave propagation in pristine concrete. P wave is clearly discerned as the fastest moving wave in the medium. S wave and reflections from the nearby boundaries can also be located in the figure. To validate the model the wave velocities are determined from the simulation. According to Fig. 7a, P wave travels 330 mm in 75.5 μs. Thus, the velocity of propagation of P waves is 4370 m/s which agrees closely with 4400 m/s as mentioned in table 1 and obtained velocity in Section 4.2.

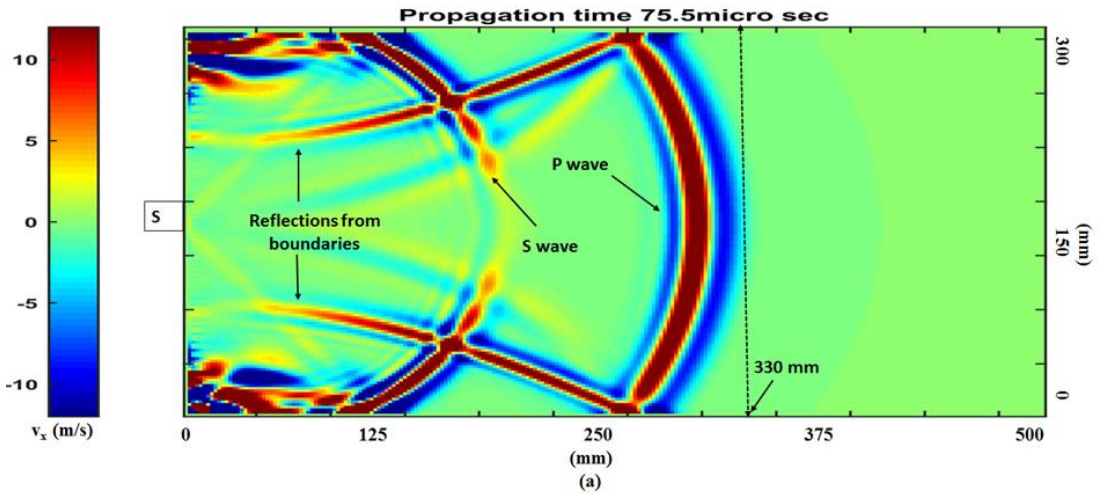

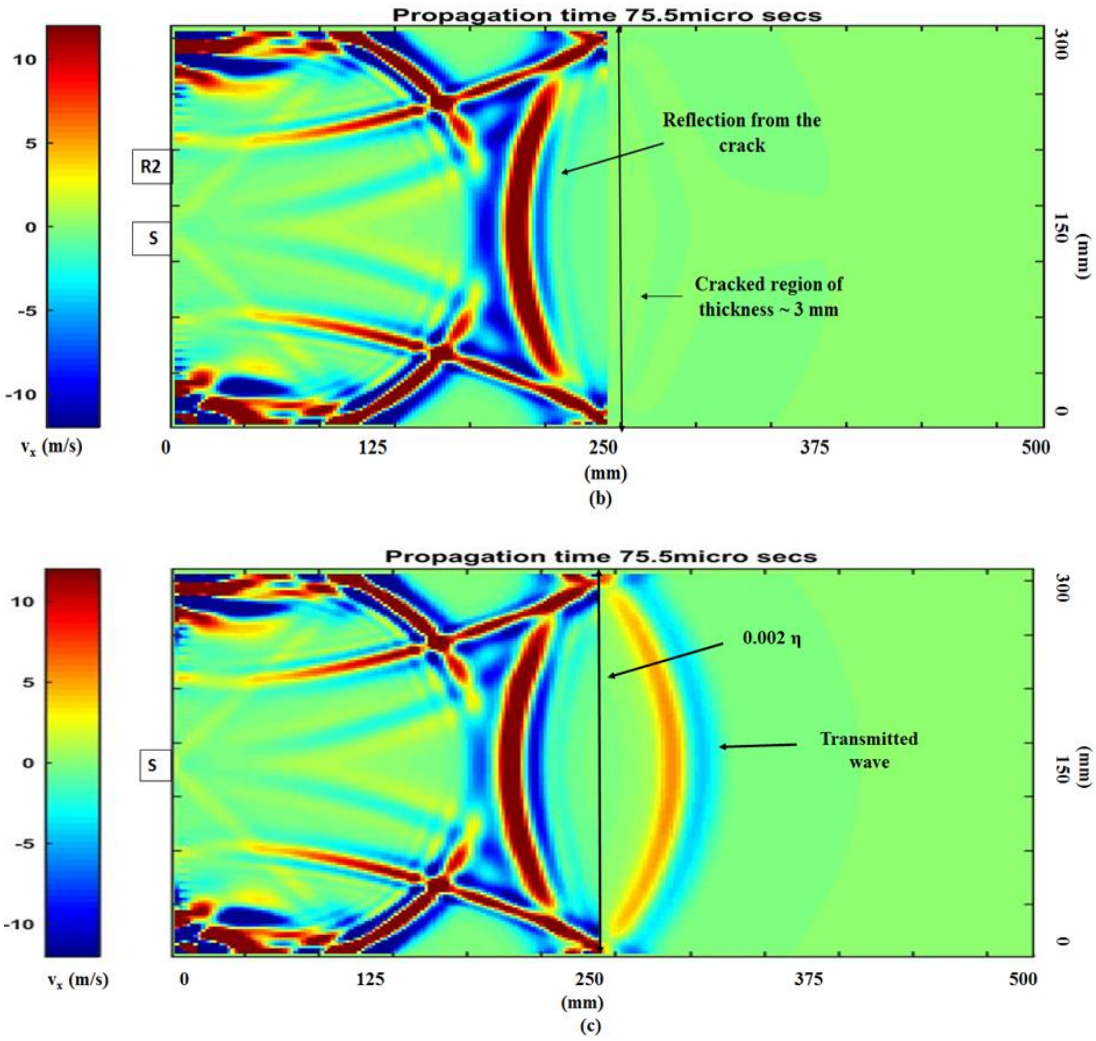

Figure 3.7: Wave propagation through (a) pristine specimen (b) fully cracked specimen (c) soft material in the cracked region. [Stress wave form: Gaussian]

Figure 3.7b presents the waves in the fully cracked specimen. As expected, in case of the fully cracked specimen, the entire wave is reflected. Evidently, the reflected wave from the crack-concrete interface can be utilised to detect the location of the crack by analysing the wave pattern recorded at the receiver location R2. In Figure 3.7c the crack is filled with a material having an acoustic impedance lower than that of concrete, such as a healing fluid. This material has density of the same order as of concrete, but its elastic modulus increases from negligible to that close to concrete as the healing progresses. Therefore, the ratio of transmission and reflection from the cracked region is dependent on the relative acoustic impedances of concrete and the

filling material. For Figure 3.7c, acoustic impedance of the filler material is chosen to be 0.2% of that of concrete. This represents the initial liquid filled state of the cracked region. A high attenuation in the transmitted wave is observed. As the healing material cures, its elastic modulus approaches that of the concrete. Consequently, a higher fraction of the incident stress wave gets transmitted through the healing region and the wave attenuation drops.

4.1.1 Reflected wave

In order to obtain the location of the unhealed portion, reflected waves for a fully cracked specimen is recorded at the location R2 (Figure 3.7b). The distance between S and R2 is 20 mm. As the velocity of the P wave and location of the crack are known to be 4400 m/s and 250 mm respectively, the reflected wave from the crack can be calculated from the distance velocity relation. Figure 3.8a shows additional peak due to the reflection from the crack. However, for the original dimension of the specimen i.e., 500 mm x 150 mm, information about the location of crack gets lost among dominating multiple reflections from the top and bottom boundaries of the specimen as shown in Figure 3.8b. The results for both cases are very similar, and it is difficult to extract any significant information about crack location from these graphs. Based on simulation results, it can be said that the near field effect and the secondary signals generated due to the reflections from the boundaries, dominate the waveform and no significant difference between the pristine and the damaged specimens could be discerned. Also, the assessment of the location of damage through reflection is strongly dependent on the geometry of the specimen.

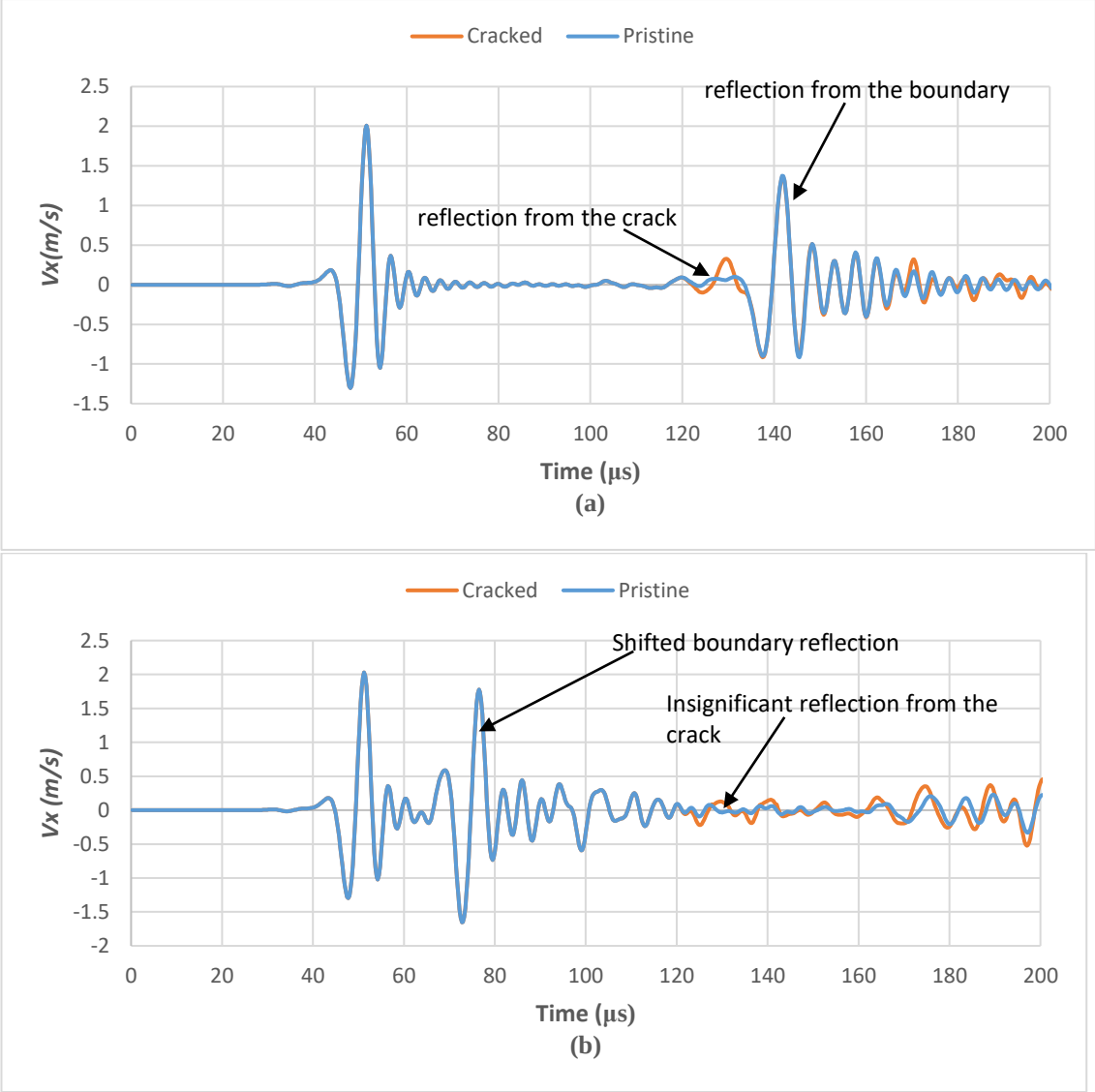

Figure 3.8: Reflection analysis at location R2 for the specimen with dimension of (a) 500 mm x 300 mm and (b) 500 mm x 150 mm

4.1.2 Progressive healing

The healing fluid flows into the crack and then undergoes a phase change gradually approaching the stiffness of concrete. In this study, the hardening phase of the healing fluid is represented by changing its acoustic impedance (η). In Figure 3.9a and 3.9b, it can be seen that when the η of the healing material approaches that of concrete, attenuation of stress waves through the healing region drops significantly. However, the velocity of the wave remains nearly the same. Therefore, wave attenuation is

expected to be a better parameter than wave velocity for monitoring progressive healing.

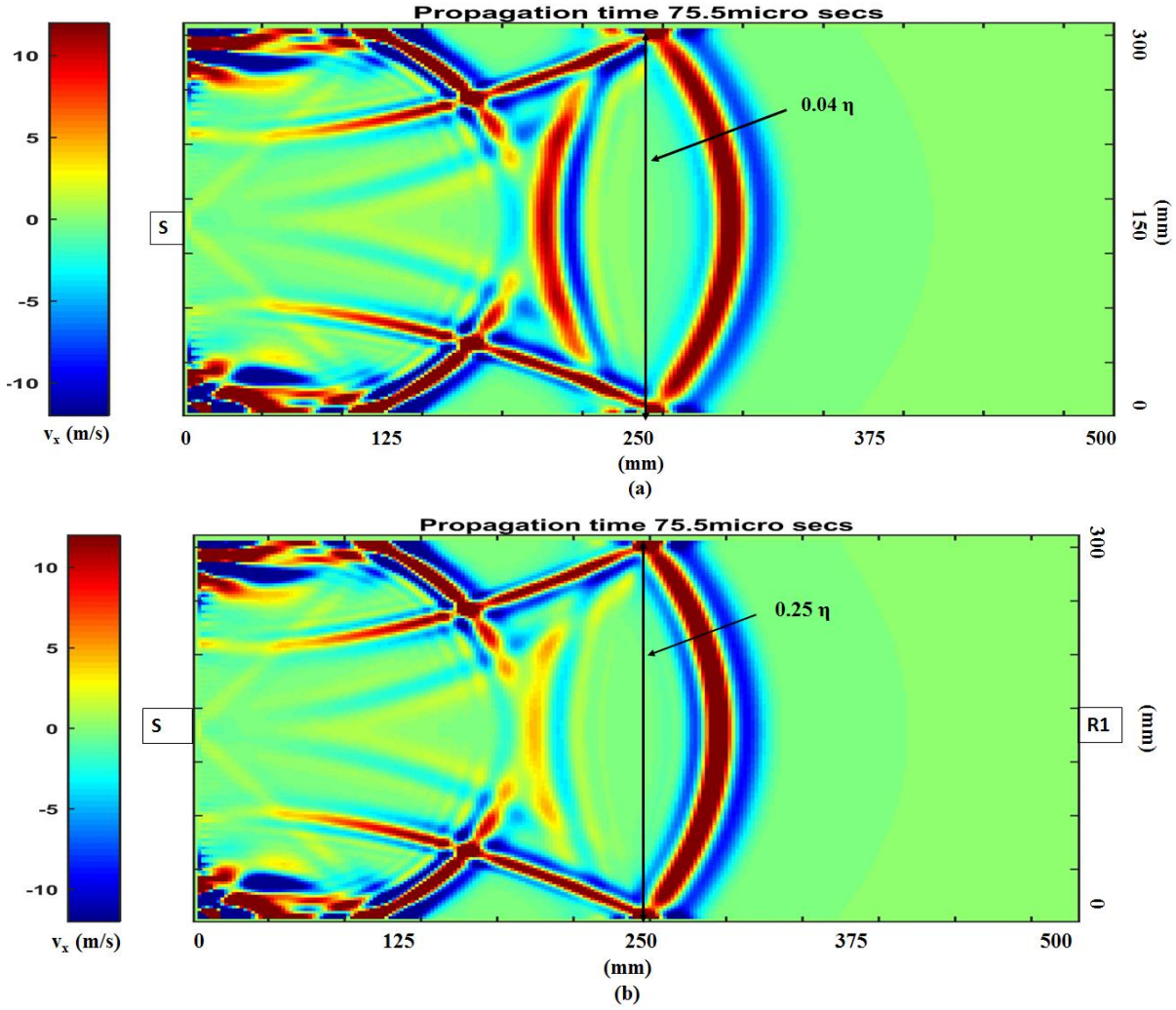

Figure 3.9: Wave propagation for different acoustic impedances (a) 0.04 η (b) 0.25 η

The transmitted wave for the specimen is recorded at the location R1 as shown in Figure 3.9b. Variation of the particle velocity component v_x with time of wave propagation is plotted for different acoustic impedances rη (r = 0.002, 0.01, 0.04, 0.25, 1) of the healing fluid in Figure 3.10a. Lowest acoustic impedance shows the initial liquid stage of the healing fluid and the highest values represents the acoustic impedance for the concrete. It can be seen that the transmitted wave changes during different phases of healing. The third peak was recorded to be the highest. Therefore, the arrival time and attenuation of the peak is observed in Figure 3.10b. It is noted that

while the arrival time remains relatively unaltered, the attenuation reduces sharply with healing. This simulation demonstrates that in experiments, monitoring signal attenuation during healing is likely to be more effective than change in the arrival time. However, for a reliable experimental data on attenuation, ensuring proper coupling of the transducers with the substrate is essential.

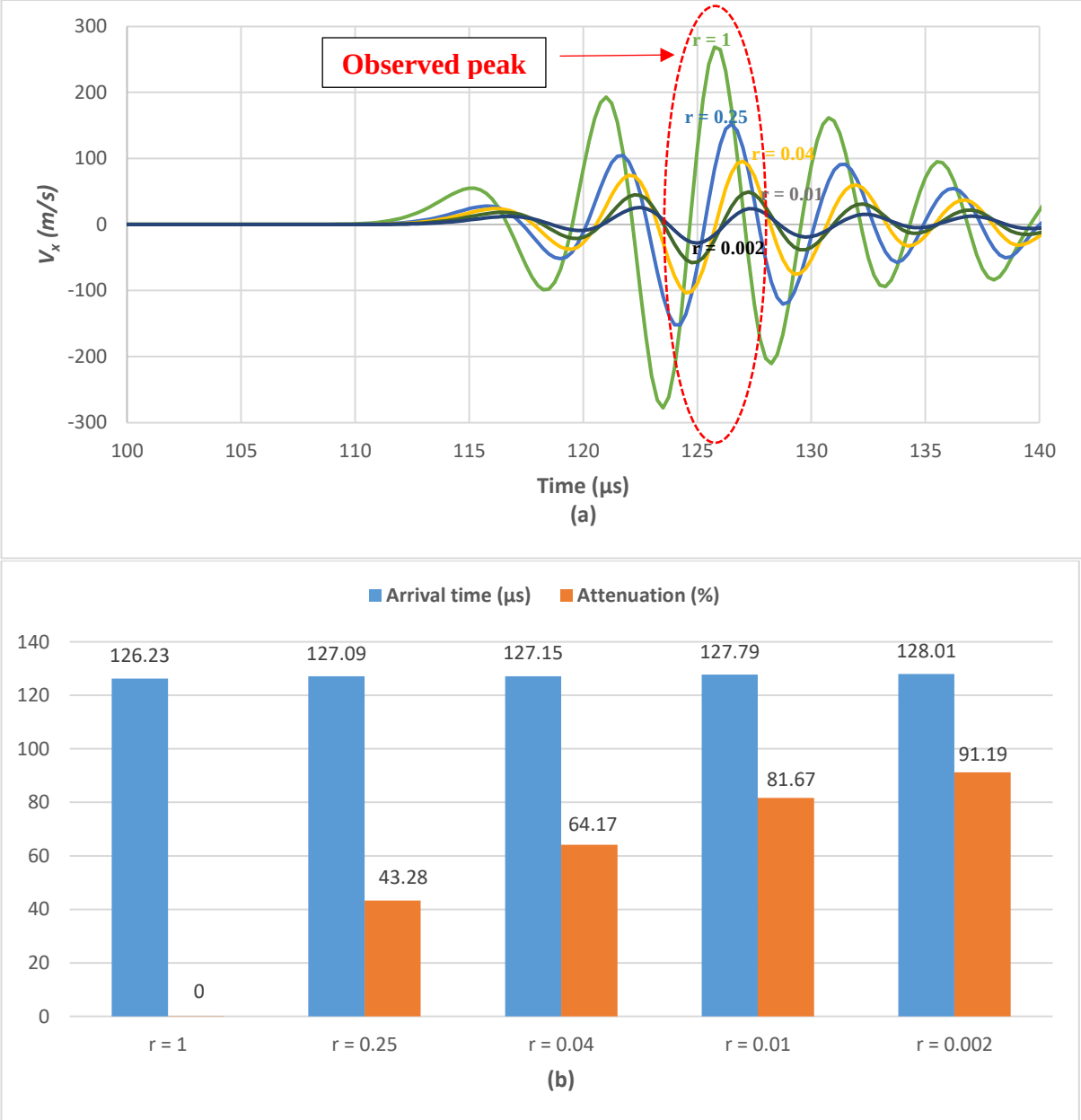

Figure 3.10: (a) v_x vs propagation time plot showing time history of the transmitted wave (b) Variation of arrival time of first peak and attenuation in the third peak

4.1.3 Partially filled cracks

This section investigates the partial healing of a crack. Figure 3.11 shows a snapshot of wave propagation for a case where only the top one-fourth of the crack is healed, but the rest of the crack is not treated. The snapshot of the propagation of the wave at 75.5µsec shows that the transmission happens only through the healed portion. Two transducer positions, S-R1 and S'-R1' have been investigated. It can be noted that the S-R1 configuration is in the unhealed portion, while S'-R1' is in the healed portion. Evidently, the path length in case of S-R1 is considerably longer than that in case of S'-R1'.

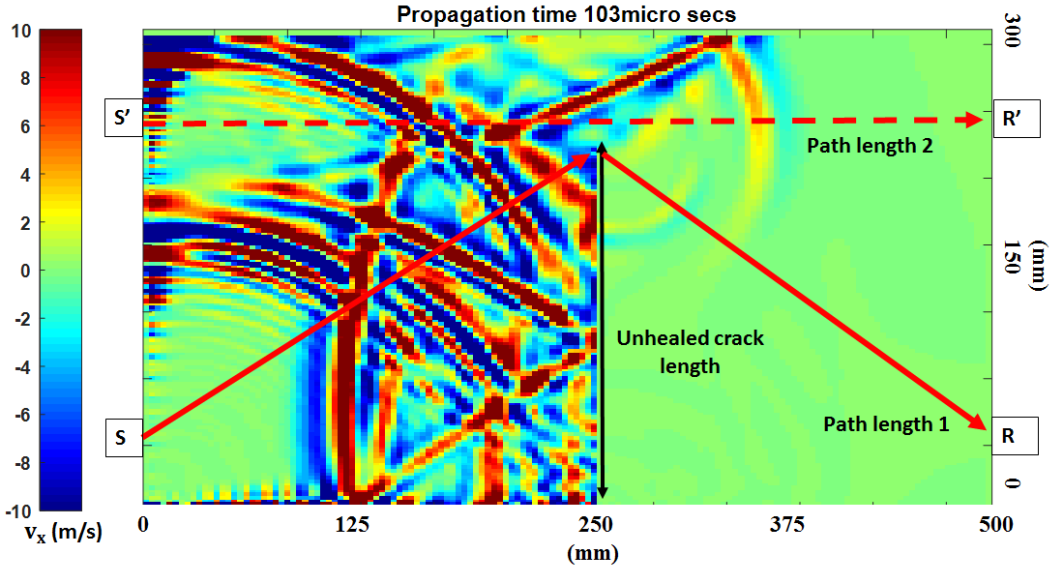

Figure 3.11: Wave propagation through partially filled cracks [Stress wave form: Gaussian]

Figure 3.12a and 3.12b show the waveforms received with S-R1 and S'-R1' configurations. The fraction (n) of the filled length of the crack (nL) is varied in the range (n = 1, 0.75, 0.50, 0. 25). Both the times of arrival of the first peak and the attenuation in the third peak differ significantly for the two positions.

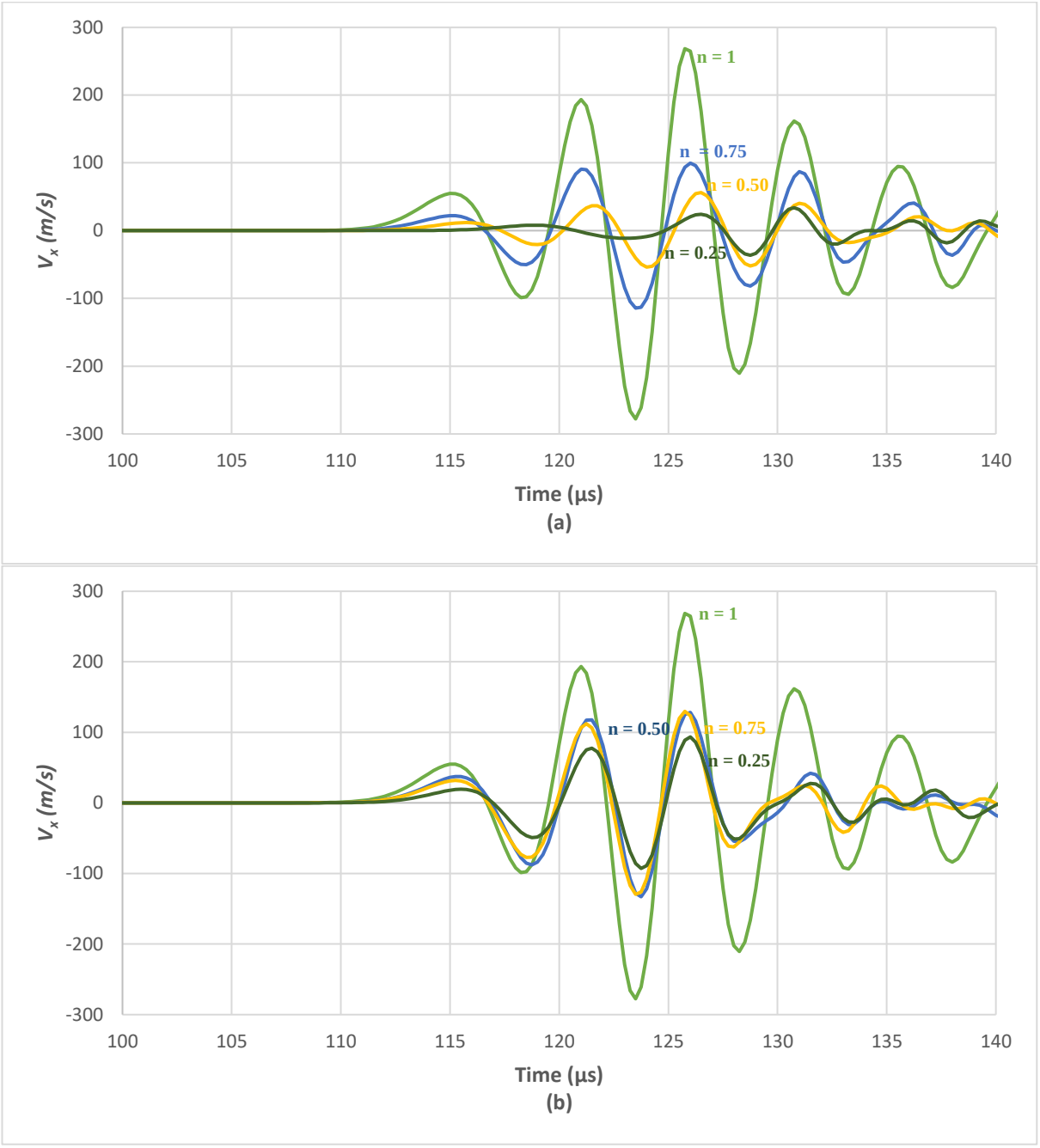

Figure 3.12: Transmitted signal received with (a) S-R1 and (b) S'-R1'

Figure 3.13a compares the arrival time of the first peak for the two transducer configurations. For n=1 the crack is fully healed. Thus, both arrival times are equal. As n becomes smaller, or the healing is of smaller fraction of the crack length the arrival times change substantially. For the S-R1 position, which is far from the healed region, the arrival time is higher than that in the S'-R1' configuration. The difference increases as the healed length reduces. This is due to the longer path length for the S-R1 configuration, as depicted in Figure 3.11. However, by comparing the arrival times at two different locations of sensors, it can be concluded that change in arrival time of the first peak or change in wave velocity is not that significant to draw a conclusion about healing. Figure 3.13b compares the attenuation in the third peak for S-R1 and S'-R1' configurations. For n=1, both configurations have identical attenuations. As n reduces, or in other words larger fraction of the crack remains unhealed, attenuation increases for both configurations; but for S-R1 configuration attenuation increases more rapidly than the S'-R1' configuration. Thus, the possibility of having an unhealed region can be found out by monitoring the attenuation in the transmitted signal at two different sensor locations. Thus, on the basis of Figure 3.13a and 3.13b, it can be concluded that attenuation variations at two different locations can give an approximate idea about the unhealed length of the crack than the arrival time of the first peak which is dependent on the position of transducers.

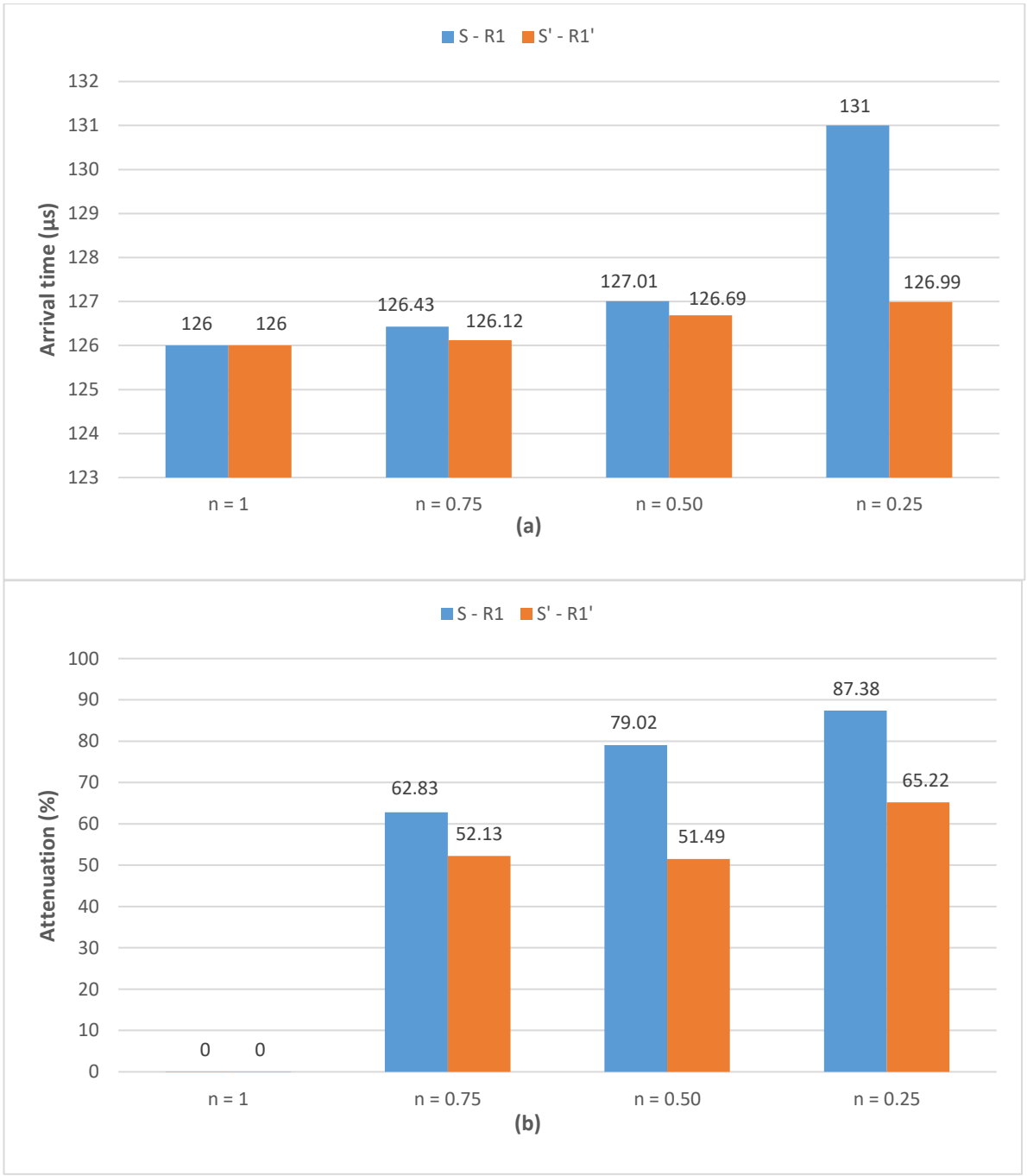

Figure 3.13:(a) arrival time and (b) attenuation variation in the observed peak for different healed lengths for bottom (S and R1) and top (S' and R1') positions of source and receiver.

Numerical results have revealed that for the present specimen the reflected wave could not be clearly discerned while the presence of cracks was identified in the transmitted wave. Therefore, the healing process can be monitored by the wave analysis transmitted through the crack. The hardening process of the healing fluid can also be traced in the transmitted waveform history. Healing of a fraction of the crack can also

be identified and the region that has remained healed can be demarcated. Attenuation of the waveform is more sensitive than the arrival time in all the cases. The experimental program is based on these observations.

4.2 Experimental results

4.2.1 Transducer configuration

Two configurations of the transducers: 1) reflection and 2) transmission, have been explored. In the reflection mode, the transducer pairs were placed on the same face of the slab, while in the transmission mode, the transducer pairs were on the opposite faces. The ultrasonic readings are taken repeatedly at different points to make sure that no region is missed. Figure 3.14(a) shows the waveforms measured in the reflection mode for uncracked, tensile crack and corrosion crack specimen. It is noted that a clear distinction could not be made between the uncracked, cracked and corroded specimens. The numerical results have already indicated that the reflection configuration is unsuitable for monitoring the crack due to the near field effect and the interference of multiple reflections from the boundaries. In the experiments too the same phenomenon is observed. Therefore, the reflection mode of measurement is abandoned and only the transmission mode results are presented for the rest of the paper.

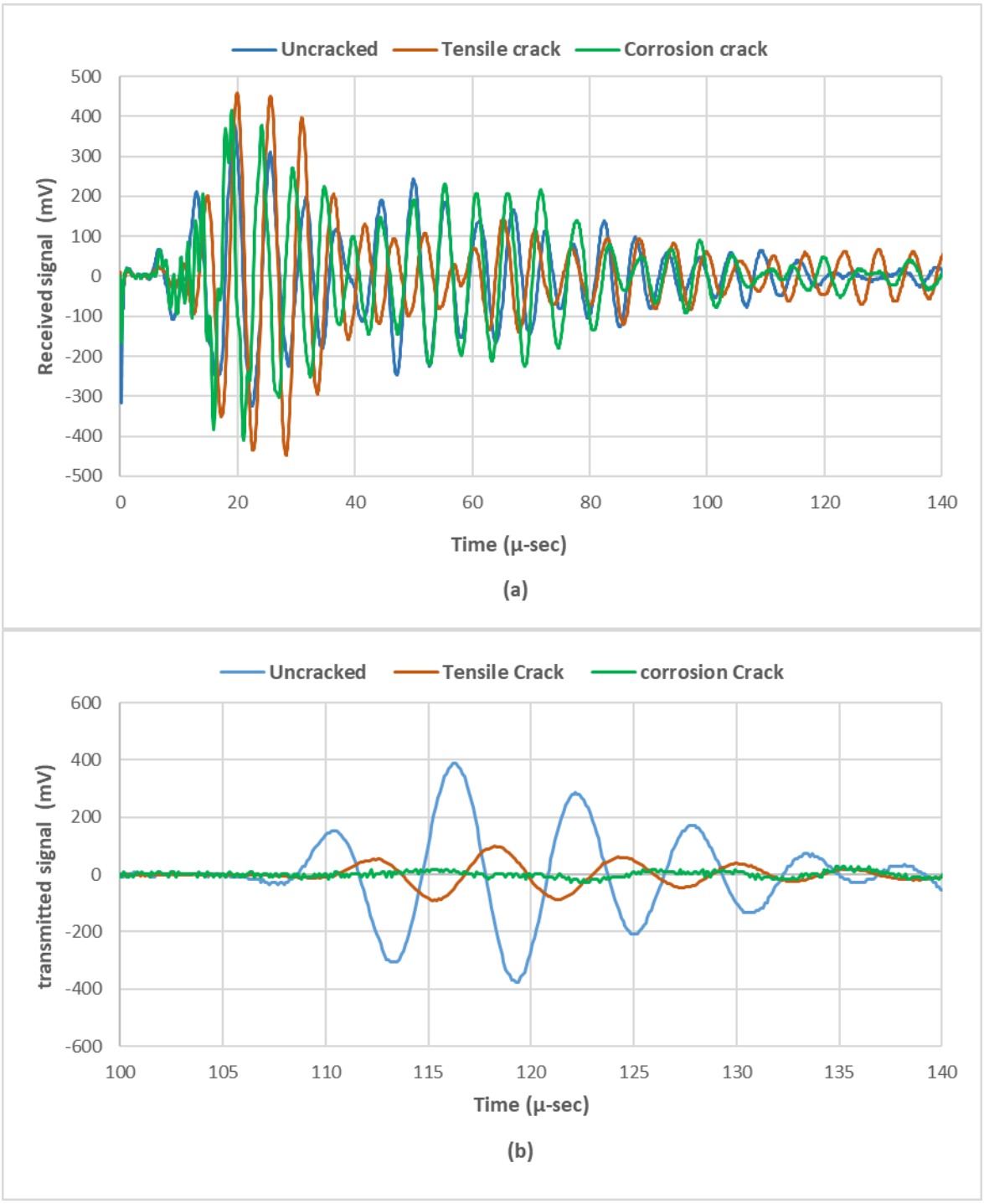

Figure 3.14:Ultrasonic signals using (a) reflection approach (b) transmission mode for uncracked, tensile crack and corrosion crack specimens.

Figure 3.14 (b) presents the recorded signals in the transmission mode. A clear difference is discernible in case of uncracked, tensile cracked, and corrosion cracked specimens. There is a distinct slowdown in the wave speed from the uncracked to the tensile cracked specimen. However, a substantial portion (~25%) of the pulse has been

transmitted though the crack. It demonstrates that the crack faces are in contact at several places in case of the tensile crack resulting in transmission, albeit with a longer path length. In case of the corrosion cracked sample, there is only a marginal transmission of the pulse. It demonstrates that the crack faces are not likely to be in contact. A negligible transmission is taking place possibly through the reinforcing bar.

For clear representation of the transmission signals, the arrival time and the attenuation variation of the largest peak are plotted as shown in Figure 3.15. It is noted that while the arrival time remains relatively unaltered, attenuation is greatly affected. Similar variations are observed in numerical study as well. These results corroborate well with the results obtained by Suaris and Fernando [50] in which attenuation of waveform was found to be more sensitive to the crack growth than wave velocity.

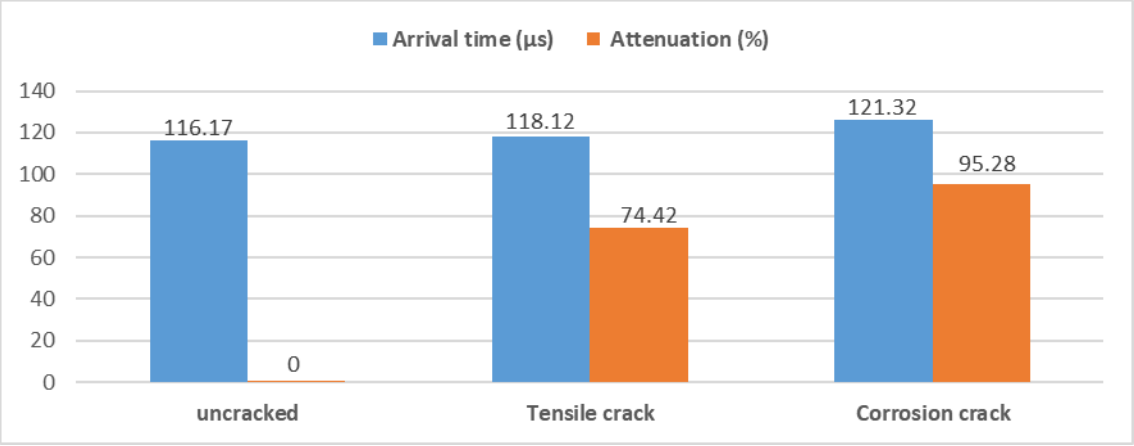

Figure 3.15:Bar graph showing variation of arrival time (largest peak) and attenuation for signals in transmission mode

4.2.2 Treatment of tensile cracks

Figure 3.16 presents the ultrasonic signals before cracking (uncracked), after cracking (cracked) and after the grout treatment (treated) for tensile cracked slab specimens. A gain of 40 dB was maintained for all the readings.

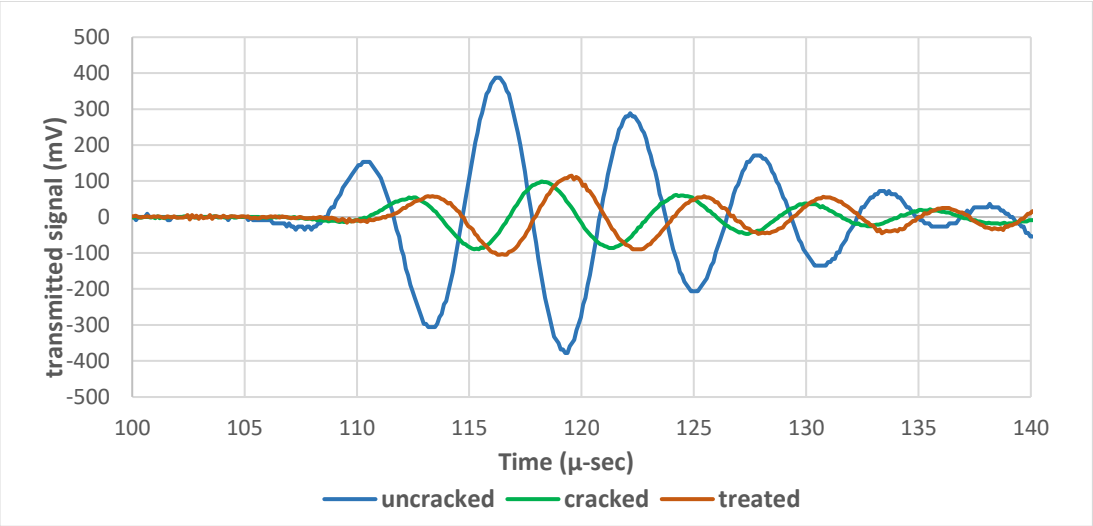

Figure 3.16: Tensile cracked specimen: before cracking (uncracked), after cracking (cracked) and after the grout treatment (treated).

From Figure 3.16, it is observed that there is a high attenuation and to a lesser extent, change in arrival time for uncracked and cracked specimen. This is due to the fact that ultrasonic waves travel faster in hardened concrete matrix than through the crack. During healing, it was expected that the attenuation shall reach that of the uncracked specimen, or in other words the waveforms shall be restored because the crack now gets filled with grout which after solidification, would have the acoustic properties close to that of concrete. The ultrasonic readings were repeatedly recorded at regular time intervals and no significant difference was observed even after 24 hours although the grout deposited at the surface of the specimen had already dried. It was observed visually during the treatment that very small quantity of the grout could be utilised. Clearly, the cementitious grout was unable to penetrate the crack and only the surface

of the specimen was covered with the grout, resulting in marginal change in recorded waveform after the treatment. The velocity and attenuation presented in Figure 3.18 corroborate this observation as no significant change could be seen for treated specimen. Similar conclusions were made by Tittleboom et al. [7] in which small change in transmission time was observed when crack width of 0.3 mm was healed with cement grout. It can be concluded that, although the cracks appeared to be covered on the surface, but the ultrasonic technique could reveal that it is not healed.

4.2.3 Treatment of corrosion cracks

Figure 3.17 presents the ultrasonic signals before cracking (uncracked), after cracking (cracked) and after grout treatment (treated) for the corrosion cracked specimen. A gain of 40 dB is maintained for the specimens before cracking and after treating with grout. For the cracked specimen before treatment the signal recorded at 40 dB was below the noise level. Thus, a gain of 60 dB was applied for the cracked specimen.

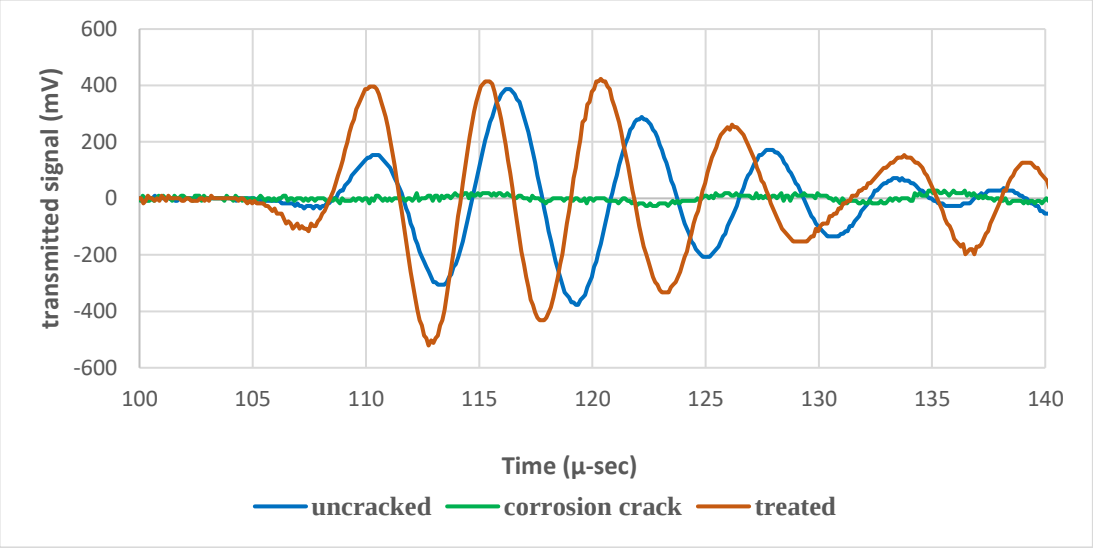

Figure 3.17:Ultrasonic transmission through corrosion cracked specimen: before cracking (uncracked), after cracking (corrosion crack) and after treatment (treated).

It can be seen that there is a marginal transmission of the pulse for corrosion cracked specimen. In this case the cracks are wider and not in contact. Thus, no wave can pass

through the crack faces. Presumably, only a small fraction of the pulse transmits through the reinforcing bar as depicted in the record. Unlike the tension cracked specimen, in case of corrosion cracked specimen the grout treatment showed a marked increase in pulse transmission through the crack faces. The cracks are as wide as a few millimetres thus, the present grout could easily penetrate through the depth of the crack. The recorded waveform for the treated specimen was close to that of uncracked specimen.

Figure 3.18 illustrates the effect of the treatment in the two crack types. In case of the tensile crack, the treatment resulted in a marginal shift in the wave velocity or wave attenuation. Thus, the present grout was unable to penetrate the thin crack. Significant reduction in attenuation could be seen in the corrosion crack specimen after healing of the wider crack caused due to corrosion. To a lesser extent, the velocity had increased too. Clearly, the voids were filled with the healing material leading to a significant recovery in the signal strength. Thus, evidence of recovery of the specimen due to the treatment could be seen. These results reveal that monitoring signal attenuation during healing is likely to be more effective than change in the arrival time/velocity. This experiment demonstrates that it is possible to discern healed cracks from the unhealed cracks using the present ultrasonic technique.

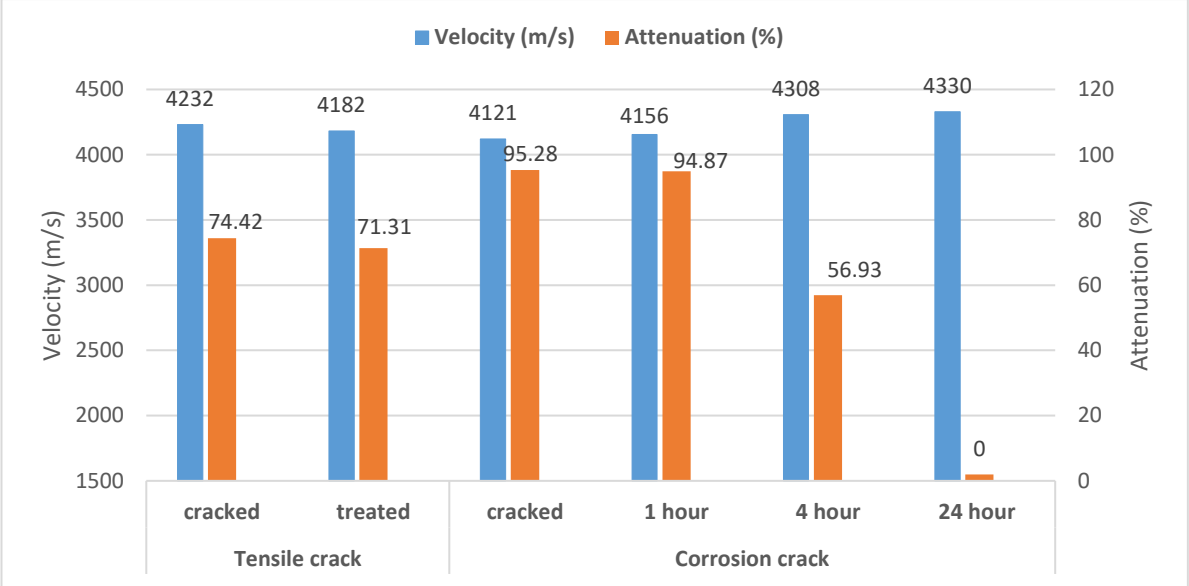

Figure 3.18: Velocity and attenuation variations for tensile and corrosion crack before and after treating

4.2.4 Progressive healing

After the grout treatment, the ultrasonic measurements were performed at regular intervals. The resulting waveforms are presented in Figure 3.19. Time “0 hour” corresponds to the time just after the cracked specimen was filled with cementitious grout and healing has just initiated. There was no perceptible change in the waveform until nearly two hours after the pour: this is the initial setting time of the grout. At four hours there was a significant increase in pulse transmission. Evidently, the hardening process of the grout has initiated. Sharma and Mukherjee [60, 61] observed that the setting process of concrete can be monitored by the guided ultrasonic waves. According to their experiment, the initial setting time is around 3 hours for vibrated concrete and 6 hours for self-compacting concrete. The present results corroborate well with their observation. In 24 hours, the signal was close to that of the uncracked sample indicating nearly full recovery. Monitoring of the sample was continued even after 24 hours but no significant change was observed. Gliozzi et al. [6] on the other hand, observed full recovery after 7 days when healed with sodium silicate solution.

Understandably, the time of healing significantly varies with the healing material. However, the transmitted ultrasonic pulse embodies the signature of the extent of healing for all materials.

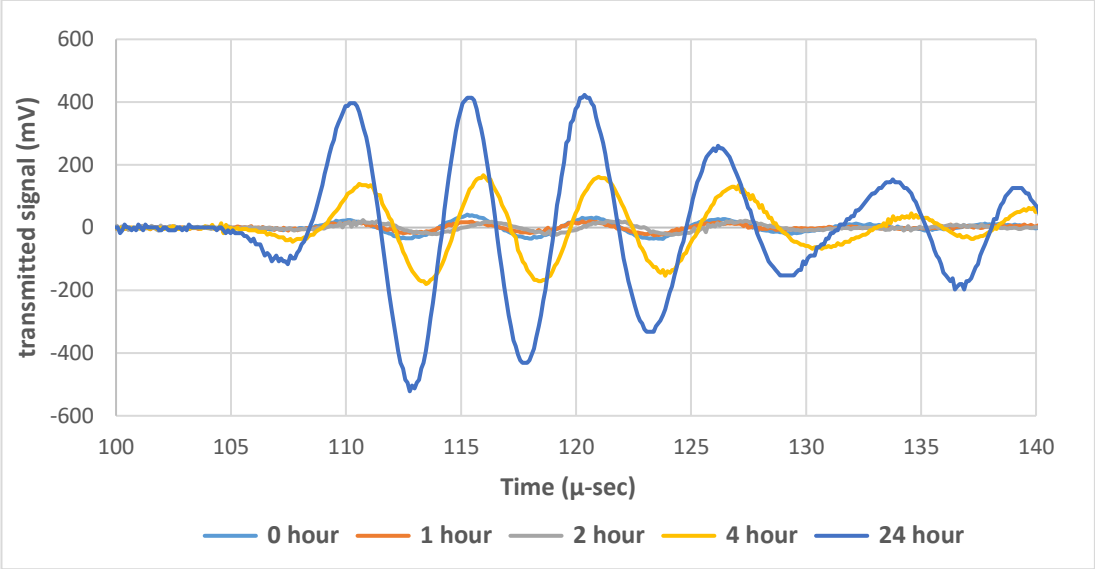

Figure 3.19: Healing stages of corrosion cracked specimen at different time intervals.

5. Conclusions

This paper presents the performance of the ultrasonic technique to monitor healing of cracks in concrete. A numerical technique is developed to predict the healing characteristics in terms of ultrasonic signals for concrete slab specimens. Based on the results of the numerical analysis, an experimental program for monitoring healing of tensile and corrosion cracks is reported.

The numerical results demonstrate that the transducer configuration is paramount in discerning damages and healing in concrete. For the present sample, the reflected signal from the crack was overwhelmed by the near field effects and boundary reflections. The cracks could be discerned clearly by monitoring the pulse transmitted through the crack. The pulse was characterised by both arrival time and signal attenuation. It is noted that the signal attenuation is generally more sensitive to

cracking and healing than transmission time. However, the reliability of measured signal is subject to the quality of the coupling of the transducers. The numerical study also revealed the relationship between the acoustic impedance of the crack filler and the transmitted pulse. This is useful in monitoring the progression of healing of the crack. The present ultrasonic technique was also able to identify partially filled cracks and locate the voids through comparison of the arrival time and signal attenuation at different positions of the crack.

The experimental technique explored the efficacy of the ultrasonic technique in discerning healing from its failure. For this purpose, a tensile crack (thin) and a corrosion crack (thick) were treated with a cementitious grout. The viscosity of the grout allowed it to fill the thick crack but not the thin crack. The ultrasonic technique was able to clearly classify the success from the failure of healing. When the crack was filled by the grout, its hardening process could be monitored by the present technique. The initial setting and the extent of hardening was characterized by variation in the signal attenuation. Finally, the signal resembles closely with that of the uncracked specimen, indicating near complete healing.

Research is underway to devise a healing system suitable for healing thin cracks. A bacterial healing fluid is very promising. The authors are also exploring other types of transducers such as piezo patches and their configurations to generate others form of waves (Rayleigh waves, for example) to discern more detailed information of the fate of healing cracks in concrete.

Acknowledgements

The authors would like to acknowledge the contribution of Australian Government Research Training Program Scholarship in supporting this research.

Funding

The authors thankfully acknowledge the financial support from Australian Research Council through Linkage Project Grant LP150100475.

Conflicts of Interest

The authors declare that they have no conflict of interest.

Data availability

The raw data required to reproduce these findings cannot be shared at this time as the data also forms part of an ongoing study.

REFERENCES

1. Neville, A.M., Properties of concrete. Vol. 4. 1995: Longman London.
2. Thanoon, W.A., et al., Repair and structural performance of initially cracked reinforced concrete slabs. Construction and Building Materials, 2005. **19**(8): p. 595-603.
3. Yokota, O. and A. Takeuchi. Injection of repairing materials to cracks using ultrasonic rectangular diffraction method. in 16th World conference on non destructive testing. 2004.
4. Blaiszik, B.J., et al., Self-healing polymers and composites. Annual review of materials research, 2010. **40**: p. 179-211.

5. Huang, H., G. Ye, and Z. Shui, Feasibility of self-healing in cementitious materials–By using capsules or a vascular system? Construction and Building materials, 2014. **63**: p. 108-118.
6. Gliozzi, A., et al., Correlation of elastic and mechanical properties of consolidated granular media during microstructure evolution induced by damage and repair. Physical Review Materials, 2018. **2**(1): p. 013601.
7. Van Tittelboom, K., et al., Use of bacteria to repair cracks in concrete. Cement and Concrete Research, 2010. **40**(1): p. 157-166.
8. Wang, J., et al. Potential of applying bacteria to heal cracks in concrete.
9. Xu, J., X. Wang, and B. Wang, Biochemical process of ureolysis-based microbial CaCO3 precipitation and its application in self-healing concrete. Applied Microbiology and Biotechnology, 2018. **102**(7): p. 3121-3132.
10. Palin, D., V. Wiktor, and H.M. Jonkers, Autogenous healing of marine exposed concrete: Characterization and quantification through visual crack closure. Cement and Concrete Research, 2015. **73**: p. 17-24.
11. Wu, M., B. Johannesson, and M. Geiker, A review: Self-healing in cementitious materials and engineered cementitious composite as a self-healing material. Construction and Building Materials, 2012. **28**(1): p. 571-583.
12. De Belie, N. and J. Wang, Bacteria-based repair and self-healing of concrete. Journal of Sustainable Cement-Based Materials, 2016. **5**(1-2): p. 35-56.
13. Joshi, S., et al., Microbial healing of cracks in concrete: a review. Journal of Industrial Microbiology & Biotechnology, 2017: p. 1-15.

14. Sangadji, S. and E. Schlangen, Self Healing of Concrete Structures-Novel approach using porous network concrete. Journal of Advanced Concrete Technology, 2012. **10**(5): p. 185-194.
15. Huang, H., G. Ye, and Z. Shui, Feasibility of self-healing in cementitious materials – By using capsules or a vascular system? Construction and Building Materials, 2014. **63**: p. 108-118.
16. Achal, V., A. Mukerjee, and M. Sudhakara Reddy, Biogenic treatment improves the durability and remediates the cracks of concrete structures. Construction and Building Materials, 2013. **48**: p. 1-5.
17. Wiktor, V. and H.M. Jonkers, Quantification of crack-healing in novel bacteria-based self-healing concrete. Cement and Concrete Composites, 2011. **33**(7): p. 763-770.
18. Jonkers, H.M., et al., Application of bacteria as self-healing agent for the development of sustainable concrete. Ecological Engineering, 2010. **36**(2): p. 230-235.
19. Wiktor, V. and H.M. Jonkers, Field performance of bacteria-based repair system: pilot study in a parking garage. Case Studies in Construction Materials, (0).
20. Erşan, Y.Ç., et al., Nitrate reducing CaCO3 precipitating bacteria survive in mortar and inhibit steel corrosion. Cement and Concrete Research, 2016. **83**: p. 19-30.
21. Souradeep, G. and H.W. Kua, Encapsulation technology and techniques in self-healing concrete. Journal of Materials in Civil Engineering, 2016. **28**(12): p. 04016165.

22. Van Tittelboom, K., Self-Healing Concrete through Incorporation of Encapsulated Bacteria-or Polymer-Based Healing Agents ('Zelfhelend beton door incorporatie van ingekapselde bacteri. 2012, Ghent University.
23. Wang, J., et al., Use of silica gel or polyurethane immobilized bacteria for self-healing concrete. Construction and Building Materials, 2012. **26**(1): p. 532-540.
24. Ferrara, L., et al., Experimental characterization of the self-healing capacity of cement based materials and its effects on the material performance: A state of the art report by COST Action SARCOS WG2. Construction and Building Materials, 2018. **167**: p. 115-142.
25. Achal, V., A. Mukerjee, and M. Sudhakara Reddy, Biogenic treatment improves the durability and remediates the cracks of concrete structures. Construction and Building Materials, 2013. **48**(Supplement C): p. 1-5.
26. Snoeck, D., et al., X-ray computed microtomography to study autogenous healing of cementitious materials promoted by superabsorbent polymers. Cement and Concrete Composites, 2016. **65**: p. 83-93.
27. Hilloulin, B., et al., Mechanical regains due to self-healing in cementitious materials: Experimental measurements and micro-mechanical model. Cement and Concrete Research, 2016. **80**: p. 21-32.
28. Gruyaert, E., et al., Self-healing mortar with pH-sensitive superabsorbent polymers: testing of the sealing efficiency by water flow tests. Smart Materials and Structures, 2016. **25**(8): p. 084007.
29. Ahn, E., et al., Principles and Applications of Ultrasonic-Based Nondestructive Methods for Self-Healing in Cementitious Materials. Materials, 2017. **10**(3): p. 278.

30. Van Tittelboom, K., et al., Acoustic emission analysis for the quantification of autonomous crack healing in concrete. Construction and Building Materials, 2012. **28**(1): p. 333-341.

31. Tsangouri, E., et al., Detecting the activation of a self-healing mechanism in concrete by acoustic emission and digital image correlation. The Scientific World Journal, 2013. **2013**.

32. Van Den Abeele, K., et al., Active and passive monitoring of the early hydration process in concrete using linear and nonlinear acoustics. Cement and Concrete Research, 2009. **39**(5): p. 426-432.

33. Garnier, V., et al., Acoustic techniques for concrete evaluation: Improvements, comparisons and consistency. Construction and Building Materials, 2013. **43**: p. 598-613.

34. Ait Ouarabi, M., et al., Ultrasonic Monitoring of the Interaction between Cement Matrix and Alkaline Silicate Solution in Self-Healing Systems. Materials, 2017. **10**(1): p. 46.

35. Aggelis, D. and T. Shiotani, Repair evaluation of concrete cracks using surface and through-transmission wave measurements. Cement and Concrete Composites, 2007. **29**(9): p. 700-711.

36. In, C.-W., et al., Monitoring and evaluation of self-healing in concrete using diffuse ultrasound. NDT & E International, 2013. **57**: p. 36-44.

37. Liu, S., et al., Evaluation of self-healing of internal cracks in biomimetic mortar using coda wave interferometry. Cement and Concrete Research, 2016. **83**: p. 70-78.

38. Hilloulin, B., et al., Monitoring of autogenous crack healing in cementitious materials by the nonlinear modulation of ultrasonic coda waves, 3D

microscopy and X-ray microtomography. Construction and Building Materials, 2016. **123**: p. 143-152.

39. Hilloulin, B., et al., Small crack detection in cementitious materials using nonlinear coda wave modulation. NDT & E International, 2014. **68**: p. 98-104.
40. Shah, A.A., Y. Ribakov, and S. Hirose, Nondestructive evaluation of damaged concrete using nonlinear ultrasonics. Materials & Design, 2009. **30**(3): p. 775-782.
41. Kim, G., et al., Drying shrinkage in concrete assessed by nonlinear ultrasound. Cement and Concrete Research, 2017. **92**: p. 16-20.
42. Popovics, S., J.L. Rose, and J.S. Popovics, The behaviour of ultrasonic pulses in concrete. Cement and Concrete Research, 1990. **20**(2): p. 259-270.
43. <cement mehta.pdf>.
44. Komlos, K., et al., Ultrasonic pulse velocity test of concrete properties as specified in various standards. Cement and Concrete Composites, 1996. **18**(5): p. 357-364.
45. Tsangouri, E., et al., Crack sealing and damage recovery monitoring of a concrete healing system using embedded piezoelectric transducers. Structural Health Monitoring, 2015. **14**(5): p. 462-474.
46. Karaiskos, G., et al., Monitoring of concrete structures using the ultrasonic pulse velocity method. Smart Materials and Structures, 2015. **24**(11): p. 113001.
47. WATANABE, T., et al., Evaluation Of Self Healing Effect In Fly-Ash Concrete By Ultrasonic Test Method. International Journal of Modern Physics B, 2011. **25**(31): p. 4307-4310.

48. Zhong, W. and W. Yao, Influence of damage degree on self-healing of concrete. Construction and building materials, 2008. **22**(6): p. 1137-1142.

49. Shiotani, T. and D.G. Aggelis, Wave propagation in cementitious material containing artificial distributed damage. Materials and Structures, 2009. **42**(3): p. 377-384.

50. Suaris, W. and V. Fernando, Detection of crack growth in concrete from ultrasonic intensity measurements. Materials and Structures, 1987. **20**(3): p. 214-220.

51. Barbero, E.J., F. Greco, and P. Lonetti, Continuum damage-healing mechanics with application to self-healing composites. International Journal of Damage Mechanics, 2005. **14**(1): p. 51-81.

52. Herbst, O. and S. Luding, Modeling particulate self-healing materials and application to uni-axial compression. International journal of fracture, 2008. **154**(1-2): p. 87-103.

53. Zemskov, S.V., H.M. Jonkers, and F.J. Vermolen, A mathematical model for bacterial self-healing of cracks in concrete. Journal of Intelligent Material Systems and Structures, 2014. **25**(1): p. 4-12.

54. Zemskov, S.V., H.M. Jonkers, and F.J. Vermolen, Two analytical models for the probability characteristics of a crack hitting encapsulated particles: Application to self-healing materials. Computational materials science, 2011. **50**(12): p. 3323-3333.

55. Gheduzzi, S., et al., Numerical and experimental simulation of the effect of long bone fracture healing stages on ultrasound transmission across an idealized fracture. The Journal of the Acoustical Society of America, 2009. **126**(2): p. 887-894.

56. Schroeder, C.T. and W.R. Scott Jr. Finite-difference time-domain model for elastic waves in the ground. in Proceedings of the SPIE: 1999 Annual International Symposium on Aerospace/Defense Sensing, Simulation, and Controls. 1999.

57. Schroder, C. and W.R. Scott, On the stability of the FDTD algorithm for elastic media at a material interface. IEEE Transactions on geoscience and remote sensing, 2002. **40**(2): p. 474-481.

58. Lee, Y.H. and T. Oh, The Measurement of P-, S-, and R-Wave Velocities to Evaluate the Condition of Reinforced and Prestressed Concrete Slabs. Advances in Materials Science and Engineering, 2016. **2016**.

59. Sangadji, S., Porous Network Concrete: a bio-inspired building component to make concrete structures self-healing. 2015.

60. Sharma, S. and A. Mukherjee, Ultrasonic guided waves for monitoring the setting process of concretes with varying workabilities. Construction and Building Materials, 2014. **72**: p. 358-366.

61. Sharma, S. and A. Mukherjee, Monitoring freshly poured concrete using ultrasonic waves guided through reinforcing bars. Cement & Concrete Composites, 2015. **55**: p. 337-347.

Chapter 4 Healing Fine Cracks in Concrete with Bacterial Cement for an Advanced Non-destructive Monitoring

Nimrat Pal Kaur, Subhra Majhi, Navdeep Kaur Dhami and Abhijit Mukherjee
School of Civil and Mechanical Engineering, Curtin University, WA 6102, Australia

Abstract

Cracks in concrete are inevitable and they can adversely affect the service life of structures. An efficient method to heal the cracks coupled with a reliable monitoring technique is of paramount importance. Standard crack healing materials are unable to penetrate thin cracks (1). This paper presents an experimental demonstration of healing of fine cracks of around 0.6 mm using the bacterial based healing technique. Simultaneously, the evidence and efficiency of bacterial healing is investigated using advanced monitoring techniques. Ultrasonic signals passing through the healing area have been recorded and the waveform has been studied to interpret the condition of the crack. It has been validated through a series of water-tightness tests. The bacterial technique was able to heal the crack to the extent that no water was seen to permeate through the crack. The evidence of bacterial healing was confirmed through scanning electron microscopy and X-ray dispersion spectrum. It was found that the ultrasonic technique is able to monitor the progression of healing.

Keywords: concrete; ultrasonic monitoring; healing; bacteria; calcium carbonate precipitation

1. Introduction

Concrete is the most widely used construction material throughout the world. However, a major concern is its susceptibility to damage in the form of cracking that can occur due to thermal stress, creep, drying shrinkage, or general loading under serviceability conditions. Cracks provide pathways for migration of fluids and aggressive chemicals that may trigger corrosion of embedded steel. As the crack formation is unavoidable during structure's service life, crack healing is necessary. Crack healing is a phenomenon in which chemical or physical processes result in formation of solid products inside the crack, thereby blocking the pathway for ingress of aggressive agents. In general, concrete is observed to have a natural ability to autogenously heal cracks of a certain extent, of around ~50μm width (2, 3) by hydration of unhydrated cement particles in presence of water (4, 5). However, this is not enough for most damages and external assistance for healing is warranted. Success of healing is influenced by three aspects: the healing material for filling the cracks; the delivery system for transporting healing material inside the crack; and the monitoring technique to ensure healing (6, 7). Figure 4.1 illustrates a paradigm for healing structures. The non-destructive monitoring system identifies damage in the structure and informs the controller to trigger the healing system. The non-destructive system monitors the extent of healing achieved. It asks the controller to stop the healing when the target is reached.

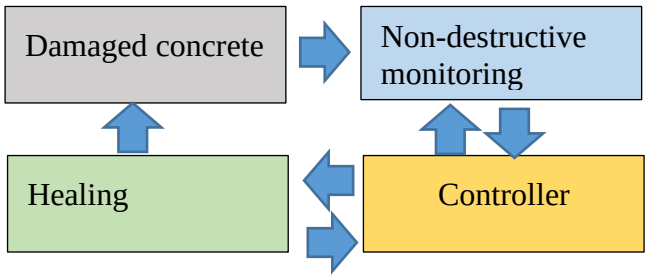

Figure 4.1: The healing-monitoring loop

The healing material can be based on cement or resins. The key factor of healing material is its ability to flow into the cracks and solidify to prevent moisture ingress. We have reported methods of healing with cement grout (1). It was noted that although cement grout was effective in filling relatively wide cracks of width of a few millimetres, it was unable to penetrate fine cracks of width less than a millimetre. A system of healing for fine cracks and pores is essential to prevent deterioration of concrete. Recently, bacteria-based system, also known as biocementation has been proposed for healing of concrete cracks. Biocementation is a process in which naturally occurring microorganisms such as bacteria, through their metabolic activities are able to precipitate calcium carbonate at the cracked zone, thus preventing harmful substances.

Several bacterial species are known to precipitate calcium carbonate through different metabolic routes (8-10). Owing to the high alkalinity of concrete the alkaliphilic strains (Bacillus group) are expected to function in concrete environment. For crack remediation enzymatic hydrolysis of urea is popular because of its high urease activity. Bacteria produce an enzyme, urease, which catalyses the hydrolysis of urea into ammonium (NH_4^+) and carbonate ions (CO_3^{2-}). At this point, when calcium ions are added, calcium carbonate is formed (11, 12).

There are several methods of applying material to repair the crack (Figure 4.2). It can be applied externally on the crack (13, 14) or it can be positioned inside concrete and activated at the occurrence of damage (9, 15). Pre-existing cracks necessitate manual repair but in case of intrinsic healing, the healing system must be placed inside concrete at the time of construction. For intrinsic healing, the material can be dispersed in the concrete matrix in capsules (Figure 4.2b) (16-18). Polyurethane or silica gel (17, 18), hydrogel (19), and expanded clay (3) have been used for encapsulation. A

vascular system where the healing fluid is delivered at the point of damage through capillaries or hollow channels has also been reported (Figure 4.2c) (9, 20, 21).

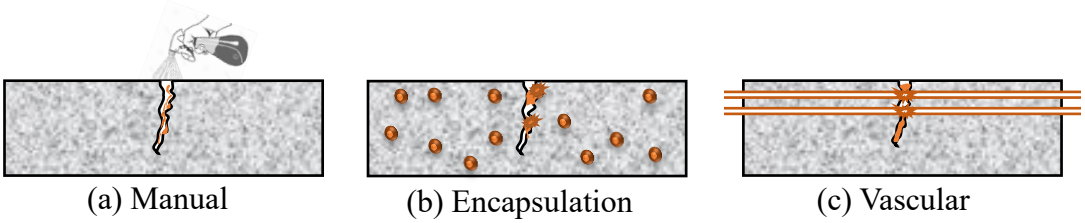

Figure 4.2: Methods of applying healing material

Apart from healing material and its transport mechanism, a reliable evaluation technique to monitor healing is of paramount importance. An account of the evaluation techniques is available in (6) and (22). Microstructural analysis through Scanning Electron Microscopy (SEM), Energy Dispersive Spectroscopy (EDS), X-ray diffraction (9, 10, 23-28) or X-ray computed tomography (29) have been reported. The sealing of the damages have been examined by the sorptivity (30, 31) and permeability tests (27, 28, 32). The mechanical properties can be analysed through strength tests (33). However, these techniques cannot be adopted in the continuous non-destructive monitoring scheme as shown in **Error! Reference source not found.**. Wave based t echnologies are more suitable for continuous monitoring. Two such techniques are acoustic emission (34-38) and ultrasonic waves (22). While acoustic emission technique may be able to detect the damage it is not capable of monitoring healing. Ultrasonic technique has both these capabilities. The monitoring can be performed by measuring a number of ultrasonic parameters. Ultrasonic pulse velocity (UPV) measurement is based on the time of flight and the simplest one to measure (20, 39). However, UPV is not found to be very sensitive to cracks. In our previous work,

ultrasonic pulse attenuation was found to be more effective in monitoring healing (1). However, pulse amplitude can vary with other parameters such as the extent of coupling achieved. The frequency content of the signal can be analysed to obtain deeper insights. Waveform analysis in various flavours such as surface-wave transmission (40); ultrasound diffusivity (41); non-linear ultrasonics (38); coda wave interferometry (42-44) and more recently, direct wave interferometry (45) have been reported. A more recent technique based on Short Time Fourier Transform (STFT) retains both time and frequency information (46). This technique has not been applied hitherto in monitoring of concrete.

This paper explores several advancements over our previously reported research. We attempt to heal cracks that could not be repaired by cement grout by a bacterial cement. The healing process is monitored in a number of ways: 1) visual, 2) chemical, 3) mechanical and 4) hydraulic. The state of the crack is monitored through successive visual imaging. Through chemical mass balance relationships, the rate of deposition of calcium carbonate is estimated. The ultrasonic pulse method is used to inspect the progress of healing. The ultrasonic signal has been processed further using an advanced STFT technique to obtain a nuanced observation of the crack healing process. Simultaneously, the hydraulic flow through the crack is monitored to estimate the degree of sealing achieved by the healing treatment. At the termination of the healing treatment, Scanning Electron Microscopy (SEM) coupled with Energy Dispersive X-ray Spectroscopy (EDS) spectrum has been performed to ensure that calcium carbonate has indeed filled the cracks.

2. Experimental program

2.1 Preparation of test specimens and damage introduction

Concrete slab specimens of size 500mm (length) x 250mm (width) x 150mm (height) with an embedded plain mild steel bar 24 mm diameter were cast as shown Figure 4.3a. The bar was protruded by 200mm on both sides for easy handling of the specimen. Ordinary Portland cement, fine aggregates (medium-sized natural/river sand) and coarse aggregates with nominal size of 10 mm was used in concrete. The ratio of cement: sand: coarse aggregate was 1: 1.6: 3.4 and water to cement ratio was 0.5. The specimens were demoulded after 24 hours of casting and moist cured for 28 days. The resulting strength of concrete after 28 days was 41 MPa.

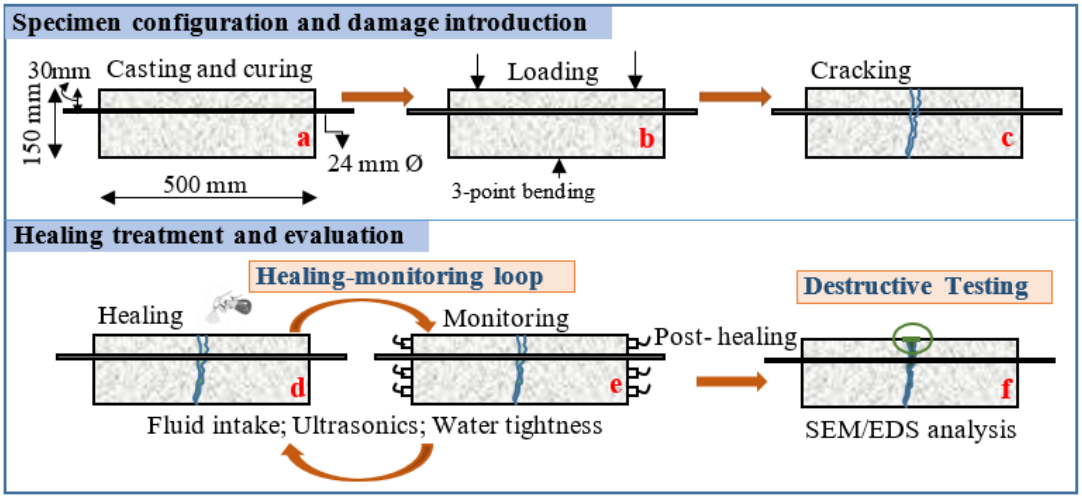

Figure 4.3: Layout of experimental plan (front view)

For evaluating healing response, damage was induced on the specimen. The slab specimens were loaded in three-point bending configuration as shown in Figure 4.3b, resulting in the formation of a crack in the middle of the slab as shown in Figure 4.3c. The stress in the reinforcement was well within its yield limit. Loading was stopped, on appearance of a visible crack. Due to the elastic recovery of the reinforcement after removing the load, the crack width reduced considerably. After unloading, crack width

was measured at different locations along the crack length using a crack measuring scale. The crack width was in the range 0.5 – 0.7 mm.

It is evident that a crack produced by three- or four-point bending has a width that varies along its depth. The crack being widest at its mouth and narrowing towards the tip. These bending cracks are generally discovered beams and plate elements. [6].

2.2 Bacteria-based healing treatment for cracks

After crack formation, the specimens were subjected to the healing treatment. The crack was in the face-up position. The bacteria-based healing treatment comprised of two components: bacterial fluid and cementing fluid. The precipitation of calcium carbonate ($CaCO_3$) results from the combination of carbonate ions (CO_3^{2-}) from the hydrolysis of urea ($CO(NH_2)_2$) and the calcium ion (Ca^{2+}) supplied in the cementing solution, as described in the following chemical reactions:

$$CO(NH_2)_2 + 2H_2O \xrightarrow{\text{Bacterial urease}} 2NH_4^+ + CO_3^{2-} \quad (4.1)$$

$$Ca^{2+} + CO_3^{2-} \rightarrow CaCO_3 \quad (4.2)$$

From reactions (4.1) and (4.2), the amount of hydrolysed urea provides an indirect estimation of calcium carbonate deposit. One mol of urea gets converted to two mol of ammonia and one mol carbonate ions. Thus, the amount of calcium supplied gives an indirect measure of calcium carbonate deposit. In our previous publication, the consumption of urea and calcium was investigated. It was noticed that equal amounts of urea and calcium were utilised to precipitate calcium carbonate (47, 48).

Sporosarcina Pasteurii (ATCC® 11859™) was used due to its high urease activity and popularity in remediation of concrete (49). The medium for culturing comprised of ammonium sulphate $(NH_4)_2SO_4$, yeast extract, and Tris buffer (pH=9) (47, 50). All liquid media were sterilized by autoclaving for 20 min at 121°C. The bacterial culture was incubated aerobically at 35°C for 24 hours and shaken at 250 rpm. Growth of

bacterial culture was checked regularly by measuring the optical density (OD) at 600nm with spectrophotometer. The average OD value was 1.2. Cementing fluid was prepared by dissolving equimolar urea and calcium chloride at 0.5M concentration in distilled water.

The treatment was performed at room temperature of 25± 1° C. The sealing was attempted through periodic pouring of the healing fluid on the surface of the crack. First, 20 ml bacterial fluid was poured into the crack and allowed to rest, followed by 20 ml cementing fluid. The cementing fluid was poured twice a day for three days. Bacterial fluid was replenished at an interval of three days. This cycle was repeated until the monitoring system reported that the target healing is achieved.

2.3 Ultrasonic investigation

Ultrasonic technique was used for recording pulse transmission through the crack at designated points. The experimental set-up for ultrasonic data acquisition is presented in Figure 4.4**Error! Reference source not found.**.

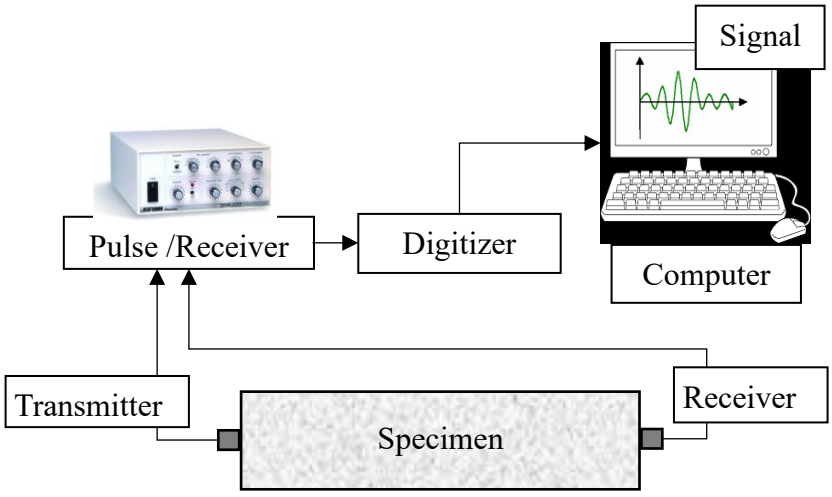

Figure 4.4: Set-up for ultrasonic data acquisition

In this method, the transmitter and the receiver were placed on the opposite faces of the slab to measure the pulse transmitted through the crack. A pair of GC200-D25 Ultran piezoelectric transducers of diameter 25mm with central frequency 200 kHz at

were used to generate compressional waves. The transducers were attached to a JSR DPR 300 pulser-receiver system to generate a pulse at 40dB. The received signal was digitized using Pico Scope 6 version 6.4.64.0 and a modular oscilloscope.

For recording the ultrasonic signals, transmitting and receiving points were marked on the specimen as shown in Figure 4.5. Two sets of points at the two sides of the slab were chosen. To avoid edge effects, the transducers were placed away from the edges of the slab. The surface of concrete was cleaned, and a petroleum based greased coupling agent was used to securely attach the transducers to the concrete surface. All readings were taken by the same persons and repeated at least three times for each measuring point (Figure 4.5). It was observed that the readings were consistent and repeatable.

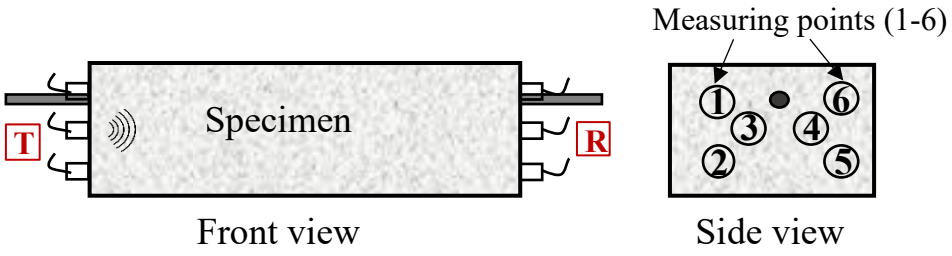

Figure 4.5: Specimen showing placement of transducers at different locations

2.4 Watertightness Test

Water permeability measurements were performed onto the crack at regular intervals while the healing treatment was on. To saturate the specimen, water was poured on it until water freely drips from the specimen. A 100ml measuring cylinder was adhesively attached on the top of the cracked surface of the specimen. The cylinder was filled with water. It was made sure that no water leaks through the adhesive joint. The level of water was observed at regular intervals. The test was performed at different locations of the crack. The flow rate was calculated based on the time taken

for 10 ml of water to drain. Each test was conducted three times. The test was terminated when the flow was below measurement least count.

2.5 Microstructural analysis

After completing the healing treatment, a slice was carefully cut from the specimen that includes the area of the crack. The slice was prepared for examination using scanning electron microscope (SEM). The material deposited in the crack was imaged. Moreover, an EDS analysis was performed to create an elemental map of the deposited material.

3. Results and discussion

The healing has been monitored by a number of means. The extent of healing has been measured by the quantity of calcium carbonate deposition. Simultaneously, the water flow through the crack has been measured.

3.1 Visual monitoring

The width of the crack has been measured at every 10 mm along the crack once in seven days throughout the period of healing. Figure 4.6 shows the initial and the healed crack. Clearly, it can be seen that the crack has been sealed.

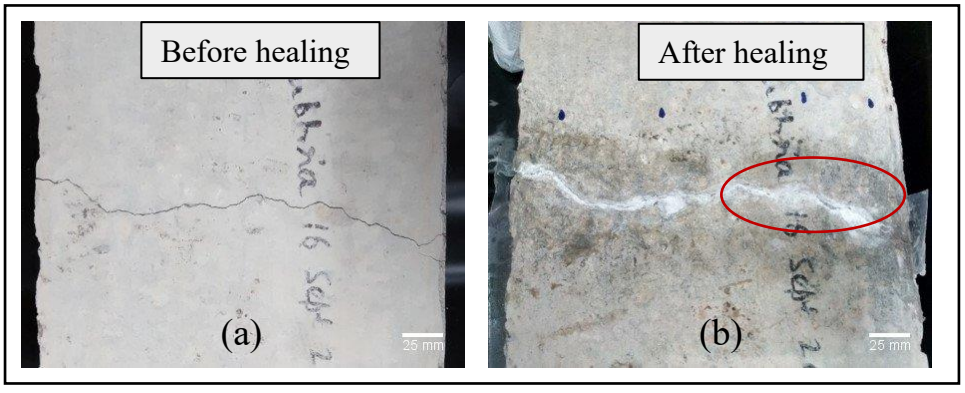

Figure 4.6: Visible calcite deposition seen on the surface post healing

The area marked in red in Figure 4.6b is seen in close up in Figure 4.7. The healing was considered 100% when the flow through the crack was below measurement level. Time for the treatment was 40 days. The amount of calcium carbonate deposited at that time was considered to be 100%. The healing at the intermediate stages were calibrated against the final amount of deposition as shown in Figure 4.7. and Figure 4.8.

The measured crack widths have been indicated in Figure 4.7a. It is seen that even at 73% healing, the crack at the surface is open although other measurements indicated that healing has been happening. This result indicates that the deposition has happened inside the crack first before the surface was sealed. From this point, deposition started appearing at the surface of the crack.Figure 4.7b shows the crack at 83% healing. Clearly, the crack mouth has been partially sealed, but it is still open at most locations. At 91% healing, most of crack mouth is sealed (Figure 4.7c). Finally, the entire crack was covered with calcium carbonate as seen in Figure 4.7d and no water could pass through the crack. It can be concluded that continuous microbial activity resulted in precipitation inside the crack finally reaching the surface. The bacterial treatment resulted in the depositions of calcium carbonate that could cover the entire crack.

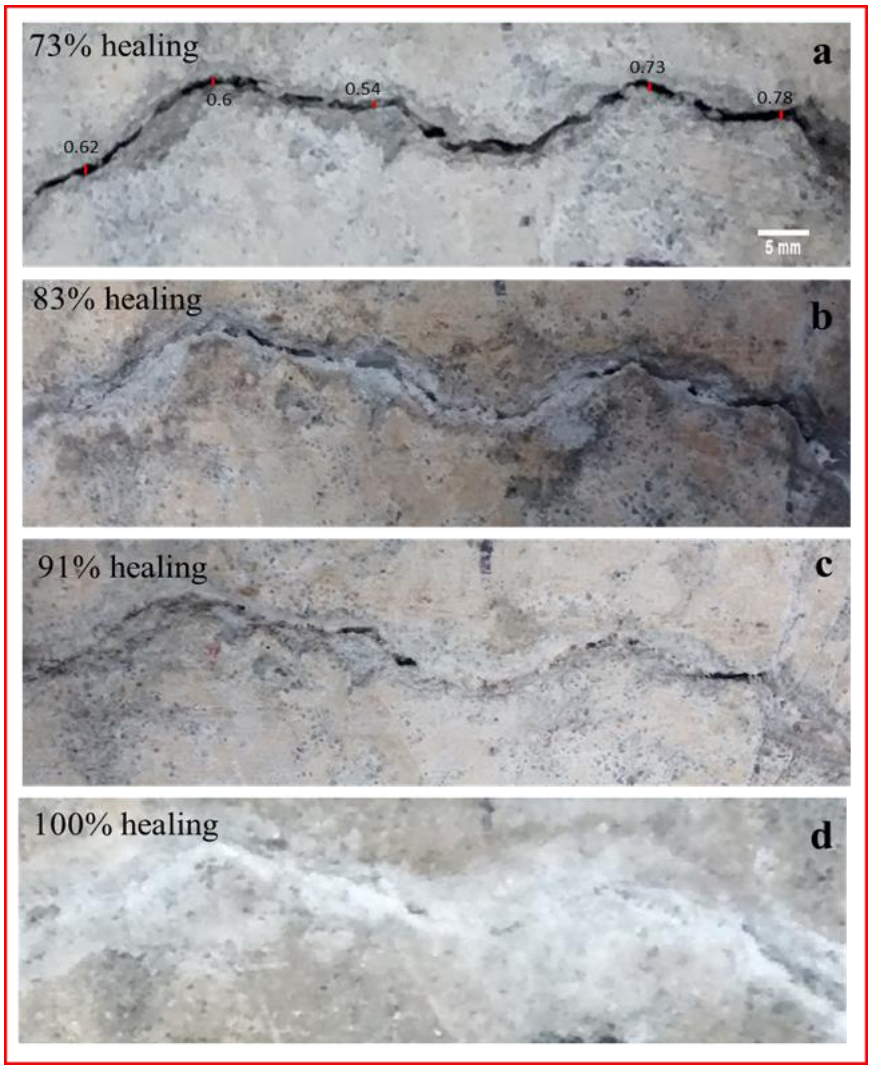

Figure 4.7: Visual observations of the crack at different stages of deposition (Note: these are the close-up images of the portion of the crack marked red in Figure 4.6b)

3.2 Chemical monitoring

The amount of cementation solution poured on the crack for each batch was recorded. As the crack gets filled, the volume of cementation fluid that can enter the crack is reduced. Figure 4.8 presents the distribution of both healing fluid and the accumulated volume of calcium carbonate at different stages of healing. Until 48% healing, 40 ml of solution could be absorbed by the crack. During this time, the calcium carbonate deposit builds up linearly. Beyond this period, the capacity of the crack to absorb the fluid reduced gradually. In the end, only 8 ml of fluid could be absorbed. As the

volume of cementation fluid was reduced, the rate of deposition of calcium carbonate also reduces. The total volume of calcium carbonate inside the crack is estimated to be between 20 and 25 cc, which is comparable with the volume of the crack. Comparing Figure 4.7 and Figure 4.8 it can be seen that even when 73% of the crack is filled, there is marginal deposit at the crack mouth. The final 25% deposition achieves the sealing of the crack.

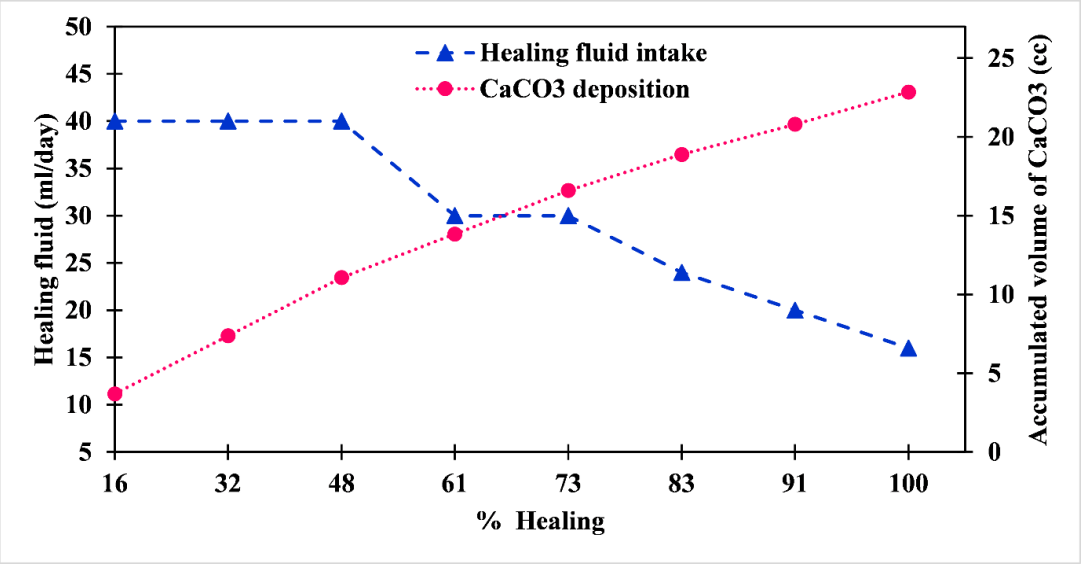

Figure 4.8: Rise in volume of calcium carbonate and reduction in healing fluid with healing progression.

3.3 Microstructural study

After the healing was completed, samples were collected from the surface of the healed area for microstructural analysis. Calcite crystals were clearly visible inside the crack in SEM images. It is noticed from Figure 4.9a, that bacterial treatment resulted in prominent presence of crystalline deposits. In addition, the elemental composition of minerals was also analysed by EDS. The presence of peaks of calcium, carbon and oxygen Figure 4.9b) confirmed calcium carbonate as the precipitation within the cracks.

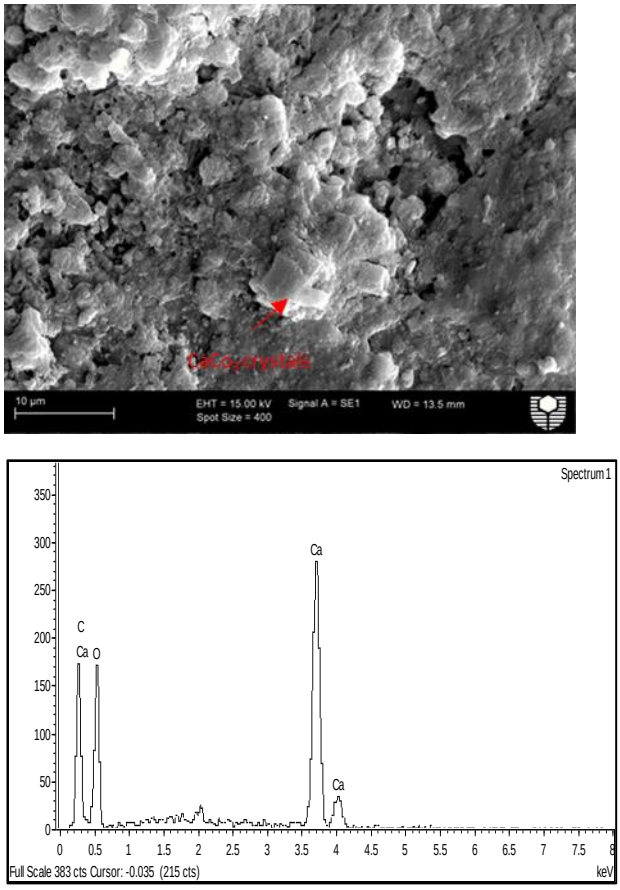

Figure 4.9: (a) SEM images of the precipitates after healing treatment (b) EDS analysis of the crystals.

3.4 Ultrasonic tests

3.4.1 Waveform analysis

Figure 4.10 presents the recorded waveforms of the uncracked specimen along with that at different healing stages for points marked 1 to 6 on the specimen (Figure 4.5). The variation of amplitude (y-axis) with time (x-axis) of the transmitted pulse is observed. It is noted that there was a significant drop in signal amplitude due to cracking. A consistent pattern of recovery was observed with the progression of healing. The signal amplitude increased considerably at all the locations. In the end, the signal at all the locations was very close to that before cracking. However, points 1, 2 and 3 show higher initial amplitudes (corresponding to 0% healing) as compared

to points 4, 5 and 6. It may be recalled that the crack was created by bending the slab. As the load was withdrawn there was considerable recovery and the width of the crack went down. Therefore, it is likely that there is internal contact between the crack faces on the left side of the slab while the right side is not in contact. Thus, the wave would travel with less resistance through points 1, 2 and 3 while at points 4, 5 and 6 it encounters separation of the crack faces.

With the progress of healing the signal amplitudes at all points have shown an increasing trend. This is because the acoustic barrier has come down as the cement is deposited inside the crack bringing the faces closer. Thus, the wave would now travel with less resistance through the closed crack. The signal amplitudes can vary subject to the local condition therefore it is seen that the signal amplitudes are slightly higher for some healed specimens as compared to uncracked specimens. Thus, ultrasonic pulse transmission is a reliable method for monitoring healing with biocement. The signal amplitude at points 1, 2 and 3 are consistently higher than that in points 4, 5 and 6. At 100% healing, the signal amplitude at 1, 2 and 3 reached 2V. While at points 4, 5 and 6 it remained in around 1V. It shows that although biocement has filled the crack the acoustic mismatch between the parent concrete and cement is not completely removed. However, a clear trend of significant increase in signal amplitude was noticed with the progress of healing in all cases. Thus, it is possible to calibrate the signal amplitude with the extent of healing using the initial amplitude of the corresponding point as baseline.

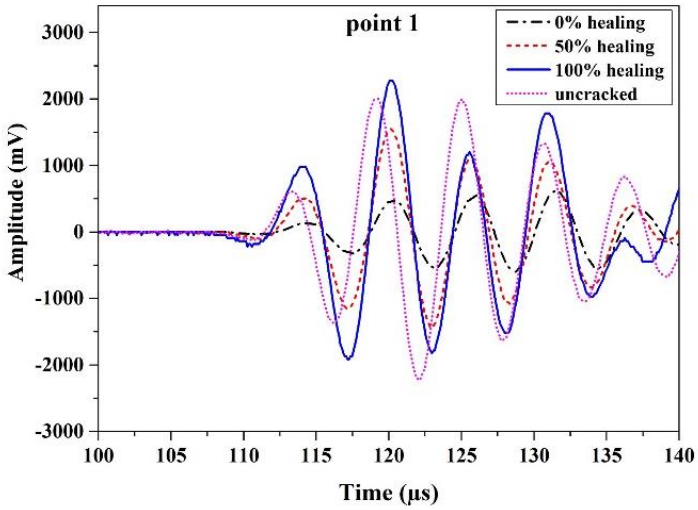
point 1
0% healing
50% healing
100% healing
uncracked
Amplitude (mV)
Time (μs)

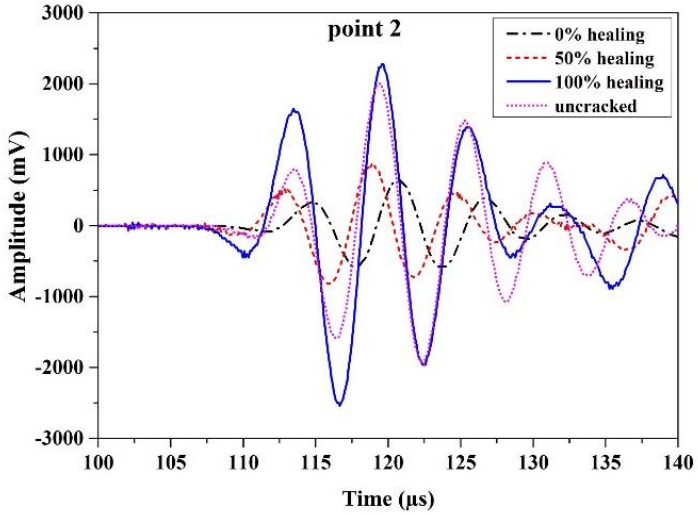
point 2
0% healing
50% healing
100% healing
uncracked
Amplitude (mV)
Time (μs)

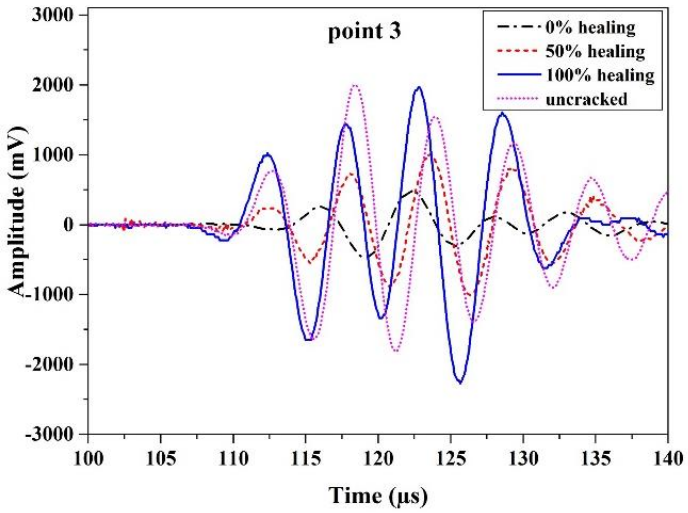
point 3
0% healing
50% healing
100% healing
uncracked
Amplitude (mV)
Time (μs)

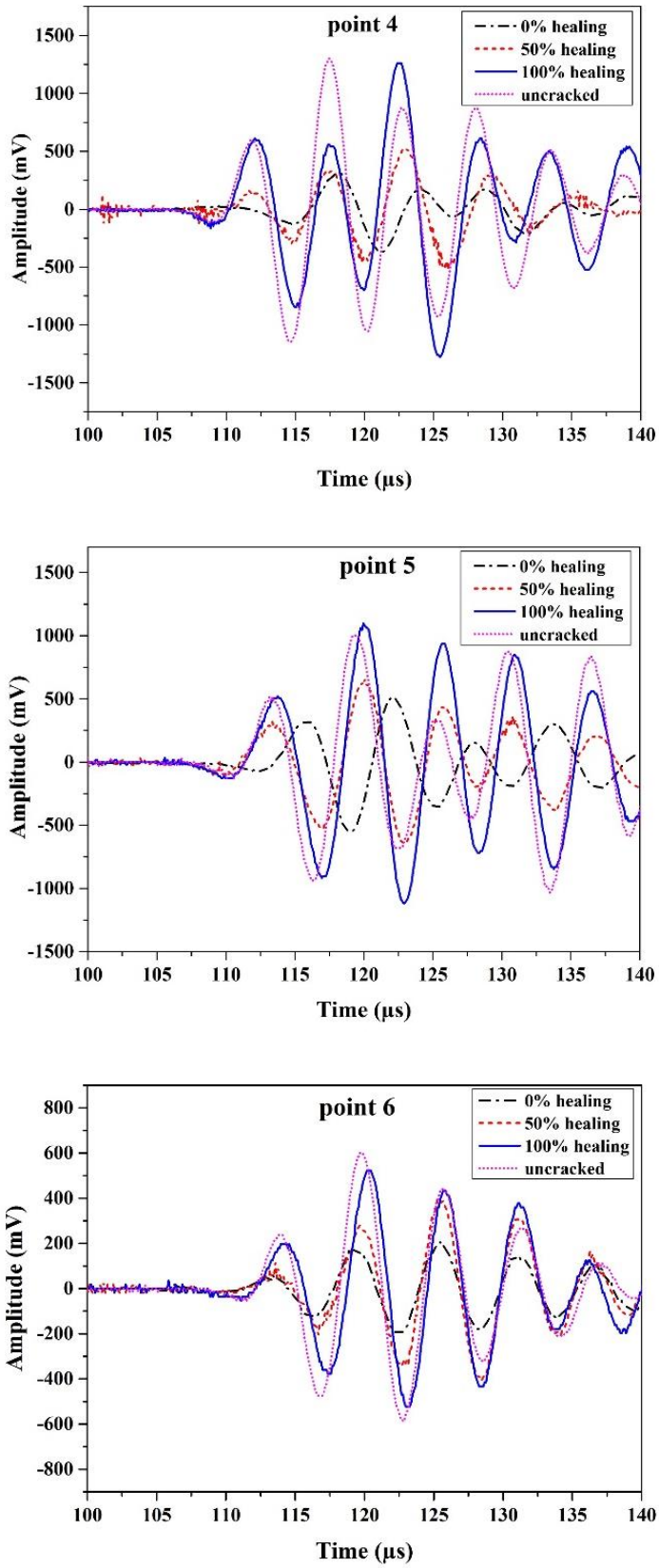

Figure 4.10: Recorded waveforms at different healing stages

The pulse velocities and the ratio of amplitudes between healed and uncracked signals have been presented in Figure 4.11. The velocity did not change appreciably due to cracking and healing. It was also noticed in our previous investigation (1). As the crack is thin, the crack faces often form irregular contacts letting some energy to pass through but most of the energy is reflected. Thus, there has been significant variation in the amplitude ratios. The ratio fell dramatically from 1 to 0.2 due to cracking. However, it recovered consistently with healing. At the end of the treatment the amplitude ratio was very close to that of uncracked specimen, confirming that healing has indeed been achieved. Thus, further results have been presented using the signal amplitude only.

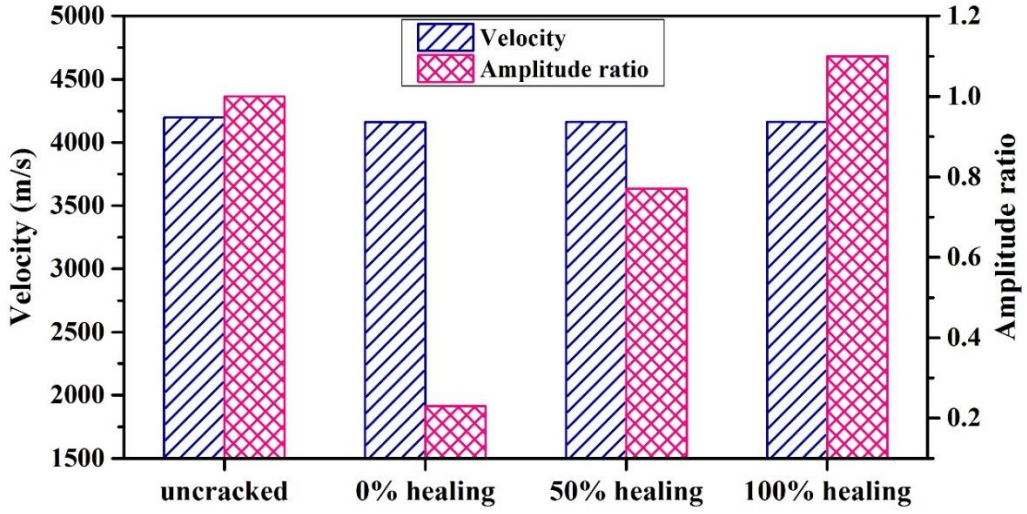

Figure 4.11: Velocity and amplitude ratio for point 1 measured at different healing percentage

It is noticed earlier that the signal amplitudes can vary subject to the local condition and there is internal contact between the crack faces Thus, the signal amplitudes have been plotted in Figure 4.12 as ratios of the initial values. It can be seen that all

amplitudes went up with healing. At the final stage, the amplitude ratio varied between 3 and 5. This is considerable signal amplification; thus, it would be possible to calibrate the extent of healing with the amplitude ratios. Comparing Figure 4.10 and Figure 4.12 it can be seen that the relative gain is lower at points where the initial amplitude is relatively high, for example points 2 and 3. These points were possibly in contact right from the beginning. Thus, healing did not change the signal amplitude considerably, however, the amplitude ratios at points with lower initial amplitude did gain considerably.

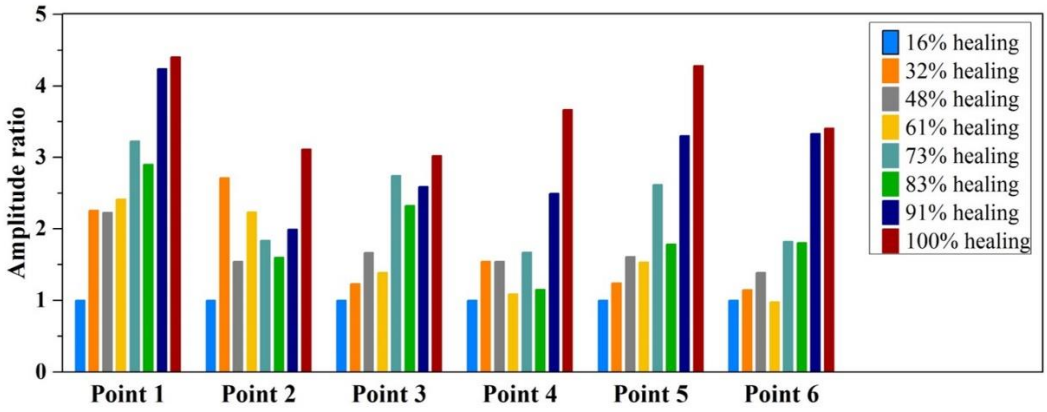

Figure 4.12: Amplitude ratios at different stages of healing

3.4.2 Time-Frequency Analysis

In the above methods, the time component of the signal is viewed. Fundamental observations about the changes in the system can be made by noting the frequency spectra of the signals. In a more advanced analysis, the frequency spectra at different time windows are obtained to observe the variations of frequency spectra with time. A technique called S-Transform is adopted here. It consists of convoluting a time delayed window with the time signal while performing a Fourier Transform. S-Transforms can be considered as an improved version of Short Time Fourier Transform (STFT) where the windowed function is Gaussian. This Gaussian function

is varied in proportion to the frequency contents of interest (46). Our previous publication contains a detailed account of the method (51).

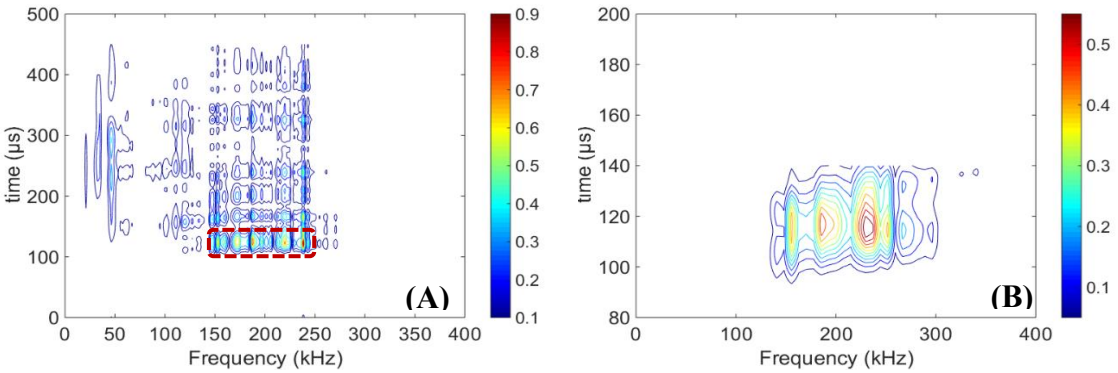

Figure 4.13: (a) Typical time-frequency spectra of the received signal for point 1 (b) spectral contour corresponding to the window (marked in red).

The time frequency spectral plot for a typical signal for point 1 is presented in Figure 4.13. The plot depicts the relative intensities of the signal at different times and corresponding to the frequencies. It can be seen that the signal intensity is concentrated at 100-140µs with a frequency of 150-300 kHz. Therefore, all other components are negligible. A zoomed view of the time-frequency window is presented in Figure 4.13b. The aggregate signal intensity in this region is estimated by integrating the signal intensity over the selected time-frequency window. These values are plotted in Figure 4.14 for all six points with advancing healing. It can be seen that all the points show an increase in signal intensity at an exponential rate. An exponential curve has been fitted through the data points:

$$I = I_0 h^n \qquad (4.3)$$

Where I is the signal intensity; I_0 is the initial signal intensity; h is the percentage of healing; and n is the exponent of healing. It may be noted that I_0 depends on the initial damage state. While n is the measure of the rate of healing. The values of n are tabulated for the six points in Table 1. The healing rates are in the range of 0.3 and

0.4. The average *n* for Points 1, 2 and 3 is lower than that for points 4, 5 and 6. It may be recalled that Points 1, 2 and 3 are from the area of the beam where the initial signal was stronger indicating relatively sound condition in comparison to Points 4, 5 and 6. Thus, the area corresponding to Points 4, 5 and 6 has healed relatively at a higher rate. From this investigation we can conclude that S-Transform is a reliable measure of healing of cracks in concrete. Eqn. 4.3 can be used to calibrate the non-destructive parameter, ultrasonic signal intensity, with the healing achieved.

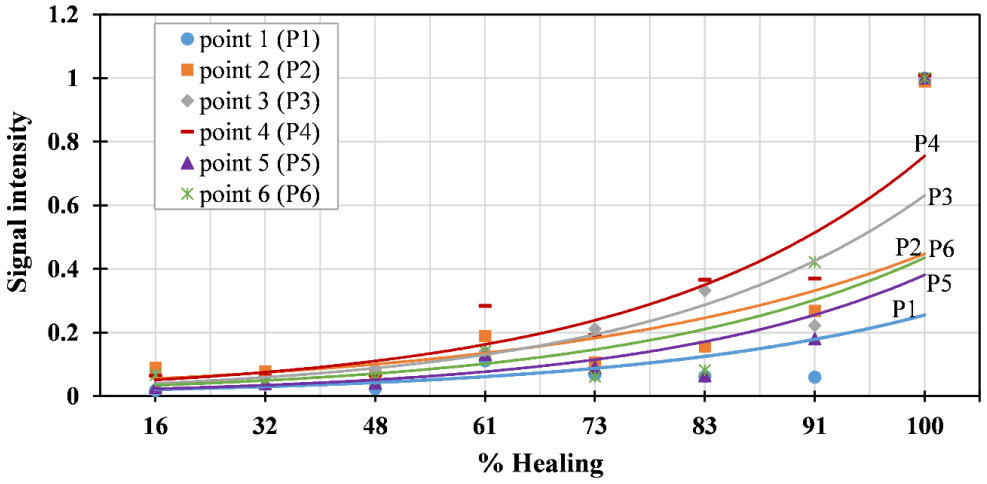

Figure 4.14: Plot of values corresponding to spectral contour at different healing stages

Table 1: Healing rate for all points

Healing rate (*n*)	Point 1	Point 2	Point 3	Point 4	Point 5	Point 6
	0.355	0.298	0.392	0.334	0.399	0.362
Average (n)	0.348			0.365		

3.5 Water tightness tests

Regain in water tightness is another important aspect for evaluating crack closure. This test consists of measuring the water flow through the cracked specimen during the progression of healing. Water flow was measured at different locations marked A, B, C, and D along the surface of the crack as shown in Figure 4.15.

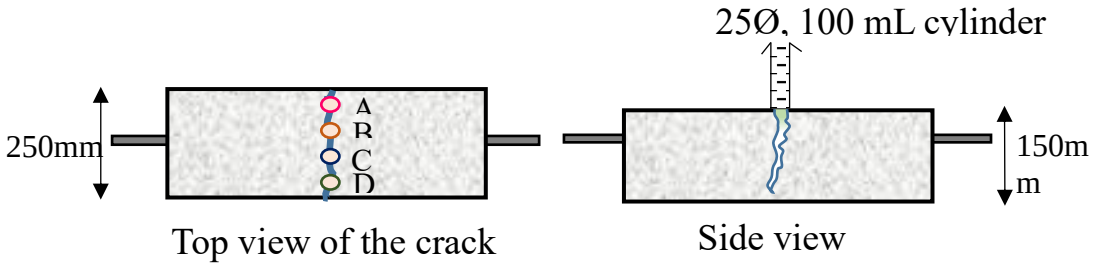

Figure 4.15: Locations and set-up for water flow test.

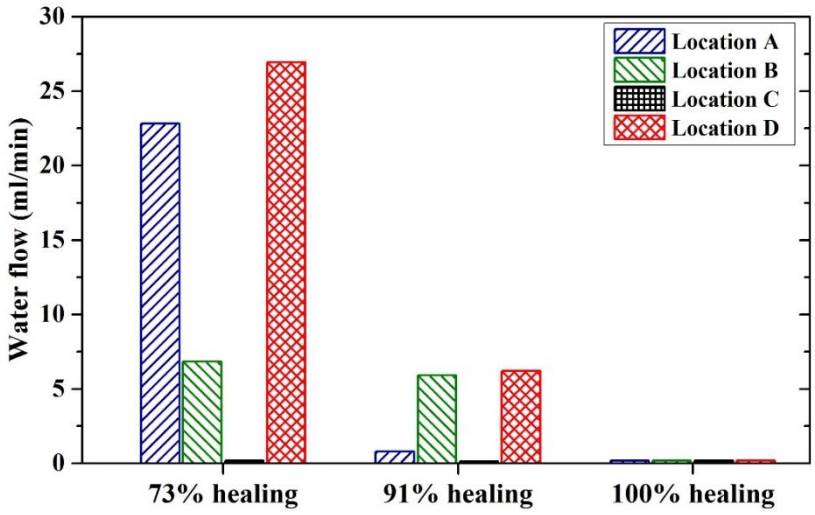

Figure 4.16: Water flow through different locations of the crack

Figure 4.16 presents the water flow for the locations marked on the specimen. Initially, as expected, the water flows freely through the crack. However, with the evolution of healing, decrease in water flow through the crack was observed. The initial reduction in water flow was negligible. This is expected, as biocement fills the crack in layers and until a substantial thickness is built up, the gap between the crack faces does not close. After 73% healing, significant recovery in water tightness was seen for locations B and C as compared to locations A and D. At 91% healing, the flow was negligible at all the four points. The evidence of near closure of the crack was obtained. At 100% healing, complete recovery in water tightness could be seen as there was no

measurable flow through the crack. These observations support well with Figure 4.7, in which visible deposition could be seen on the cracked surface at different stages of healing.

4. Conclusions

This paper demonstrates the performance of bacterial healing system for healing cracks of around 0.6 mm width that could not be filled with the conventional cement grout. In addition, a method of non-destructive monitoring ultrasonic technique, simultaneously as healing progresses has been reported. An advanced signal processing technique for calibrating healing with the ultrasonic records has been developed. The extent of healing has been validated with water tightness checks. Deposition of calcium carbonate inside the crack has been visualised.

It is observed that the bacterial treatment resulted in deposition of calcium carbonate inside the crack, possibly forming a layer on both the crack faces in each cycle. The crack was sealed when the layers from the opposite faces of the crack touched each other. Initially, there was no visual evidence of sealing of the crack, but finally there was abundant surface deposition. This demonstrates that the sealing starts from the crack tip reaching the crack mouth in the end.

Ultrasonic technique was capable of monitoring the progression of healing. The extent of healing is characterized by an increase in signal amplitude. Periodic monitoring of the transmitted pulse, throughout the healing period revealed that signal amplitude can be correlated with the extent of healing. It is noted that signal amplitude is more sensitive than pulse velocity that has been used hitherto.

The advanced S-Transform of the signal helped us to identify the time-frequency window that captures the change in the signal with healing. The signal intensity within that time window showed an exponential increase with the progress of healing. An exponential curve was fitted to the data to and calibrated to obtain the initial condition and the healing rate. It was noticed that the healing rate is in the range of 0.3 and 0.4 for all the points sampled. Thus, the present technique was found to be reliable and repeatable for evaluating healing. This information will be useful in future research on non-destructive monitoring of healing.

Ultrasonic results were augmented by water tightness and SEM/EDS analysis. It was noticed that the water tightness is achieved after a significant level is healing has taken place. Thus, water tightness of the sample would be a useful check for ensuring a high level of healing. Complete recovery in water tightness could be seen at around 90% healing. SEM/EDS analysis has confirmed the hypothesis that carbonate crystals are formed in layers on the crack faces. The crack is closed and water tightness is achieved when the layers from the opposite faces of the crack touch each other with no gaps left. At that instant, the crack is completely sealed.

Acknowledgements

The authors would like to acknowledge the contribution of Australian Government Research Training Program Scholarship in supporting this research. The authors also acknowledge the use of Curtin University's Microscopy & Microanalysis Facility, whose instrumentation has been partially funded by the University, State and Commonwealth Governments.

Conflicts of Interest

The authors declare that they have no conflict of interest.

References

1. Kaur NP, Shah JK, Majhi S, Mukherjee A. Healing and Simultaneous Ultrasonic Monitoring of Cracks in Concrete. Materials Today Communications. 2018.
2. Edvardsen C. Water permeability and autogenous healing of cracks in concrete. Materials Journal. 1999;96(4):448-54.
3. Palin D, Wiktor V, Jonkers HM. Autogenous healing of marine exposed concrete: Characterization and quantification through visual crack closure. Cement and Concrete Research. 2015;73:17-24.
4. Hearn N. Self-sealing, autogenous healing and continued hydration: what is the difference? Materials and structures. 1998;31(8):563.
5. Suleiman A, Nehdi M. Effect of environmental exposure on autogenous self-healing of cracked cement-based materials. Cement and Concrete Research. 2018.
6. Ferrara L, Van Mullem T, Alonso MC, Antonaci P, Borg RP, Cuenca E, et al. Experimental characterization of the self-healing capacity of cement based materials and its effects on the material performance: A state of the art report by COST Action SARCOS WG2. Construction and Building Materials. 2018;167:115-42.
7. Sangadji S. Porous Network Concrete: a bio-inspired building component to make concrete structures self-healing. 2015.
8. Wang J, Ersan YC, Boon N, De Belie N. Application of microorganisms in concrete: a promising sustainable strategy to improve concrete durability. Applied microbiology and biotechnology. 2016;100(7):2993-3007.
9. Souradeep G, Kua HW. Encapsulation technology and techniques in self-healing concrete. Journal of Materials in Civil Engineering. 2016;28(12):04016165.

10. Joshi S, Goyal S, Mukherjee A, Reddy MS. Microbial healing of cracks in concrete: a review. Journal of Industrial Microbiology & Biotechnology. 2017:1-15.
11. Castanier S, Le Métayer-Levrel G, Perthuisot J-P. Ca-carbonates precipitation and limestone genesis—the microbiogeologist point of view. Sedimentary geology. 1999;126(1-4):9-23.
12. Xu J, Wang X, Wang B. Biochemical process of ureolysis-based microbial CaCO 3 precipitation and its application in self-healing concrete. Applied microbiology and biotechnology. 2018;102(7):3121-32.
13. Choi S-G, Wang K, Wen Z, Chu J. Mortar crack repair using microbial induced calcite precipitation method. Cement and Concrete Composites. 2017;83:209-21.
14. Wiktor V, Jonkers H. Field performance of bacteria-based repair system: Pilot study in a parking garage. Case Studies in Construction Materials. 2015;2:11-7.
15. Sánchez M, Al-Tabbaa A, De Belie N, Ferrara L, Jefferson A, editors. Self-healing approaches for the preventive repair of concrete structures: SARCOS COST Action. 2nd International RILEM/COST Conference on Early Age Cracking and Serviceability in Cement-based Materials and Structures (EAC-02); 2017: RILEM Publications.
16. Wang K, Huang W, Lomboy G, Pei Y, QI Z. Silica Encapsulation Of Ureolytic Bacteria For Self-Healing Of Cement-Based Composites. US Patent App. 15/703,682; 2018.
17. Wang J, Van Tittelboom K, De Belie N, Verstraete W. Use of silica gel or polyurethane immobilized bacteria for self-healing concrete. Construction and Building Materials. 2012;26(1):532-40.

18. Van Belleghem B, Kessler S, Van den Heede P, Van Tittelboom K, De Belie N. Chloride induced reinforcement corrosion behavior in self-healing concrete with encapsulated polyurethane. Cement and Concrete Research. 2018;113:130-9.
19. Wang J, Snoeck D, Van Vlierberghe S, Verstraete W, De Belie N. Application of hydrogel encapsulated carbonate precipitating bacteria for approaching a realistic self-healing in concrete. Construction and building materials. 2014;68:110-9.
20. Huang H, Ye G, Shui Z. Feasibility of self-healing in cementitious materials–By using capsules or a vascular system? Construction and Building materials. 2014;63:108-18.
21. Minnebo P, Thierens G, De Valck G, Van Tittelboom K, De Belie N, Van Hemelrijck D, et al. A Novel Design of Autonomously Healed Concrete: Towards a Vascular Healing Network. Materials. 2017;10(1):49.
22. Ahn E, Kim H, Sim S-H, Shin SW, Shin M. Principles and Applications of Ultrasonic-Based Nondestructive Methods for Self-Healing in Cementitious Materials. Materials. 2017;10(3):278.
23. Khaliq W, Ehsan MB. Crack healing in concrete using various bio influenced self-healing techniques. Construction and Building Materials. 2016;102:349-57.
24. Ramachandran SK, Ramakrishnan V, Bang SS. Remediation of concrete using micro-organisms. ACI Materials Journal-American Concrete Institute. 2001;98(1):3-9.
25. Van Breugel K, editor Is there a market for self-healing cement-based materials. Proceedings of the First International Conference on Self-Healing Materials, Noordwijk, The Netherlands; 2007.
26. Van Tittelboom K, De Belie N, De Muynck W, Verstraete W. Use of bacteria to repair cracks in concrete. Cement and Concrete Research. 2010;40(1):157-66.

27. Achal V, Mukerjee A, Sudhakara Reddy M. Biogenic treatment improves the durability and remediates the cracks of concrete structures. Construction and Building Materials. 2013;48(Supplement C):1-5.
28. De Belie N, Wang J. Bacteria-based repair and self-healing of concrete. Journal of Sustainable Cement-Based Materials. 2016;5(1-2):35-56.
29. Wang J, Dewanckele J, Cnudde V, Van Vlierberghe S, Verstraete W, De Belie N. X-ray computed tomography proof of bacterial-based self-healing in concrete. Cement and Concrete Composites. 2014;53:289-304.
30. Alghamri R, Kanellopoulos A, Al-Tabbaa A. Impregnation and encapsulation of lightweight aggregates for self-healing concrete. Construction and Building Materials. 2016;124:910-21.
31. Achal V, Mukherjee A, Reddy MS. Microbial concrete: way to enhance the durability of building structures. Journal of materials in civil engineering. 2010;23(6):730-4.
32. Gruyaert E, Debbaut B, Snoeck D, Díaz P, Arizo A, Tziviloglou E, et al. Self-healing mortar with pH-sensitive superabsorbent polymers: testing of the sealing efficiency by water flow tests. Smart Materials and Structures. 2016;25(8):084007.
33. Hilloulin B, Hilloulin D, Grondin F, Loukili A, De Belie N. Mechanical regains due to self-healing in cementitious materials: Experimental measurements and micro-mechanical model. Cement and Concrete Research. 2016;80:21-32.
34. Van Tittelboom K, De Belie N, Lehmann F, Grosse CU. Acoustic emission analysis for the quantification of autonomous crack healing in concrete. Construction and Building Materials. 2012;28(1):333-41.

35. Tsangouri E, Aggelis D, Van Tittelboom K, De Belie N, Van Hemelrijck D. Detecting the activation of a self-healing mechanism in concrete by acoustic emission and digital image correlation. The Scientific World Journal. 2013;2013.
36. Van Den Abeele K, Desadeleer W, De Schutter G, Wevers M. Active and passive monitoring of the early hydration process in concrete using linear and nonlinear acoustics. Cement and Concrete Research. 2009;39(5):426-32.
37. Garnier V, Piwakowski B, Abraham O, Villain G, Payan C, Chaix JF. Acoustic techniques for concrete evaluation: Improvements, comparisons and consistency. Construction and Building Materials. 2013;43:598-613.
38. Ait Ouarabi M, Antonaci P, Boubenider F, Gliozzi A, Scalerandi M. Ultrasonic Monitoring of the Interaction between Cement Matrix and Alkaline Silicate Solution in Self-Healing Systems. Materials. 2017;10(1):46.
39. Karaiskos G, Deraemaeker A, Aggelis D, Van Hemelrijck D. Monitoring of concrete structures using the ultrasonic pulse velocity method. Smart Materials and Structures. 2015;24(11):113001.
40. Aggelis D, Shiotani T. Repair evaluation of concrete cracks using surface and through-transmission wave measurements. Cement and Concrete Composites. 2007;29(9):700-11.
41. In C-W, Holland RB, Kim J-Y, Kurtis KE, Kahn LF, Jacobs LJ. Monitoring and evaluation of self-healing in concrete using diffuse ultrasound. NDT & E International. 2013;57:36-44.
42. Liu S, Bundur ZB, Zhu J, Ferron RD. Evaluation of self-healing of internal cracks in biomimetic mortar using coda wave interferometry. Cement and Concrete Research. 2016;83:70-8.

43. Hilloulin B, Legland J-B, Lys E, Abraham O, Loukili A, Grondin F, et al. Monitoring of autogenous crack healing in cementitious materials by the nonlinear modulation of ultrasonic coda waves, 3D microscopy and X-ray microtomography. Construction and Building Materials. 2016;123:143-52.
44. Hilloulin B, Zhang Y, Abraham O, Loukili A, Grondin F, Durand O, et al. Small crack detection in cementitious materials using nonlinear coda wave modulation. NDT & E International. 2014;68:98-104.
45. Deraemaeker A, Dumoulin C. Embedding ultrasonic transducers in concrete: A lifelong monitoring technology. Construction and Building Materials. 2019;194:42-50.
46. Stockwell RG, Mansinha L, Lowe R. Localization of the complex spectrum: the S transform. IEEE transactions on signal processing. 1996;44(4):998-1001.
47. Porter H, Dhami NK, Mukherjee A. Synergistic chemical and microbial cementation for stabilization of aggregates. Cement and Concrete Composites. 2017;83:160-70.
48. Dhami NK, Reddy MS, Mukherjee A. Significant indicators for biomineralisation in sand of varying grain sizes. Construction and Building Materials. 2016;104:198-207.
49. Dhami NK, Reddy MS, Mukherjee A. Biomineralization of calcium carbonates and their engineered applications: a review. Frontiers in microbiology. 2013;4.
50. Wang J, De Belie N, Verstraete W. Diatomaceous earth as a protective vehicle for bacteria applied for self-healing concrete. Journal of industrial microbiology & biotechnology. 2012;39(4):567-77.

51. Majhi S, Mukherjee A, George N, Karaganov V. Corrosion Monitoring in Steel Bars using Laser Ultrasonic Guided Waves and Advanced Signal Processing. Structural Health Monitoring. 2018 Communicated.

Chapter 5 Performance of Different Calcium Sources on Bacterial Healing of Concrete

Nimrat Pal Kaur, Navdeep Kaur Dhami and Abhijit Mukherjee
School of Civil and Mechanical Engineering, Curtin University, WA 6102, Australia

Abstract

In concrete, cracks are unavoidable, and they may have a negative impact on the structure's service life. In a previous investigation, the authors have demonstrated healing of cracks with Microbially-induced calcium carbonate precipitation (MICP) with calcium chloride ($CaCl_2$) as the source of calcium. However, there is a concern that $CaCl_2$ may induce corrosion in the steel reinforcement bars. This paper is an attempt to assess the effect of calcium source on corrosion of bars during healing of cracks. Two different calcium sources, calcium chloride and calcium acetate, have been used. The healing performance with both sources has been reported. Various non-destructive parameters such as visual examinations, ultrasonics and water permeability tests were carried out to evaluate healing. Watertightness tests validated the extent of healing. Corrosion potential has been assessed with electro-chemical techniques as well as guided wave ultrasonics. After healing, the bars have been extracted to assess them destructively. It is noted that the electrochemical tests give somewhat misleading results due to the presence of electrolytes in the healing fluid. There is a good correlation between the ultrasonic transmission and corrosion.

1. Introduction

Cracks are one of the key factors that affect the service life of concrete because they provide pathways for aggressive agents to enter and cause corrosion of embedded steel bars. Corrosion is a form of damage which is often hidden until reaching a catastrophic failure. It is, therefore, essential to repair the cracks and promote healing at an early stage to enhance durability and increase service life of structures. Recently, the authors demonstrated a process of healing cracks through biocementation [1]. In the process of biocementation, naturally occurring bacteria and calcium-based nutrients combine to form calcium carbonate in the cracked zone, stopping harmful substances from entering that zone. Calcium carbonate is highly compatible with cement-based materials which makes it a promising and healing technique. Bio-cementation has demonstrated encouraging results in the healing of cracks because of its reaction time and lower viscosity [2-4].

Biocement consists of bacteria and a source of calcium. Inside the crack, bacteria convert the soluble calcium into an insoluble form causing sealing of the crack. Calcium carbonate is precipitated by several bacterial species via several metabolic pathways [5-7]. The alkaliphilic strains (Bacillus group) are known to work effectively for crack restoration because of the high alkalinity of concrete. Urease is a bacterial enzyme that catalyses the hydrolysis of urea to create ammonium (NH_4^+) and carbonate ions (CO_3^{2-}). The interaction of carbonate ions (CO_3^{2-}) produced by the hydrolysis of urea ($CO(NH_2)_2$) and the calcium ion (Ca^{2+}) provided in the cementing solution results in the precipitation of calcium carbonate ($CaCO_3$), as explained in the chemical processes below [8, 9]:

$$CO(NH_2)_2 + 2H_2O \xrightarrow{\text{Bacterial urease}} 2NH_4^+ + CO_3^{2-} \quad (5.1)$$

$$Ca^{2+} + {CO_3}^{2-} \rightarrow CaCO_3 \quad (5.2)$$

From reactions (5.2), it is evident that an electrolyte is needed to supply Ca^{2+}. Generally, calcium chloride is used as a calcium source. However, chlorides are perceived as the main cause of corrosion in concrete. Thus, other sources of calcium such as calcium acetate, calcium lactate, calcium glutamate, and calcium nitrate are explored [10]. Jonkers et al. [11] selected *Bacillus pseudofirmus* and *B. cohnii* and calcium lactate for self-healing purposes. Farrugia et al. [12] selected *Lysinibacillus sphaericus* as a bacterial strain and calcium chloride and calcium acetate as calcium sources for healing of mortar specimens. Zheng et al. [13] selected *Bacillus alcalophilus* and calcium nitrate and calcium lactate as calcium sources for healing. The calcium sources were mixed in mortar specimens and then cured for self-healing efficiency. Lapeyrusse et al. [14] studied the effect of calcium gluconate and calcium lactate in mortar specimens. Vijay and Murmu [15] mixed *bacillus subtilis* with concrete along with calcium lactate to study the effect of compressive strength and self-healing capability of concrete. It is noted that in most of the studies bacteria or calcium source are added directly into concrete or mortar. However, their role in corrosion of bars embedded in concrete is yet unexplored.

Corrosion begins by attacking the protective coating on embedded steel bars, and once that layer is destroyed, the concrete becomes highly reactive or ionised, allowing the electrochemical corrosion process to begin. Attempts have been made to incorporate autonomous healing of cracks with encapsulated polymers. Belleghem et al. [16] used encapsulated polyurethane for autonomous healing of cracks. Wet and dry cycling of the healed specimens in saline environment revealed that self-healed specimens suffered a lower mass loss due to corrosion in comparison to the untreated ones. It was also concluded that autonomous healing performed better than manual injection of

polymer. Feiteira et al. [17] studied healing of cracks under dynamic loading. They noted that a low viscosity polymer was able to self-heal cracks that are opening up to 50%. It is also noted that shelf life of polymer-based capsules is only about a year. Use of MICP for healing cracks is attractive due to extremely low viscosity of the healing fluid. In Achal et al. [18], a specially isolated bacterium has been used in the concrete mix along with calcium chloride and it was observed that the bacterial concrete has better corrosion resistance than the control concrete. Wang et al. [19] used hydrogel encapsulated bacterial spores for self-healing of concrete and observed that cracks treated with nutrients and bacterial hydrogel healed more quickly than cracks in prepared with nutrients and non-bacterial hydrogel. Self-healing with encapsulated bacterial fluid is also reported. Xu et al. [20] used ceramsite particles as a carrier for bacterial healing agent embedded in concrete. Crack width upto 450 μm was healed and was observed that reinforcement corrosion was controlled by the crack closure from microbial precipitation. However, as the bacterial healing fluid contains electrolytes, there is a concern that it may initiate corrosion in the reinforcement. Hitherto, reports of corrosion study during bacterial healing of cracks is unknown to the authors.

This investigation is a systematic study of possible corrosion in reinforcement during the bacterial healing of cracks in concrete. A crack has been created in concrete and healed using the biocementation process. The healing agent was injected through the cracked surface of the concrete. Two calcium sources namely calcium chloride ($CaCl_2$) and calcium acetate ($Ca(CH_3COO)_2$) were used for biocementation. Healing performance of both calcium sources have been observed through visual, chemical, ultrasonic and water flow tests. Simultaneously, corrosion has been monitored using

the conventional electrochemical techniques as well as the ultrasonic guided wave method. Finally, destructive tests have been performed to assess any loss of strength of the reinforcing bars due to the healing process.

2. Materials and Methods

Reinforced concrete slab specimens have been cast. After curing, bending load was applied on the samples to develop a crack. The crack was then healed with biocementation. Two different sources of calcium, calcium chloride (CL) and calcium acetate (CA), have been used to evaluate any possible effect of the calcium source on corrosion of the steel bar. Healing has been monitored by both water permeability and ultrasonic wave techniques. Corrosion has been monitored by electro-chemical methods and guided wave technique.

2.1 Preparation of reinforced concrete specimen and cracking

Concrete slab specimens with dimensions of 500mm long, 250mm wide, and 150mm high were cast. Ordinary Portland cement, fine aggregates (medium-sized), and coarse aggregates (nominal size of 10 mm) were used in the concrete casting process. A standard plain mild steel reinforcement bar with a nominal diameter of 24 mm and a length of 900mm was used. Water-cement ratio was 0.5 and cement-to-sand-to-coarse-aggregate ratio was 1: 1.62:3.4. The specimens were demoulded after 24 hours of casting and wet cured for 28 days. The concrete compressive strength was 43 MPa. The bar was protruded 200mm on both sides for electrochemical and ultrasonic connections.

A three-point bending system was used to load concrete specimens, causing a crack to form in the middle of the slab. Stress on the reinforcement was close to the limit of its

yielding capacity. The loading was stopped as soon as a visible crack was seen. After removal of load, the crack width was significantly reduced as a result of the reinforcement's elastic recovery. After unloading, all specimens had their crack width measured using a crack measuring scale at various points along the crack length. The crack width was between 0.3 and 0.5 mm.

2.2 Microorganism and culture medium

Sporosarcina Pasteurii (ATCC® 11859TM) was chosen because of its high urease activity and widespread use in concrete remediation. Ammonium sulphate (NH4)2SO4, yeast extract, and Tris buffer (pH=9) was used to cultivate the bacteria. All liquid media were autoclaved for 20 minutes at 121°C. The bacterial culture was shaken at 250 rpm for 24 hours in an aerobic environment. The optical density (OD) of the bacterial culture was measured on a regular basis using a spectrophotometer at a wavelength of 600nm. The average OD value was 1.2.

2.3 Preparation of cementing fluids

Two types of healing fluids were prepared for biocementation. Type1 was prepared by dissolving 0.5M urea and 0.5M calcium chloride in distilled water and was named as CL (chloride healed) and Type2 was prepared by dissolving 0.5M urea and 0.5M calcium acetate in distilled water and was named as CA (acetate healed).

2.4 Healing Treatment

The specimens were given healing treatment after the cracks had formed. There were two parts to the treatment: bacterial fluid and cementing fluid. The procedure was carried out at a temperature of 25°± 1° C. The crack was sealed by pouring healing fluid on the surface of the crack on a regular basis. The cementing fluid was poured twice a day for three days. Every three days, the bacterial fluid was replenished. This

cycle was continued until the monitoring system showed that the healing target had been achieved.

2.5 Watertightness test

Water permeability measurements were taken on the crack at regular intervals throughout the healing process. Water was placed on the specimen to soak it until water freely dripped from it. On top of the cracked surface, a 100ml measuring cylinder was adhered using super glue and silicon. Water was poured into the cylinder. No water was allowed to leak through the adhesive junction. At regular intervals, the water level was checked. The test was carried out at several points along the crack. Each test was repeated three times. When the flow was below the measuring least count, the test was terminated.

2.6 Ultrasonic measurements

2.6.1 Ultrasonic measurements through concrete

At specific sites, an ultrasonic method was utilised to record pulse transmission through the crack. Figure 5.1 shows the experimental setup for ultrasonic data gathering. In this technique, the transmitter and receiver were positioned on opposite sides of the slab. Piezoelectric transducers (GC200-D25) of 25mm diameter and 200kHz central frequency were utilised to create compressional waves. The transducers were connected to a JSR DPR 300 pulser-receiver system to generate a pulse at 40dB. The received signal was digitised using Pico Scope 6 version 6.4.64.0 and a modular oscilloscope.

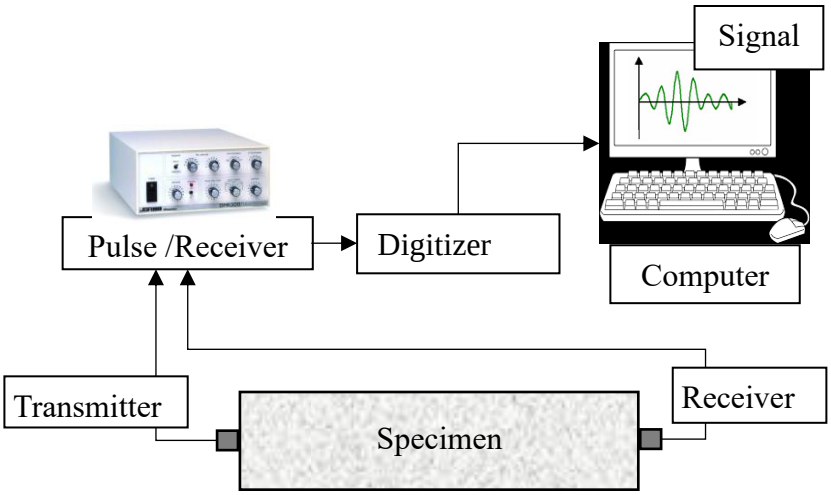

Figure 5.1: Set-up for ultrasonic data acquisition

Figure 5.2 shows the locations of the transmit and receive points on the specimen that were used to capture the ultrasonic waves. The transducers were placed at a distance from the slab's edges in order to eliminate edge effects. The concrete surface was cleaned, and the transducers were securely attached to the surface with a petroleum-based greased coupling agent. Each measurement point had its measurements taken a minimum of three times. The readings were found to be consistent and repeatable.

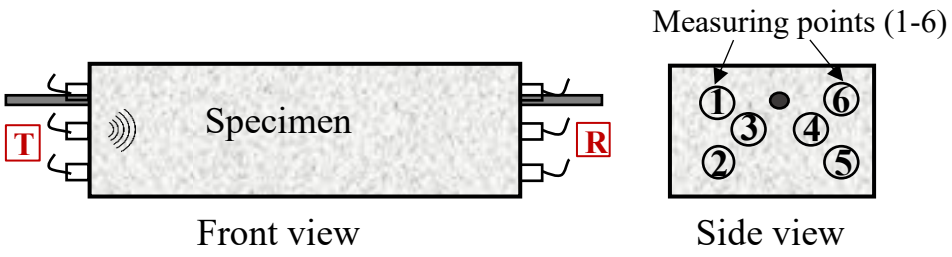

Figure 5.2: Specimen showing different locations of transducers

2.6.2 Ultrasonic measurements through steel bar

To study the behaviour of steel with respect to healing fluids, the specimens were monitored by ultrasonic guided wave modes. Figure 5.3 depicts the ultrasonic data collection setup. A pair of Warsash Scientific piezoceramic patches with diameter 10 mm and thickness 0.5 mm were used to generate guided waves in rebar. The resonance

frequency of piezoceramic patches was around 250 kHz. The patches were connected to the rebar such that the excitation wave mode from the transmitter T travels through the rebar to its opposite surface where the receiving transducer R is placed. A function generator (RIGOL DG1035) was used to generate ultrasonic signal and the signal was amplified with a power amplifier (Ciprian HVA 400 A). The received signal was digitized using a Picoscope version 6.4.64.0 and recorded by a computer. All signals were repeated at least three times for each specimen. It was observed that the readings were repeatable.

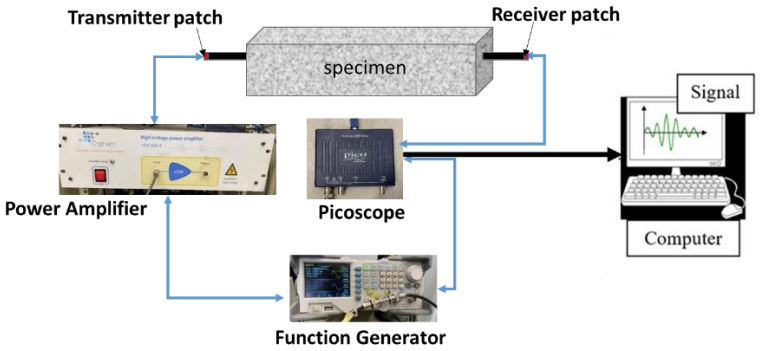

Figure 5.3: Set-up for ultrasonic measurements through steel bar

2.7 Electrochemical measurements

2.7.1 Half-cell measurements

Both specimens were monitored daily during healing process to detect the corrosion potential of embedded reinforcing bars in concrete relative to a reference half-cell placed on the concrete surface. The reinforcement potentials were recorded by voltage measurements between a reference electrode and the working electrode every 24 hours for the entire duration of the experiment. The reference half-cell used in the present study was a standard copper/copper sulphate (CSE) electrode and the rebar as working electrode. The CSE electrode was placed on the concrete surface and potentials were measured by means of a voltmeter. The rebar was connected to the positive terminal and CSE electrode to the negative terminal of the voltmeter. The concrete functions

as an electrolyte and a wetted conductivity sponge was placed underneath the reference electrode to have proper electrical contact. As shown in Figure 5.4, the measured potential difference can be used to predict the risk of corrosion of reinforcement at the test site. ASTM C876 - 91 Standard Test Method was followed for Half-Cell Potentials of uncoated reinforcing steel in concrete.

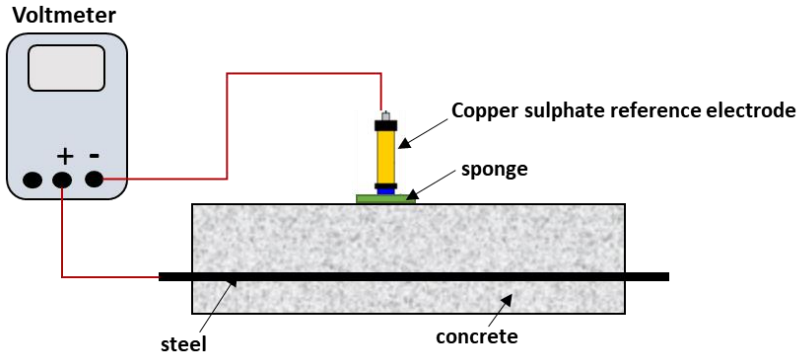

Figure 5.4: Half-cell Potential set-up

2.7.2 Linear Polarisation Resistance (LPR) measurements

Linear Polarisation Resistance (LPR) measurements were recorded daily during healing progression for both specimens to estimate the corrosion rate of steel in concrete. Potentiostat was used to record the corrosion current and corrosion potential which gives an indication of how steel is corroding. The LPR test was conducted using three electrode system with Copper/copper sulphate (CSE) electrode as reference electrode (RE), stainless steel plate as counter electrode (CE) and the rebar as working electrode (WE). To perform the test, a wet sponge was placed on surface of concrete to maintain the contact between electrodes. A schematic representation of the setup is shown in Figure 5.5.

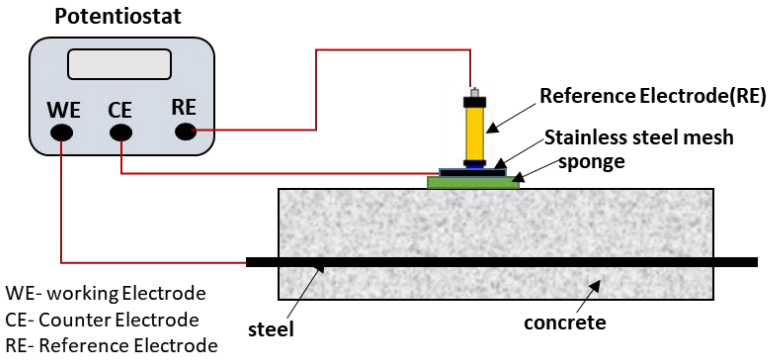

Figure 5.5: Potentiostat set-up

A constant potential was applied and the change in current was measured. Extrapolating the linear sections of the anodic and cathodic branches (Tafel areas) of the curves from the potentiodynamic plots, the corrosion potential and current were calculated. The corrosion current Icorr is determined by the intersection of the two extrapolated lines.

2.8 Mass loss and tensile strength of rebars

To examine the difference in mechanical characteristics in all specimens due to exposure to healing fluids, destructive tests such as mass loss and tensile strength were performed. The specimens were broken and the reinforcing bar for each specimen was cleaned as per ASTM G1-90 with deionized water to remove any adhered corrosion products. They were then weighed to assess how much mass had been lost owing to corrosion. After that, the specimens were put through a uniaxial tensile test using a universal testing equipment (UTM). During the tensile test, the applied load and deformation plots were recorded to better understand how the specimen's mechanical properties changed.

3. Results and Discussion

The results of monitoring healing as well as possible corrosion are presented in this section. A comparison between CL and CA has been made all through.

3.1 Monitoring healing

Healing is monitored through visual inspection as well as instrumentally. The extent of healing was measured by the quantity of calcium carbonate deposition. Time for the treatment was 40 days. The amount of calcium carbonate deposited at that time was considered to be 100%. The healing at the intermediate stages (Figure 5.7 and Figure 5.8) were calibrated against the final amount of deposition.

With gradual healing, the water flow rate across various areas of the crack was also monitored. Finally, a fast and implementable method of assessing healing using ultrasonic signals has been demonstrated.

3.1.1 Visual monitoring

Figure 5.6 and Figure 5.7 shows various stages of healing for CL and CA healed specimens respectively. The crack has been sealed in both specimens, which can be seen clearly. The area marked in red in Figure 5.6a for CL specimen is seen in close up in Figure 5.6b, c and d. It is seen that at 50% healing (Figure 5.6c), although the crack opening has been partially sealed, it remains open at the specimen's corner (Figure 5.6c). This indicated that healing initiates from the centre of the specimen and progresses to the corners. Figure 5.6d shows the crack at 100% healing. Clearly, the crack opening was completely sealed, and no water could pass through it. The deposition for CA specimen can be seen in Figure 5.7. It can be inferred that microbial activity was present inside the crack, which caused precipitation to build up and

eventually reach the surface. The use of calcium chloride and calcium acetate as calcium sources led to calcium carbonate deposits that could cover the whole crack.

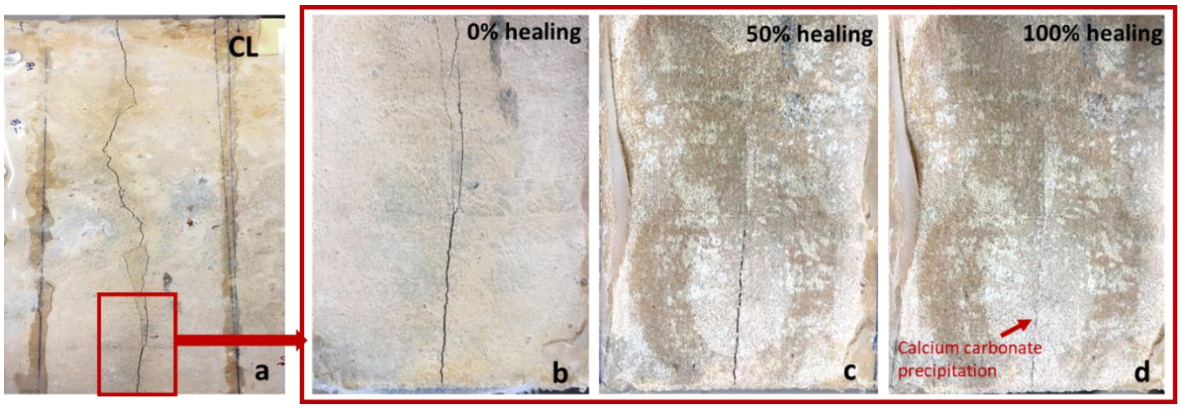

Figure 5.6: Stages of crack healing for CL specimen

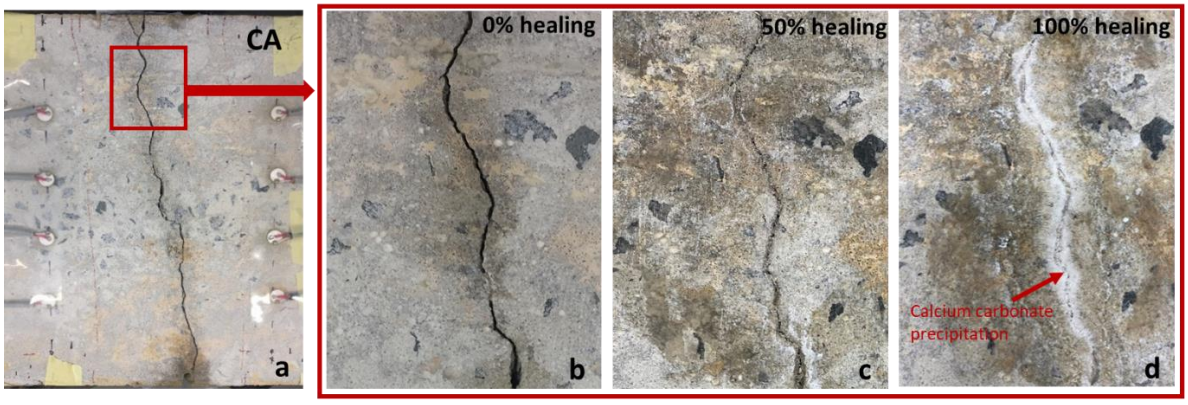

Figure 5.7: Stages of crack healing for CA specimen

3.1.2 Chemical monitoring

The amount of cementation solution poured on the crack for CL and CA healed specimens was recorded. Figure 5.8 presents the volume of healing fluid that could be poured in the crack. It can be seen that with time the volume of cementation fluid that can enter the crack has reduced. The accumulated volume of calcium carbonate with progression of healing is also presented. At the start of healing of the CL specimen, 28 ml of solution could be absorbed by the crack. This continued until 35% healing. The calcium carbonate deposit grows in a linear fashion during this time. After this time, the crack's ability to absorb fluid gradually decreased. In the end, just 8 millilitres

of liquids were able to be absorbed. As the amount of cementation fluid is decreased, the rate of calcium carbonate deposition reduces. The estimated amount of calcium carbonate in the crack is 15 cc. The CA specimen could absorb 28 ml of solution at the commencement of healing. This continued until 47% healing and then reduced gradually. Finally, the crack could absorb just 5 ml of fluid. It should be noted that since the crack was generated by bending the slab, the interior pattern may vary across samples. However, in the present case, both samples healed nearly at the same rate. Initially, the CA sample took a little longer to kick start healing although the duration for total healing was similar.

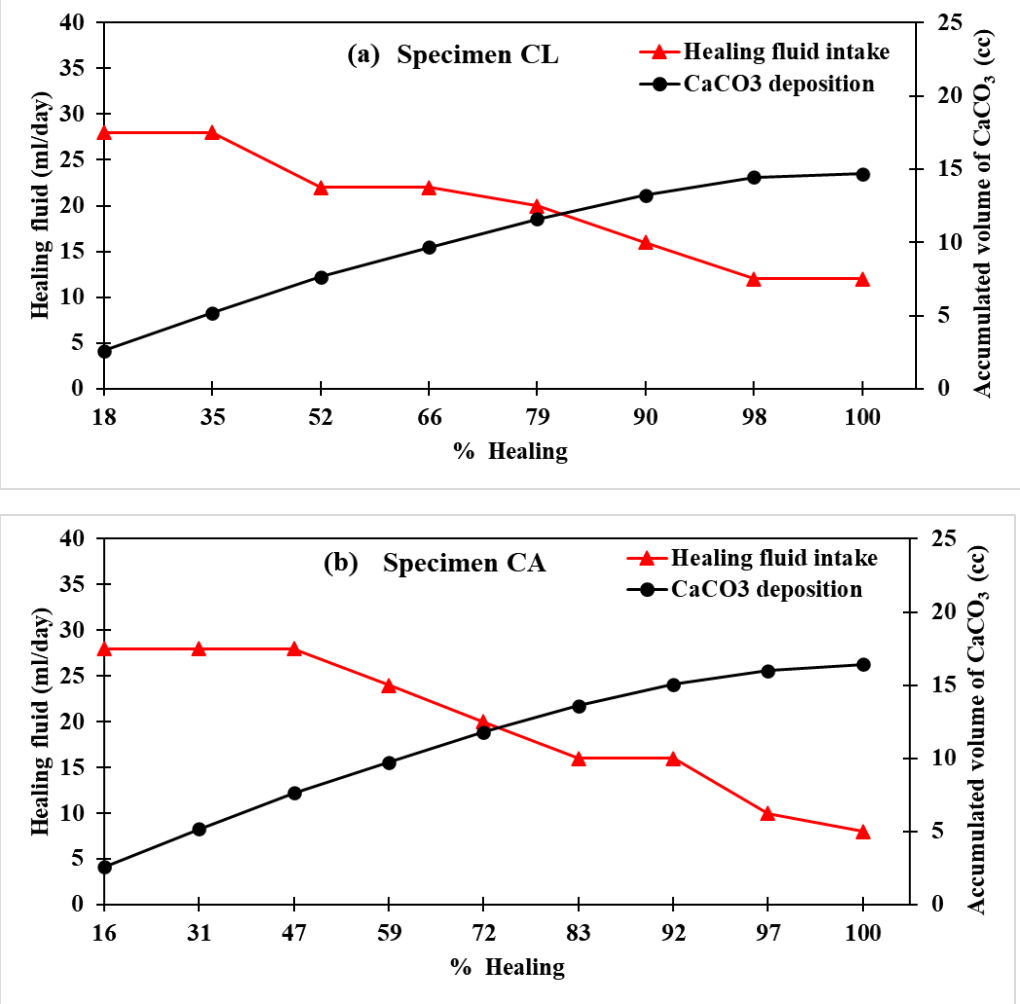

Figure 5.8: Rise in volume of calcium carbonate and reduction in fluid intake with progression of healing.

3.1.3 Watertightness tests

Another essential way for measuring crack closure is the re-establishment of water tightness. In this test, water flow through the cracked specimen was measured as it was being healed. A, B, C, and D are the locations along the crack's surface where water flow was measured (Figure 5.9).

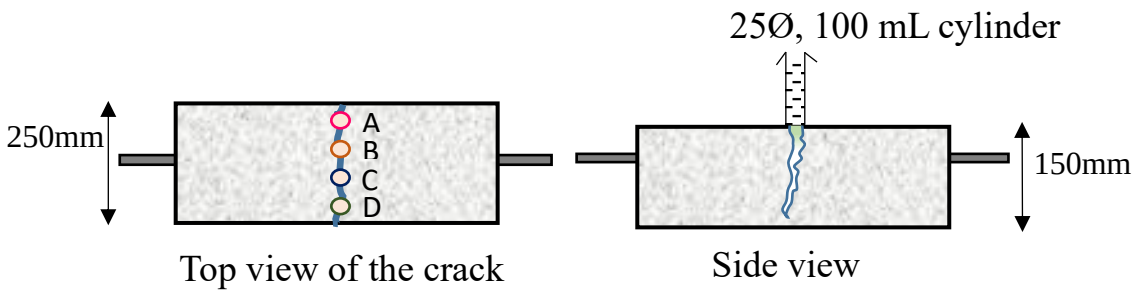

Figure 5.9: Water flow test set-up

For the locations indicated on the specimen CL and CA, Figure 5.10 (a) and (b) show the water flow. The water flows freely through the crack at first. However, as the crack healed, there was less water flowing through it. The initial drop in water flow was insignificant. This is to be expected, as biocement fills in the crack layer by layer, and the gap between the crack faces doesn't close until enough biocement has been built up. After 50% healing for specimen CL, the water tightness of locations B and C had a huge improvement compared to locations A and D, which had a small improvement. At 92% healing, there was no flow in locations B and C, but there was a lot of flow at the corners. Visually it was observed that the crack started to fill up from the central region. At 100% healing, there was no measurable flow through the crack and even the corners became totally watertight.

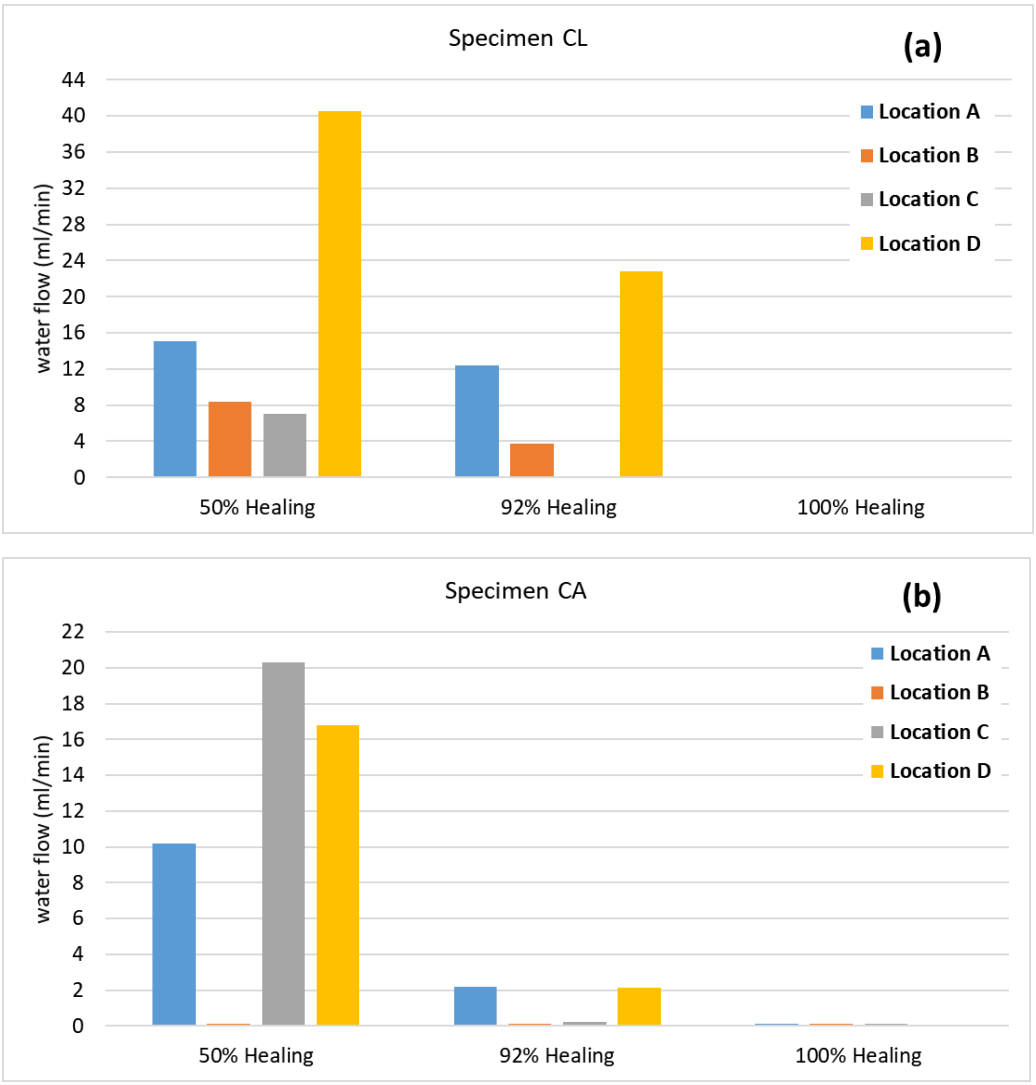

Figure 5.10: Water flow through different locations of the crack for (a) specimen CL and (b) specimen AC

For specimen CA, after 50% healing, the watertightness of locations B and D had a big improvement compared to locations A and D. At 92 percent healing, the flow was much less in all locations. This indicated that the crack was almost completely sealed. There was no flow through the crack at 100% healing, which meant that watertightness had been restored. Thus, with both CL and CA full recovery of watertightness could be achieved.

3.1.4 Ultrasonic monitoring through concrete

CL and CA specimens at different stages of healing are shown in Figure 5.11 and Figure 5.12. They show the waveforms that are sent through the specimen at the points marked 1 to 6. (Figure 5.2). The change in amplitude (y-axis) with time (x-axis) of the pulse that is sent is shown. With the process of healing, a consistent pattern of recovery was seen. The signal amplitudes increased considerably at all the locations. As evident the cement is placed within the crack, the acoustic barrier breaks down, bringing the faces closer together. This was seen for both CL and CA healed specimen. Thus, ultrasonic pulse transmission is an effective way to monitor the progress of concrete crack healing. A similar pattern of considerable rise in signal amplitudes was detected with the process of healing at all points (point 1-6).

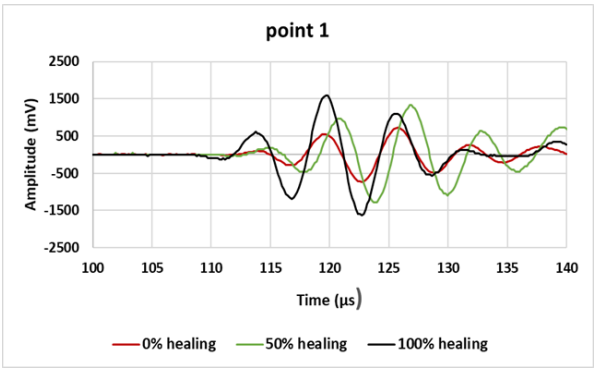

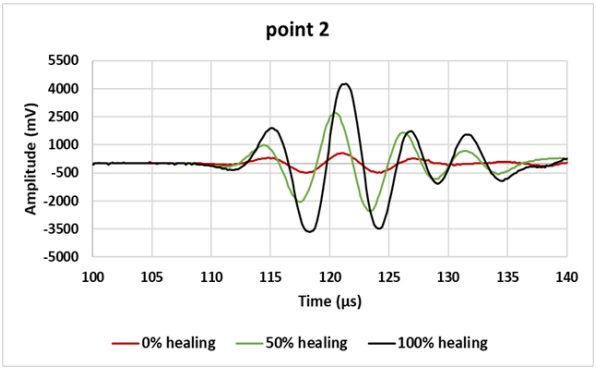

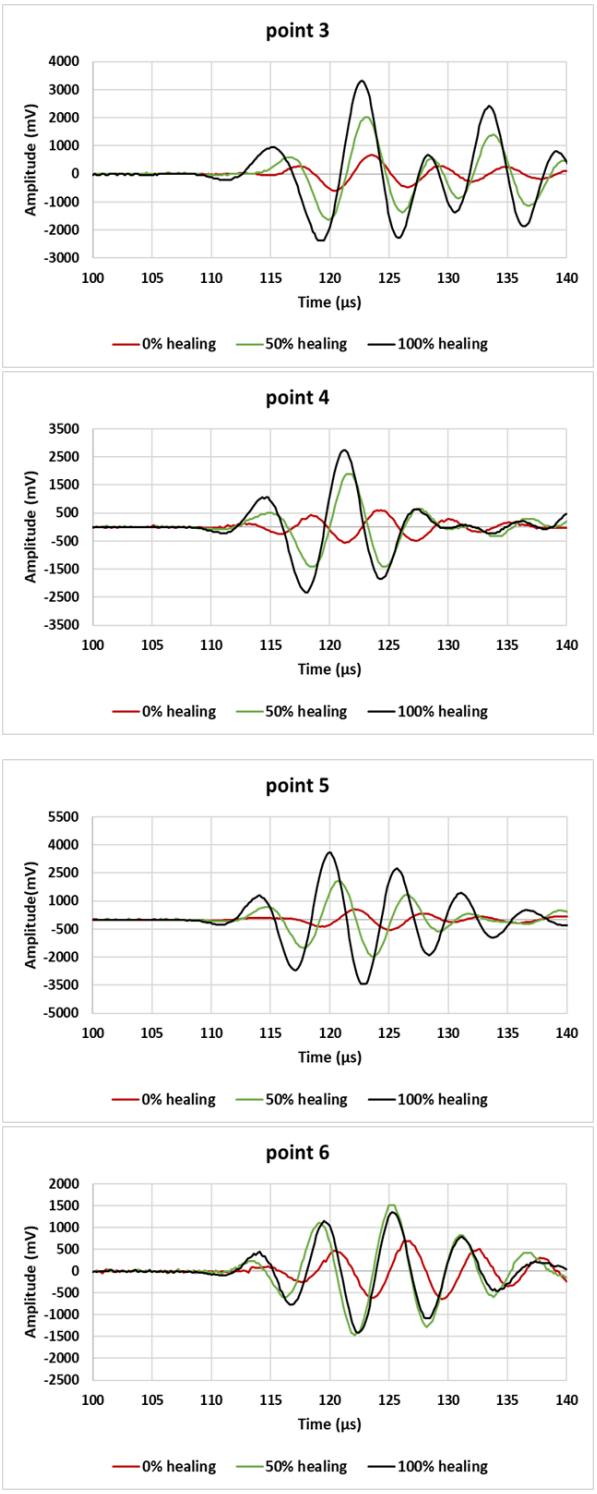

Figure 5.11: Amplitudes for points 1-6 for CL specimen at different stages of healing.

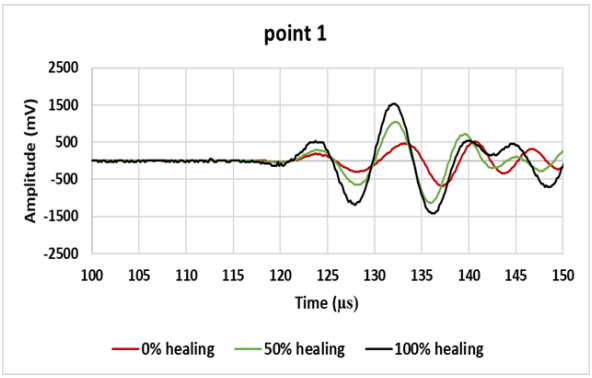
point 1
Amplitude (mV)
2500
1500
500
-500
-1500
-2500
100 105 110 115 120 125 130 135 140 145 150
Time (µs)
0% healing
50% healing
100% healing

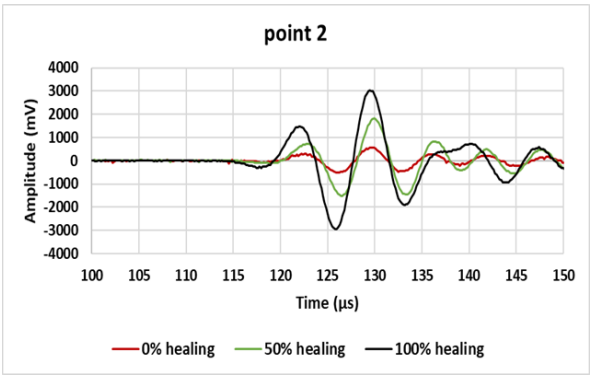
point 2
Amplitude (mV)
4000
3000
2000
1000
0
-1000
-2000
-3000
-4000
100 105 110 115 120 125 130 135 140 145 150
Time (µs)
0% healing
50% healing
100% healing

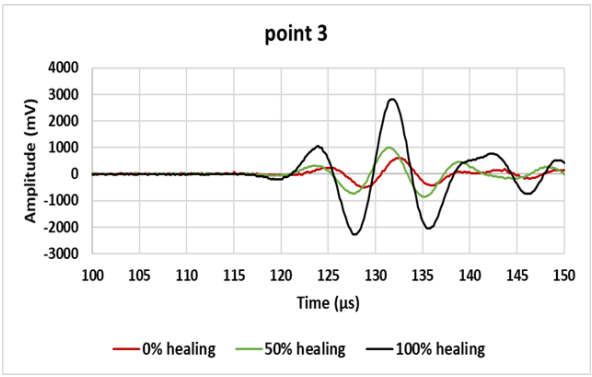
point 3
Amplitude (mV)
4000
3000
2000
1000
0
-1000
-2000
-3000
100 105 110 115 120 125 130 135 140 145 150
Time (µs)
0% healing
50% healing
100% healing

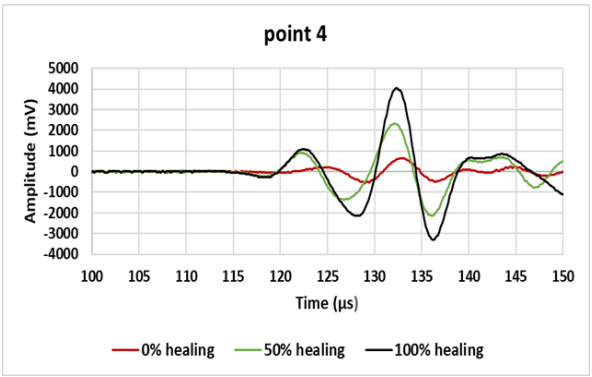
point 4
Amplitude (mV)
5000
4000
3000
2000
1000
0
-1000
-2000
-3000
-4000
100 105 110 115 120 125 130 135 140 145 150
Time (µs)
0% healing
50% healing
100% healing

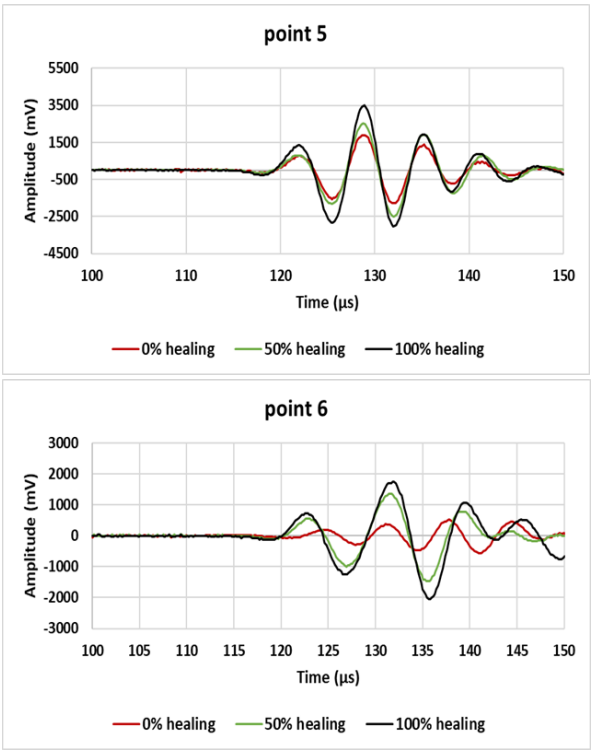

Figure 5.12: Amplitudes for CA specimen at different stages of healing

3.2 Monitoring of corrosion

Corrosion in concrete is usually monitored using the electro-chemical techniques. However, efficacy of these methods in case of healing with chlorides and acetates needs to be examined as they depend on ionic flux. Therefore, simultaneously ultrasonic guided wave technique has also been employed.

It is widely known that once chloride penetrates into concrete depassivation and electrochemical corrosion of the steel bars will occur, which affects the durability of the reinforced concrete. Calcium acetate is a more appropriate calcium source than calcium chloride for the application of MICP in reinforced concrete structures because it avoids the corrosion of steel bars caused by chloride ion. The use of calcium chloride and calcium acetate in various approaches is discussed and compared in the sections below.

3.2.1 Electrochemical Measurements

Figure 5.13 represents the electrochemical results for specimens during healing progression. Figure 5.13 (a) shows the half-cell potential vs CSE results. It was observed that for both CL and CA specimens the initial observed potential was -112mV and -218mV respectively, which indicated that the steel was in passive condition and no corrosion was occurring. According to ASTM C876-09, if the half-cell potential is more positive than -200mV, there is 90% probability of no corrosion. As the healing continues, drop in potential was seen and both specimens followed same trend. At 100% healing the potential was -500mV for CL specimen and -427mV for CA specimen. This indicated that the corrosion has initiated, and the specimens have reached active state of corrosion. It may be recalled that half-cell method only gives the probability of corrosion and various factors such as temperature, humidity or moisture content might affect the results.

Figure 5.13 (b) and (c) represent the LPR measurements for specimens during healing progression. Figure 5.13 (b) shows the corrosion potential. It was observed that both CL and CA specimens followed similar pattern. The initial observed corrosion potential was around -400mV for both specimens and a consistent drop was seen during healing progression. The final potential was -590mV for CL and -515mV for CA specimen. The corrosion current was seen from Figure 5.13 (c) and it was observed that there was significant increase in corrosion current for CL specimen as compared to CA specimen. This indicates that the rate of corrosion is likely to be higher in case of CL in comparison to CA. Although these techniques indicate likelihood of corrosion, a quantitative estimate of corrosion is elusive.

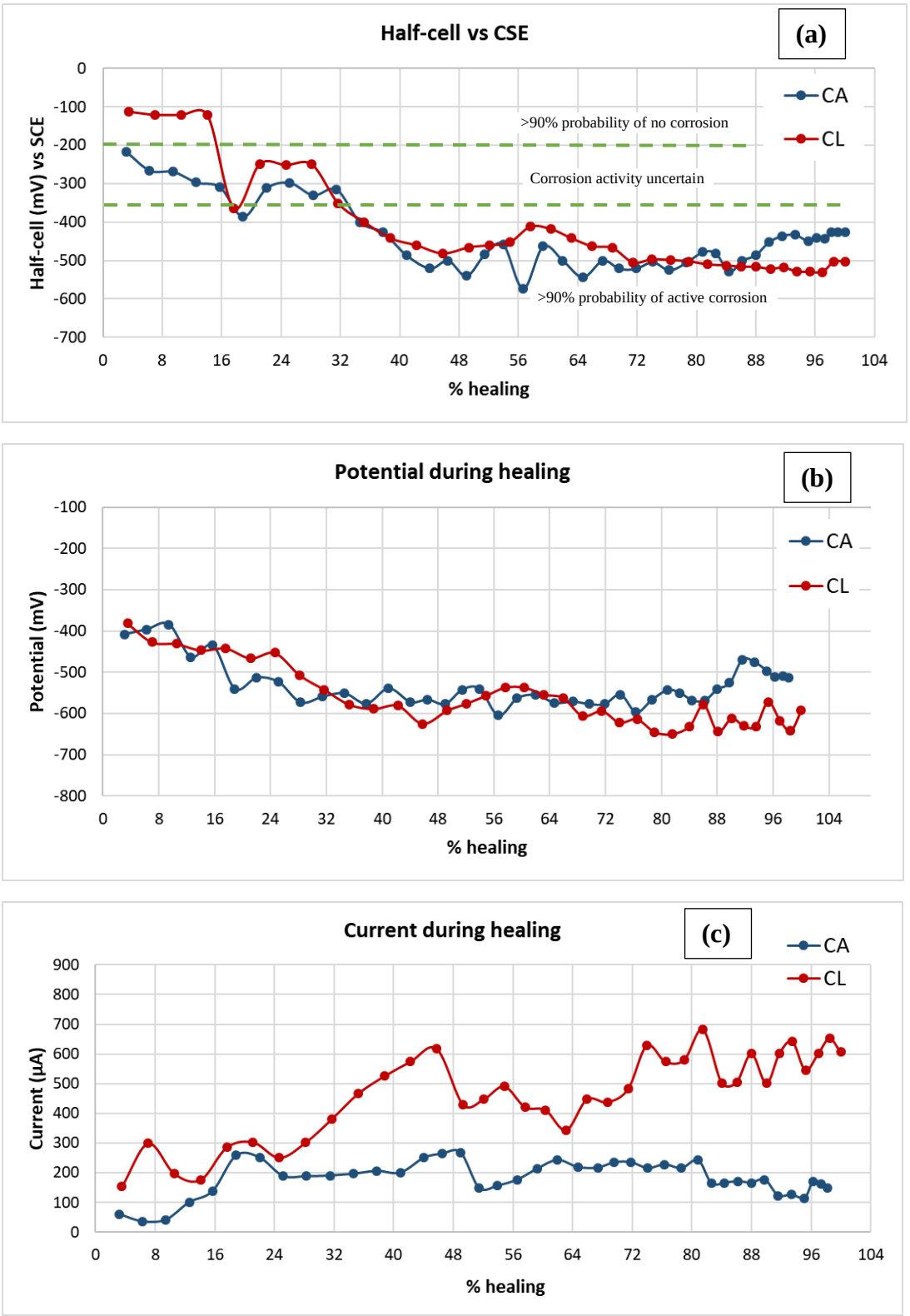

Figure 5.13: Electrochemical readings for specimens during healing. (a) Half-cell vs CSE values; (b) Current vs time; (c) Potential vs time

3.2.2 Ultrasonic guided wave measurements

Efficacy of ultrasonic guided waves in monitoring corrosion is already reported [21]. This method is applied for studying the effect of healing fluids on embedded reinforcement corrosion. The ultrasonic characteristics of the waveguide was recorded by permanently attaching piezo patches to the steel bar (Figure 5.3). The specimens were monitored using a sweeping-frequency guided wave. The received waveform was analysed to investigate the state of corrosion in the bar. A frequency sweep was conducted from 240 kHz to 400 kHz at an interval of 20 kHz to determine the best excitation frequency. The strongest signal was found to be for 300 kHz frequency. The results for 300 kHz frequency are therefore presented in this paper. A 20-cycle Hanning-window tone burst signal was used to excite the guided waves:

$$\sin 2\pi ft \times \left(\frac{1}{2} + \frac{1}{2}\cos\left(2\pi\left(\frac{t - t_{max}}{t_{max}}\right)\right)\right) \quad (5.3)$$

$$t_{max} = n \times \frac{1}{f} \quad (5.4)$$

Where f is the central excitation frequency; t is the time domain of the waveform; t_{max} is the maximum time of the waveform and n is the number of cycles.

Figure 5.14 presents the received signals in time domain for CL and CA specimen for 0 and 100% healing. A decrease in signal amplitudes was observed for both specimens at 100% healing. This indicates that there has been some effect on the bar or its surroundings. Variation of ultrasonic signal with progressive corrosion has been explained in [21]. It is noted that at the initial stage, a thin layer of corrosion product on the surface of the bar improves the bond between the steel bar and the surrounding concrete. Thus, energy leaks through the steel-concrete interface resulting in the attenuation of the signal. The signal regains amplitude when the surface layer breaks down resulting in a loss of bond. Thus, the bars are likely to have developed a thin

surface layer at this stage. To study the variation in the signal, the energy of the transmitted wave is calculated during healing of the specimens.

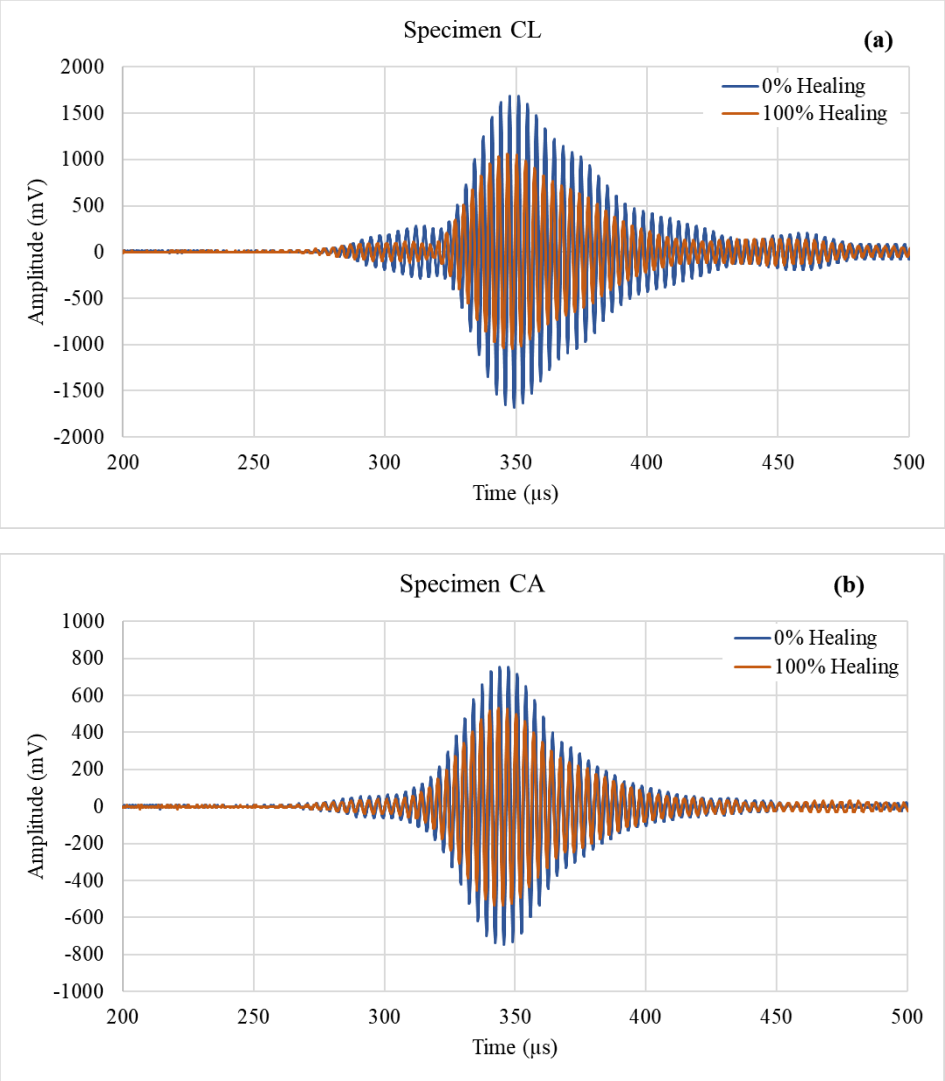

Figure 5.14: Transmission index for specimens CL and CA during healing progression for 300 kHz frequency.

The norm of the transmitted energy is determined by recording the transmitted time signals sequentially. Fast Fourier Transform is applied on the time signals as:

$$A(F_I) = \mathrm{FFT}(f(x)) \tag{5.5}$$

Where $A(F_i)$ is the Fast Fourier Transform of the i^{th} time signal $f(t)_i$

The norm of energy is computed over a frequency window $\omega \pm B/2$.

$$E_i = \sum_{\omega-B/2}^{\omega+B/2} A(F_i) \quad (5.6)$$

Where ω is the excitation frequency and B is the bandwidth.

The transmission index is calculated as 1's complement of the ratio of the ith energy norm (E_i) and the initial energy norm E_0.

$$TI(i) = 1 - \frac{E_i}{E_0} \quad (5.7)$$

Figure 5.15 presents TI for specimens CA and CL during healing progression. It was observed that TI for CA specimen were fluctuating with a decreasing trend during entire healing period. This indicated the formation of the pits, leading to the deterioration of the bar. The surface of bar becomes irregular that reduces the energy of the transmitted signal. The TI for CL specimen shows decreasing trend upto 45% healing which indicates the steel-concrete interface starts to debond but simultaneously there is a build-up calcium carbonate inside the crack due to the presence of healing fluids. The TI then remains steady until 100% healing. Previous studies show that such variations in signal indicates thin surface corrosion. This was confirmed through destructive tests after the completion of the exposure period.

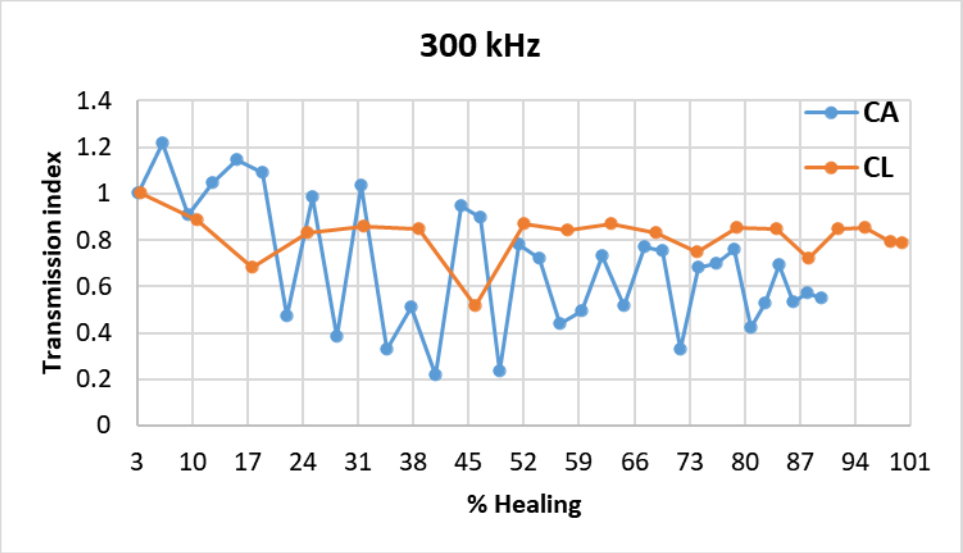

Figure 5.15: Transmission index for different frequencies for specimens CA and CL

3.7 Destructive tests

The rebars were visually examined after healing. Figure 5.16 shows the condition of rebar for both CL and CA specimens. Only a marginal amount of corrosion on the surface of the bars was noted. However, in case of CL specimens, corrosion was more concentrated in the region of the crack than the CA specimen. For CA specimens small patches were spread all along the embedded length of the bar. The mass loss for CL and CA was 0.19% and 0.12% respectively. The stress-strain curves for the healed specimens are presented in Figure 5.17 along with that of a fresh bar. It is noted that all the bars had very similar graphs. CA followed the curve of the fresh bar except in the end. The strain at failure was slightly reduced. CL too showed a close agreement with other bars. However, its yield point and the maximum strain was marginally lower. This is likely due to the localised corrosion observed in case of CL. Evidently, the corrosion in the bar due to the use of the electrolytes in the healing fluid is marginal both for CL and CA.

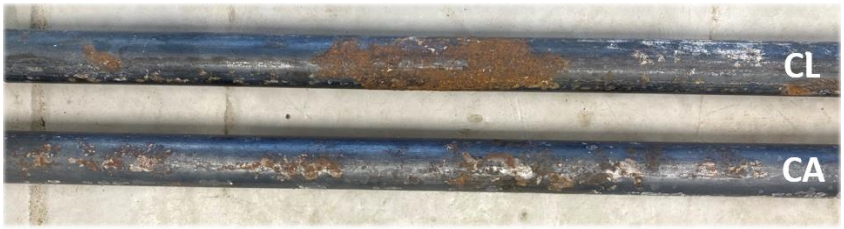

Figure 5.16: Visual inspection of rebar

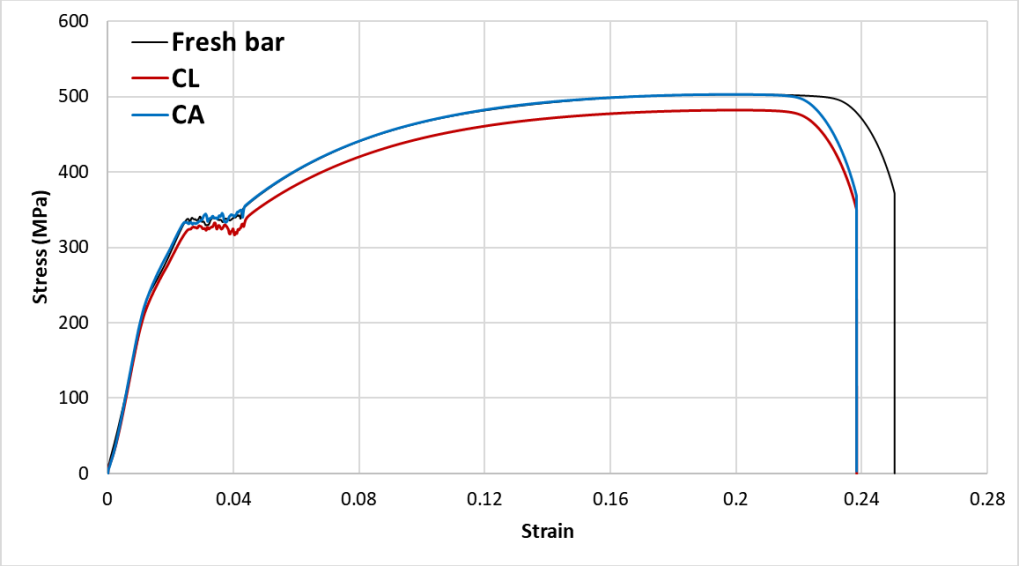

Figure 5.17: Stress-strain curves

4. Conclusions

This paper investigates the corrosion of steel bars in reinforced concrete due to the use of bacterial healing of cracks. Two discern the effect of different electrolytes, calcium chloride and calcium acetate have been used as calcium source. The novelty of the investigation is to simultaneously monitor corrosion using both electrochemical methods as well as ultrasonic guided wave technique. Calcium carbonate deposition inside the crack has been visually observed. Water tightness assessments and ultrasonic techniques were used to confirm the level of healing.

It was observed that the bacterial treatment resulted in deposition of calcium carbonate inside the crack. The healing fluids prepared using calcium chloride and calcium acetate were able to seal the crack and deposition could be seen on the surface of the crack. Water flow tests also indicated the sealing as no water was seen to permeate through the crack.

Ultrasonic signals through concrete were able to capture various stages of healing. A rise in signal amplitude indicated the level of healing. As a result, the ultrasonic approach was able to track the healing process.

Due to the presence of electrolytes in the healing fluid, as expected, the electrochemical monitoring indicated the probability of corrosion during the healing process. In contrast, the guided wave technique examines the physical the physical condition of the bar; thus, it gives more nuanced information. It indicated that the bars have developed a thin interfacial layer of corrosion products at the steel-concrete interface that has strengthened the bond. The destructive tests confirmed this prediction as a thin layer of rust was visible. In case of CL it was more concentrated in the central region while in case of CA, it was distributed in small patches along the length of the bar. The tension test of the bars showed that the effect of corrosion is negligible. This investigation demonstrates that bacterial healing of cracks in concrete may marginally affect the bar; however, its effect on the overall performance of the reinforced concrete member is negligible.

In this investigation, only a small number of specimens have been tested. It is necessary to perform the test with a large ensemble of samples to quantitively estimate the performance of the reinforced concrete samples, especially in the long term. Such a test program is underway.

Acknowledgements

The authors would like to acknowledge the contribution of Australian Government Research Training Program Scholarship in supporting this research.

Conflicts of Interest

The authors declare that they have no conflict of interest.

References

1. Kaur, N.P., et al., *Healing fine cracks in concrete with bacterial cement for an advanced non-destructive monitoring.* Construction and Building Materials, 2020. **242**: p. 118151.
2. Pal Kaur, N., et al., *Healing and Simultaneous Ultrasonic Monitoring of Cracks in Concrete.* Materials Today Communications, 2018.
3. Ramachandran, S.K., V. Ramakrishnan, and S.S. Bang, *Remediation of concrete using micro-organisms.* ACI Materials Journal-American Concrete Institute, 2001. **98**(1): p. 3-9.
4. Choi, S.-G., et al., *Mortar crack repair using microbial induced calcite precipitation method.* Cement and Concrete Composites, 2017. **83**: p. 209-221.
5. Wang, J., et al., *Application of microorganisms in concrete: a promising sustainable strategy to improve concrete durability.* Applied microbiology and biotechnology, 2016. **100**(7): p. 2993-3007.
6. Souradeep, G. and H.W. Kua, *Encapsulation technology and techniques in self-healing concrete.* Journal of Materials in Civil Engineering, 2016. **28**(12): p. 04016165.
7. Joshi, S., et al., *Microbial healing of cracks in concrete: a review.* Journal of Industrial Microbiology & Biotechnology, 2017: p. 1-15.
8. Castanier, S., G. Le Métayer-Levrel, and J.-P. Perthuisot, *Ca-carbonates precipitation and limestone genesis—the microbiogeologist point of view.* Sedimentary geology, 1999. **126**(1-4): p. 9-23.

9. Xu, J., X. Wang, and B. Wang, *Biochemical process of ureolysis-based microbial CaCO 3 precipitation and its application in self-healing concrete.* Applied microbiology and biotechnology, 2018. **102**(7): p. 3121-3132.

10. Xu, J., et al., *Effects of Calcium Source on Biochemical Properties of Microbial CaCO3 Precipitation.* Frontiers in microbiology, 2015. **6**.

11. Jonkers, H.M., et al., *Application of bacteria as self-healing agent for the development of sustainable concrete.* Ecological engineering, 2010. **36**(2): p. 230-235.

12. Farrugia, C., et al., *The application of Lysinibacillus sphaericus for surface treatment and crack healing in mortar.* Frontiers in Built Environment, 2019. **5**: p. 62.

13. Zheng, T., C. Qian, and Y. Su, *Influences of different calcium sources on the early age cracks of self-healing cementitious mortar.* Biochemical Engineering Journal, 2020: p. 107849.

14. Ducasse-Lapeyrusse, J., et al., *Effect of calcium gluconate, calcium lactate, and urea on the kinetics of self-healing in mortars.* Construction and Building Materials, 2017. **157**: p. 489-497.

15. Vijay, K. and M. Murmu, *Effect of calcium lactate on compressive strength and self-healing of cracks in microbial concrete.* Frontiers of Structural and Civil Engineering, 2019. **13**(3): p. 515-525.

16. Van Belleghem, B., et al., *Chloride induced reinforcement corrosion behavior in self-healing concrete with encapsulated polyurethane.* Cement and Concrete Research, 2018. **113**: p. 130-139.

17. Feiteira, J., E. Gruyaert, and N. De Belie, *Self-healing of moving cracks in concrete by means of encapsulated polymer precursors.* Construction and Building Materials, 2016. **102**: p. 671-678.

18. Achal, V., et al., *Corrosion prevention of reinforced concrete with microbial calcite precipitation.* ACI Materials Journal, 2012. **109**(2): p. 157-164.

19. Wang, J., et al., *X-ray computed tomography proof of bacterial-based self-healing in concrete.* Cement and Concrete Composites, 2014. **53**: p. 289-304.

20. Xu, J., et al., *Application of ureolysis-based microbial CaCO3 precipitation in self-healing of concrete and inhibition of reinforcement corrosion.* Construction and Building Materials, 2020. **265**: p. 120364.

21. Majhi, S., et al., *Corrosion detection in steel bar: A time-frequency approach.* NDT & E International, 2019. **107**: p. 102150.

Chapter 6 Long Term Corrosion Monitoring of Bacterially Healed Concrete Using Electrochemical and Ultrasonic Techniques

Nimrat Pal Kaur, Yikuan Wang, Navdeep Kaur Dhami and Abhijit Mukherjee
School of Civil and Mechanical Engineering, Curtin University, WA 6102, Australia

Abstract

Bacterial biocementation has been shown to have the unique capability of healing of cracks in concrete. However, there is a concern that the materials used in biocement may cause corrosion. This paper reports performance of bacterially healed reinforced concrete when exposed to chloride induced reinforcement corrosion. Cracks in reinforced concrete specimens were healed using two different calcium sources. After healing, the samples were subjected to 3.5% sodium chloride exposure to salt water for 120 days. The state of corrosion was assessed through standard electrochemical techniques such as half-cell and linear polarisation methods as well as ultrasonic guided waves. After the exposure period, the bars were extracted out of concrete and mass loss and tensile tests were conducted. It was found that electrochemical measurements indicated corrosion activity in the cracked specimens, but the uncracked specimen did not indicate corrosion during the entire exposure period. Presence of electrolytes in the healing fluid seems to have influenced the electrochemical measurements and gave a misleading indication of corrosion. The ultrasonic guided waves that assess both effects of corrosion, loss of metal and bar-concrete interfacial debonding, was found to realistically assess the state of corrosion in all the samples. The rate of corrosion had slowed down significantly as a result of healing.

1. Introduction

Reinforced concrete (RC) members are generally designed as cracked sections wherein concrete is allowed to crack in the tension zone. Although such cracks do not affect strength, but they can severely affect durability as cracks provide pathways for water and other aggressive agents such as chlorides to reach the reinforcements embedded inside concrete. As a result, corrosion of rebars may occur (Stratfull 1968, Shao-feng et al. 2011). Onset of corrosion accelerate deterioration of concrete as formation of rust which occupies volume 6 -10 times the volume of original steel (Broomfield 2003, Montemor et al. 2003). This in turn produces internal stresses and leads to widening of cracks, resulting in accelerated deterioration of concrete (Neville 1995, Song and Saraswathy 2007). Thus, healing the cracks to stop ingress of chlorides can greatly alleviate the problem corrosion and increase the service life of concrete structures.

Research to heal the cracks in concrete with materials such as cement grouts (Anagnostopoulos 2014, Panasyuk et al. 2014, Kaur et al. 2018), polymers (Panasyuk et al. 2014) and biocement (De Belie and Wang 2016, Kaur et al. 2020) have been reported. Bacteria based healing system known as Microbial Induced Calcite Precipitation (MICP) has been found to be particularly effective in healing thin cracks in concrete due to its lower viscosity (Achal et al. 2015, Kaur et al. 2020). MICP is a process in which naturally occurring microorganisms such as bacteria, through their metabolic activity induce precipitation of calcium carbonate from a healing fluid containing calcium and carbon ions (Dhami et al. 2012, Dhami et al. 2013). Several types of bacterial metabolic pathways for healing have been investigated in the last decade. Aerobic respiration of bacteria is among the first to be applied in crack self-healing. In this method spores and nutrients are added in concrete and precipitation

can be induced by bacterial oxidation of organic matters (Jonkers et al. 2010). Other pathway known as enzymatic urea hydrolysis, has been used in concrete other than self-healing. In this method, urea is catalysed into ammonium and carbonate by urease that is produced by bacteria resulting in increase of pH, and precipitation (Stocks-Fischer et al. 1999). Carbon dioxide sequestration with carbonic anhydrase pathway has also been explored (Qian et al. 2015). Recently, denitrification via bacteria was proposed as another pathway in which precipitation can be induced by biological nitrate reduction with additional corrosion inhibiting effect (Erşan et al. 2016, Erşan et al. 2016). In terms of the concrete healing, ureolytic pathway is preferred because of its high precipitation rate (Wang et al. 2016, Dubey et al. 2022). Despite the high efficiency in precipitation, there have been concerns that presence of chloride ions in the healing may have an undesirable effect of inducing corrosion in steel.

Typically, calcium chloride is used as the source of calcium. Some studies have reported the use of alternate sources of calcium (De Muynck et al. 2008, Jonkers et al. 2010, Wang et al. 2014, Erşan et al. 2016, Ling and Qian 2017). Various calcium sources such as calcium chloride, calcium lactate, calcium glutamate, calcium acetate and calcium nitrate are available (Xu et al. 2015). Jonkers et al. (Jonkers et al. 2010) selected *Bacillus pseudofirmus* and *B. cohnii* and calcium lactate for self-healing purposes. Farrugia et al. (Farrugia et al. 2019) selected *Lysinibacillus sphaericus* as a bacterial strain and calcium chloride and calcium acetate as calcium sources for healing of mortar specimens. Zheng et al. (Zheng et al. 2020) selected *Bacillus alcalophilus* and calcium nitrate and calcium lactate as calcium sources for healing. The calcium sources were mixed in mortar specimens and then cured for self-healing efficiency. Lapeyrusse et al. (Ducasse-Lapeyrusse et al. 2017) studied the effect of calcium gluconate and calcium lactate in mortar specimens. Vijay and Murmu (Vijay

and Murmu 2019) mixed *bacillus subtilis* with concrete along with calcium lactate to study the effect of compressive strength and self-healing capability of concrete. It is noted that in most of the studies bacteria or calcium source are added directly into concrete or mortar for self-healing purposes.

To determine the efficacy of healing, it is important to realistically assess the state of corrosion over the period of exposure. Traditionally, corrosion has been assessed by the electrochemical methods (Broomfield 2003, Sharma and Mukherjee 2011, Poursaee 2016). Among the various electrochemical methods, potential measurement is widely used for detecting corrosion activity in embedded steel bars. These measurements only provide information for corrosion probability (Song and Saraswathy 2007). Half-cell potential measurement has been standardised in ASTM C 876 for in situ detection of corrosion. However, the measurements can be affected by many site conditions such as temperature, humidity, moisture content, degree of polarisation, and cover depth (Elsener 2002, Assouli et al. 2008). In the case of bacterially healed concrete, presence of electrolytes in the form of source of calcium may affect the measurement. Linear Polarisation Resistance (LPR) technique has also been widely used for determining the corrosion rate measurement of reinforcing steel in concrete. These measurements provide a valuable insight into the instantaneous corrosion rate, thus giving more detailed information than potential measurements. However, these measurements too are affected by the presence of the calcium source in the healing fluid. These methods indicate the ongoing electrical activity but do not assess the physical condition of either the bar or its interface with concrete. An alternative method that is able to assess the physical condition of the bar may be more reliable.

In the last few decades, ultrasonic techniques such as wave propagation through the rebar has been used for detecting corrosion in concrete (Sharma and Mukherjee 2011, Lu et al. 2013, Trtnik and Gams 2014, Rodrigues et al. 2020, Majhi et al. 2021). Ultrasonic technique is based on the wave signals that reflect information along the wave path. Based on wave signals, the pulse velocity is frequently used to examine the damaged state. In a corroded RC structure, the scattering phenomenon of waves by cracks and the reduction of transmitted wave due to a change in acoustic impedance caused by the rust on the concrete-rebar interface results in additional amplitude attenuation when compared to an undamaged state (Popovics et al. 1990, Yeih and Huang 1998, Shiotani and Aggelis 2009). Sharma and Mukherjee (Sharma and Mukherjee 2014) monitored the solidification process of freshly poured concrete using the rebar as a wave guide. The technique was also demonstrated for monitoring rebar corrosion (Sharma and Mukherjee 2011, Sharma et al. 2015). Using specific core and surface seeking wave modes, they were able to discern even the type of corrosion (Sharma and Mukherjee 2013, Sharma and Mukherjee 2015). Aggelis and Shiotani (Aggelis and Shiotani 2007) used a combination of Rayleigh and longitudinal waves to study the effectiveness of using epoxy for filling the cracked bridge decks.

Although the bacterial system is greatly effective in healing cracks (Kaur et al. 2020), its efficacy in impeding reinforcement corrosion is not evaluated. This paper reports performance of bacterial healed samples when exposed to accelerated corrosion. Healed samples have been compared with samples in undamaged and damaged states. Several corrosion parameters have been monitored in this investigation. The search for the ideal parameter to study the efficacy of healing in impeding reinforcement corrosion has been reported in this paper.

2. Experimental Program

The objective of the experiment is to assess the healing ability of the bacterial technique and its effect on long term exposure to harsh corrosive environment. To address the concern of presence of chlorides in the healing agent, two calcium sources in the form of chloride and acetate have been used. Both electrochemical and ultrasonic measurements have been performed for monitoring corrosion. The experimental programme was carried out in following steps:

1. Casting of reinforced concrete specimens and cracking
2. Healing with bacterial fluid and simultaneous monitoring
3. Subjecting the uncracked, cracked and healed specimens to sodium chloride solution ponding and simultaneous monitoring
4. Determining mass loss and tensile strength of rebar

Four types of specimens were prepared. Undamaged or pristine specimen was denoted as “UD”; Damaged/cracked specimen was denoted as “D”; Specimen with a damage/crack and healed using calcium chloride + urea as cementation solution was denoted as “DHC” and specimen with a damage/crack and healed using calcium acetate + urea as cementation solution was denoted as “DHA”.

2.1 Preparation of test specimens and cracking

Reinforced concrete specimens were prepared using Ordinary Portland cement, fine aggregates (medium-sized) and coarse aggregates (nominal size of 10 mm). A standard plain mild steel reinforcing bar of 24 mm nominal diameter and 900mm length and was used. The ratio of cement: sand: coarse aggregate was 1: 1.62: 3.4. Slab specimens of size 500mm (length) x 250mm (width) x 150mm (height) with an embedded steel bar were cast. The water-cement ratio was 0.5 and the resulting

compressive strength of concrete after 28 days was 43 MPa. The bar was protruded by 200mm on both sides for making electrochemical and ultrasonic connections. All specimens were demoulded after 24 hours from casting and moist cured for 28 days.

The slab specimens were loaded in three-point bending configuration resulting in the formation of a crack in the middle of the slab. After unloading, crack width was measured at different locations along the crack length using a crack measuring scale. The crack width was in the range 0.25 – 0.45 mm.

2.2 Preparation of healing fluids and treatment

The bacterial strain used in this study was *Sporosarcina Pasteurii* (ATCC® 11859™) due to its high urease activity (Dubey et al. 2022). The bacteria were cultured in liquid medium comprising of ammonium sulphate (NH4)2SO4, yeast extract, and Tris buffer (pH=9). All liquid media were sterilized by autoclaving for 20 min at 121°C. The bacterial culture was incubated aerobically at 37°C for 24 hours and shaken at 250 rpm. Growth of bacterial culture was checked regularly by measuring the optical density (OD) at wavelength of 600nm with spectrophotometer. The average OD value was 1.2.

Two types of cementing fluids were prepared for biocementation. Type1 was prepared by dissolving equimolar urea and calcium chloride at 0.5M concentration in distilled water and Type2 was prepared by dissolving urea and calcium acetate at 0.5 M concentration in distilled water.

The treatment was performed at room temperature of 25± 1° C. The sealing was attempted through periodic pouring of the healing fluid on the surface of the crack. First, bacterial fluid was poured into the crack and allowed to rest, followed by cementing fluid. The cementing fluid was poured twice a day for three days. Bacterial

fluid was replenished at an interval of three days. This cycle was repeated until complete healing was achieved.

2.3 Corrosion monitoring and exposure regime

All specimens were exposed to corrosive environment and monitored daily for a period of 120 days. A 3.5% NaCl solution was ponded on top of the specimens to induce chloride ion ingress through the cracked zone as shown in Figure 6.1. Specimens were inspected daily by visual monitoring, electrochemical tests such as Half-cell and Linear Polarisation resistance (LPR) technique as well as guided wave measurements. After 120 days exposure, specimens were broken to retrieve the entire bar for mass loss and tensile strength testing.

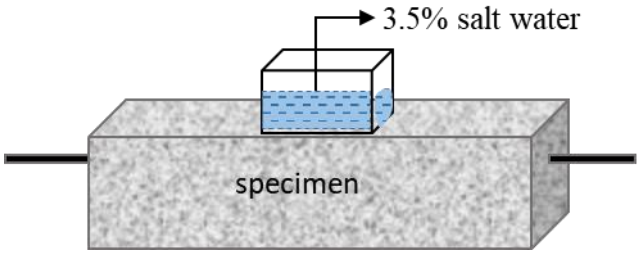

Figure 6.1. Specimen exposure to salt water

2.4 Half-cell measurements

In the present study, all specimens were monitored daily to detect the corrosion potential of embedded reinforcing bars in concrete relative to a reference half-cell placed on the concrete surface. The reinforcement potentials were recorded by voltage measurements between a reference electrode and the working electrode every 24 hours for the entire duration of the experiment. The reference half-cell used in the present study was a standard copper/copper sulphate (CSE) electrode and the rebar as working electrode. The CSE electrode was placed on the concrete surface and potentials were measured by means of a voltmeter. The rebar was connected to the positive terminal

and CSE electrode to the negative terminal of the voltmeter. The concrete functions as an electrolyte and a wetted conductivity sponge was placed underneath the reference electrode to have proper electrical contact. The risk of corrosion of the reinforcement in the immediate region of the test location may be related empirically to the measured potential difference as shown in Figure 6.2. ASTM C876 - 91 Standard Test Method was followed for Half-Cell Potentials of uncoated reinforcing steel in concrete.

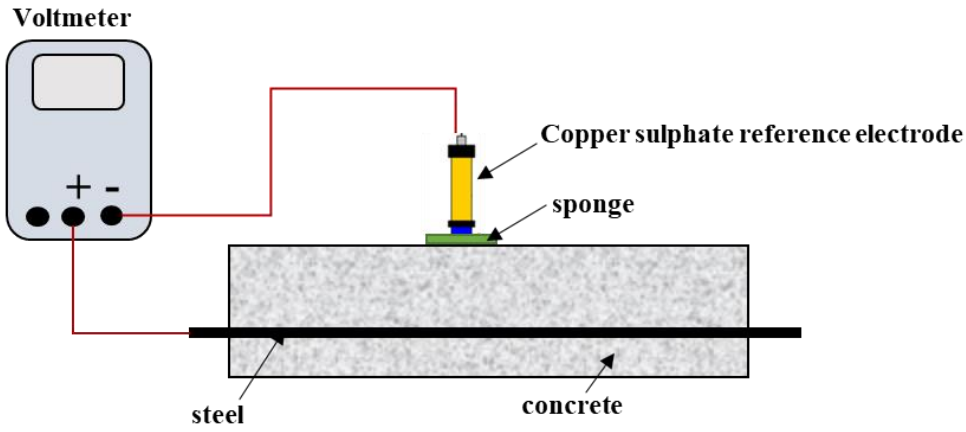

Figure 6.2. Half-cell Potential set-up

2.5 Linear Polarisation Resistance (LPR) measurements

Linear Polarisation Resistance (LPR) measurements were recorded daily for all the specimens for the entire exposure period to estimate the corrosion rate of steel in concrete. Potentiostat was used to record the corrosion current and corrosion potential which gives an indication of how steel is corroding. The LPR test was conducted using three electrode system with Copper/copper sulphate (CSE) electrode as reference electrode (RE), stainless steel plate as counter electrode (CE) and the rebar as working electrode (WE). To perform the test, a wet sponge was placed on surface of concrete to maintain the contact between electrodes. A schematic representation of the setup is

shown in Figure 6.3. A constant potential was applied and the change in current was measured. Extrapolating the linear sections of the anodic and cathodic branches (Tafel areas) of the curves from the potentiodynamic plots, the corrosion potential and current were calculated. The corrosion current Icorr is determined by the intersection of the two extrapolated lines.

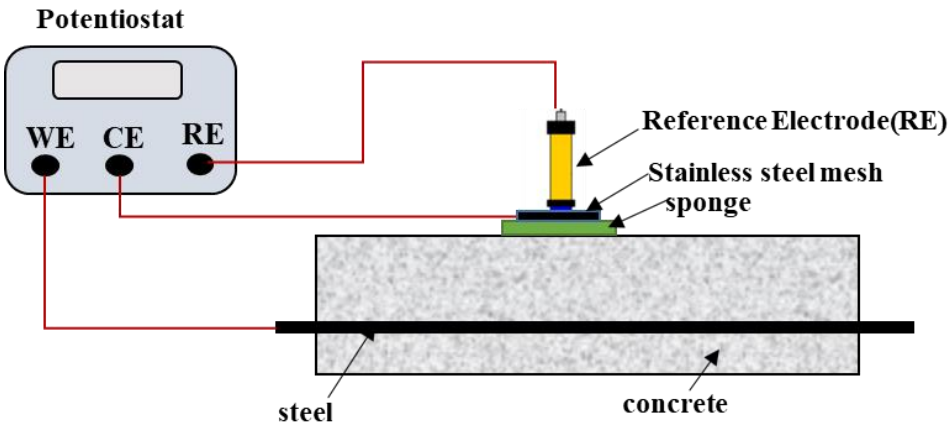

Figure 6.3. Potentiostat set-up

2.6 Guided wave inspection of reinforced bar

All the specimens were monitored by ultrasonic guided wave modes. Set-up for ultrasonic data acquisition system is shown in Figure 6.4. A pair of Warsash Scientific piezoceramic patches with diameter 10mm and thickness 0.5mm were used to generate guided waves in rebar. The patches were connected to the rebar such that the excitation wave mode from the transmitter T travels through the rebar to its opposite surface where the receiving transducer R is placed. A function generator (RIGOL DG1035) was used to generate ultrasonic signal and the signal was amplified with a power amplifier (Ciprian HVA 400 A). The received signal was digitized using a Picoscope version 6.4.64.0 and recorded by a computer. All signals were repeated at least three times for each specimen. It was observed that the readings were repeatable.

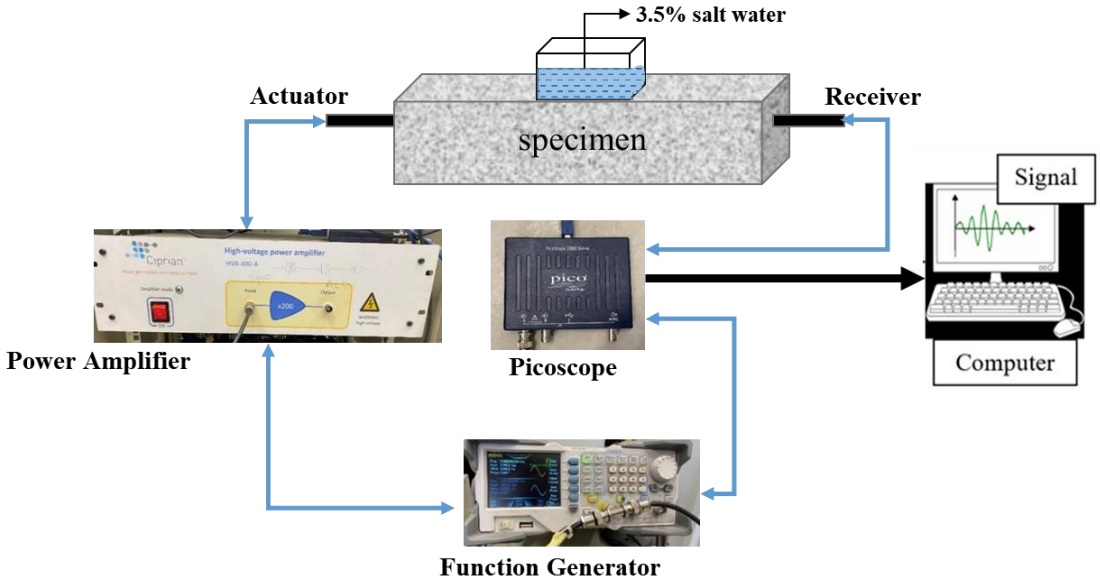

Figure 6.4. Set-up for ultrasonic data acquisition

2.7 Mass loss and tensile strength of rebars

Destructive tests such as mass loss was conducted to observe the specimens due to corrosion. The reinforcing bar for each specimen was cleaned as per ASTM G1-90 with deionized water to remove any adhered corrosion products. They were then weighed to determine mass lost due to corrosion.

3. Results And Discussion

3.1 Half-cell Potential Measurements

Figure 6.5 shows the results for half-cell potential for all specimens. ASTM C876-09 states that if the half-cell potential is more positive than -200mV, there is 90% probability of no corrosion. For UD specimen (Figure 6.5a) the initial observed potential was -98mV which implies that the steel was in passive condition and no corrosion was occurring. After one week of ponding, there was drop in potential to -141 mV and maintained a stable potential of about -150 mV throughout the entire

duration of the experiment. This indicated that no active corrosion was detected in the UD specimen.

Specimen D (Figure 6.5a) on the other hand had initial observed potential of -151 mV. This indicated that the steel was in passive condition before the exposure to NaCl solution. After 7 days of exposure to NaCl solution, the potential reached -180 mV. This indicated that NaCl solution has entered inside the crack and steel has now gone to active corrosion state. A sudden drop in potential to -251 mV was noticed after 14 days which then continued to decrease at a slow rate as shown in Figure 6.5 (a). The potential observed at termination of experiment was -571.3 mV indicating 90 % probability of corrosion (ASTM standards). This would be further compared with the actual condition of the rebar after breaking the specimen.

The healed specimens (Figure 6.5b), on the other hand, showed active state of corrosion already at the commencement of exposure. The initial observed potential for DHC and DHA specimen was -290 mV and -365 mV respectively. As per ASTM, this indicated high probability of corrosion. It may be noted that both specimens have been exposed to calcium salts at the time of healing. Thus, half-cell measurement is likely to be affected due to the presence of the healing fluid in these specimens. With time, the potential continued to be on more negative for both specimens at a slow rate for entire duration of the experiment. The final potential at the termination of the experiment for DHC was – 537 mV and for DHA was – 567 mV.

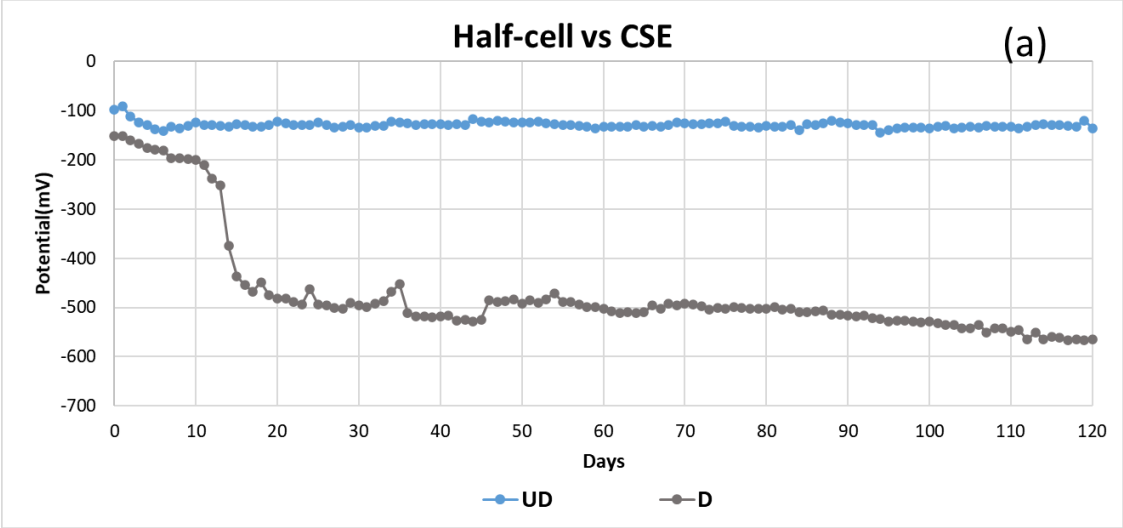

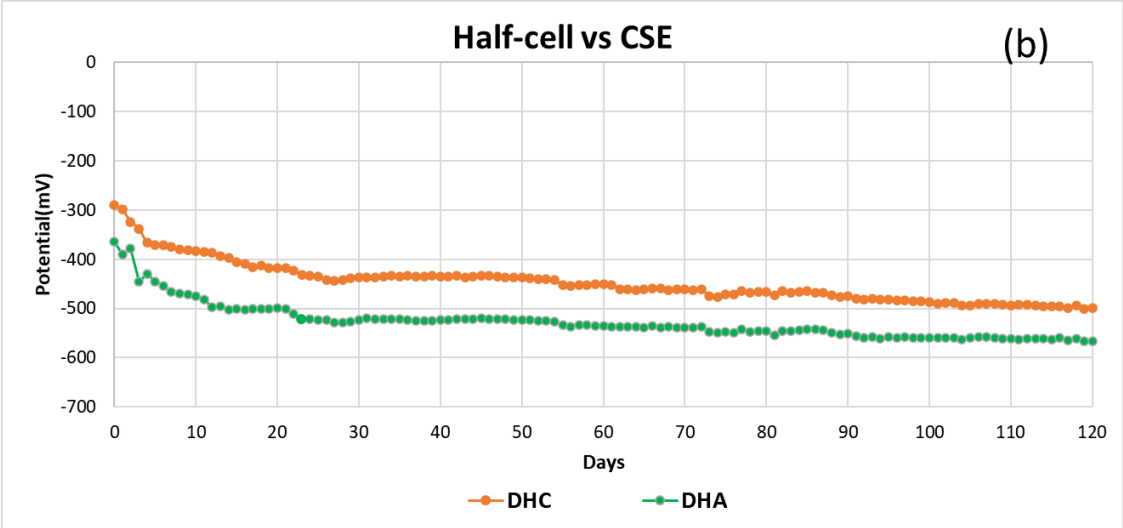

Figure 6.5. Half-cell measurements with time for (a) UD and D specimen (b) DHC and DHA specimen

3.2 LPR Measurements

The LPR measurements were recorded daily for all specimens throughout the exposure period. The potentiodynamic scans were analysed by extrapolating the Tafel plots. Corrosion current (I_{corr}) and corrosion potential (E_{corr}) were obtained by intersection of linear portions of the anodic and cathodic branches of the Tafel curves. Figure 6.6 presents the results for Icorr and Ecorr for all specimens. As seen from Figure 6.6a and 6.6b, UD specimens maintained low and stable corrosion current

values in the range 124 µA and 137 µA and corrosion potential values in the range -268 mV and -419 mV throughout the exposure period. I_{corr} in the D specimen started from a similar value as in case of UD specimen. However, at 14^{th} day there was a sudden jump in the current to 600 µA indicating initiation of corrosion. Thereafter I_{corr} remained in the vicinity of 600 µA. The initial E_{corr} was -425 mV. It rose -625 mV and remained in the vicinity for the entire period of exposure. Clearly, LPR measurements are a good indicator of corrosion. The presence of crack in the D sample has a great influence on corrosion. The crack allows easy access of chlorides that cause corrosion. These observations are consistent with the half-cell measurements for D specimen. Clearly, this experiment could discern different rates of corrosion of UD and D specimens.

The E_{corr} and I_{corr} for healed specimens is presented in Figure 6.6c and 6.6d. As in half-cell measurements, the E_{corr} at the commencement of exposure was already -400 mV indicating active corrosion. With exposure, the E_{corr} went down further and reached around -600 mV on the 40^{th} day and remained at that level. The I_{corr} started at around 200 µA for both DHA and DHC. However, while it rose gradually in DHA, for DHC rose more sharply reaching 400 µA on 22^{nd} day. Clearly, the electrochemical trends for the healed samples showed likelihood of corrosion albeit at a slower rate than the D sample but considerably higher than the UD sample. It may be recalled that the LPR measurement is likely to be affected due to the presence of the electrolytes in the healing fluid in these samples. These results would be compared with the guided wave measurements that directly examine the physical condition of the bar rather than the presence of chemicals. Moreover, destructive tests have been conducted by extracting the rebar out of specimens after termination of the experiment to determine the effect on the physical properties of the bar.

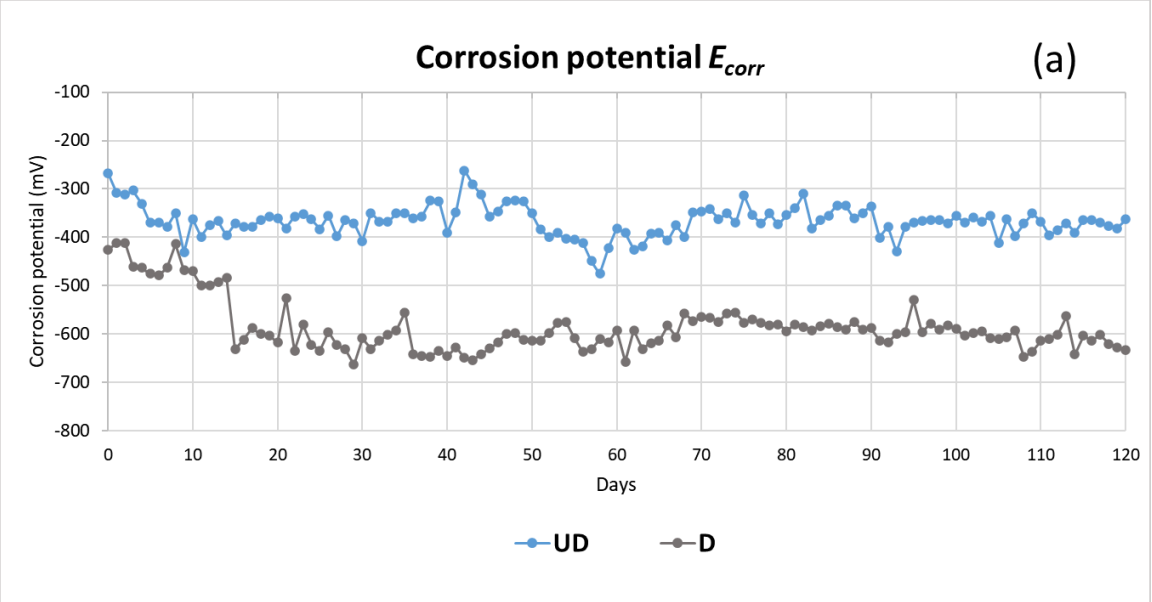
Corrosion potential E_{corr}
(a)
Corrosion potential (mV)
-100
-200
-300
-400
-500
-600
-700
-800
0
10
20
30
40
50
60
70
80
90
100
110
120
Days
UD
D

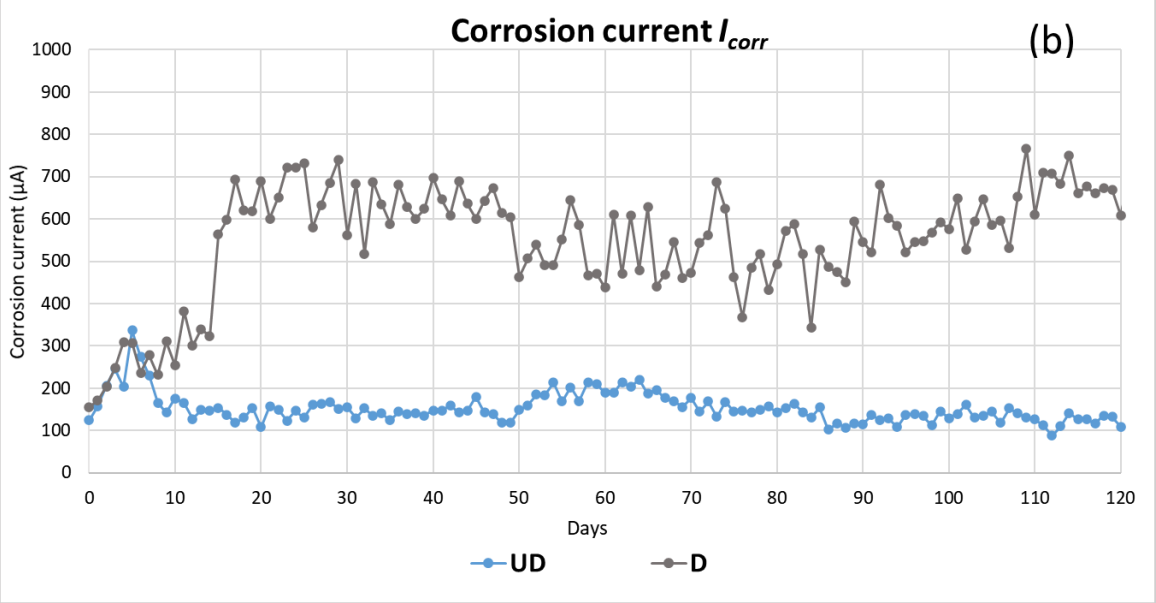
Corrosion current I_{corr}
(b)
Corrosion current (μA)
1000
900
800
700
600
500
400
300
200
100
0
0
10
20
30
40
50
60
70
80
90
100
110
120
Days
UD
D

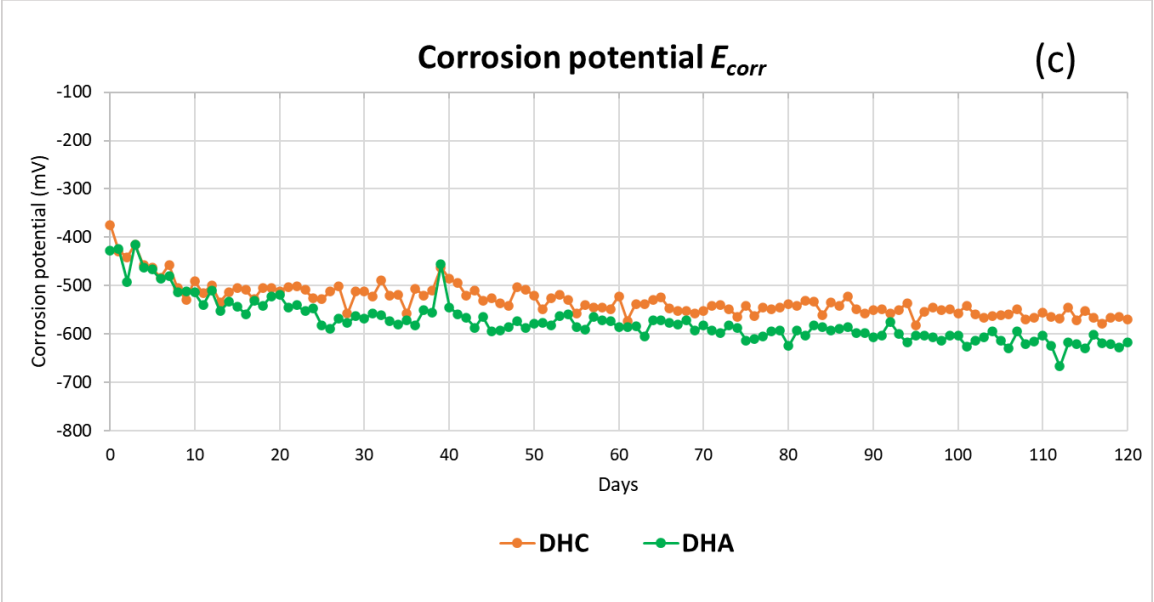

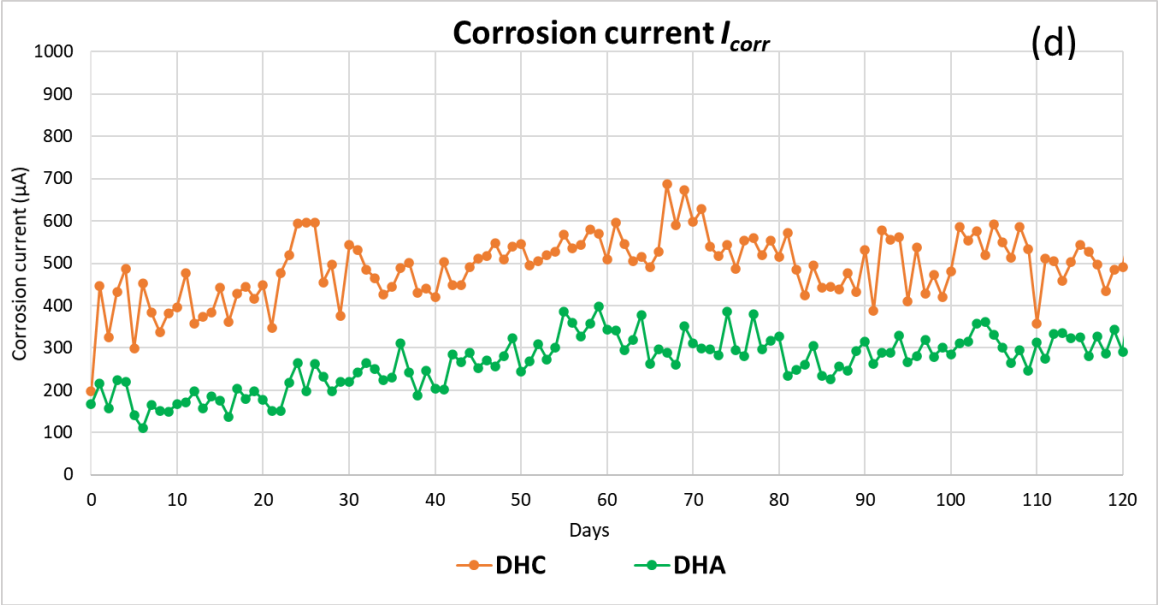

Figure 6.6. Linear polarisation measurements

3.3 Guided wave inspection of reinforced bar

Throughout the exposure period, the specimens were monitored at regular intervals by ultrasonic guided waves passing through the steel bar. The ultrasonic time response of the waveguide was recorded by attaching piezo patches to the steel bar (Figure 6.4). A Hanning windowed sine waveform was applied as excitation. The frequency of excitation was varied within a broad range to arrive at the most suitable value. The

wave is received at the other end of the bar. The received waveform is analysed to investigate the state of corrosion in the bar.

The signals were recorded using frequency sweep from 240 kHz to 400 kHz at an interval of 20 kHz to determine the best excitation frequency. The strongest signal was found to be for 300 kHz frequency. The results for 300 kHz frequency are therefore presented in this paper. A 20-cycle Hanning-window tone burst signal was used to generate the guided waves:

$$\sin 2\pi ft \times \left(\frac{1}{2} + \frac{1}{2}\cos\left(2\pi\left(\frac{t - t_{max}}{t_{max}}\right)\right)\right) \quad (6.1)$$

$$t_{max} = n \times \frac{1}{f} \quad (6.2)$$

Where f is the central excitation frequency, t is the time domain of the waveform, t_{max} is the maximum time of the waveform and n is the number of cycles.

Figure 6.7a presents the received signals in time domain for the UD specimen at days 0 and 120. Clearly, there is very little difference in the signals. At day 120 the signal had a small attenuation that indicates a marginal change in the waveguide. The D specimen (Figure 6.7b), on the other hand, had a significant attenuation in signal, indicating major change in the waveguide. Thus, the D sample is likely to have suffered much higher level of corrosion than the D sample. Thus, the ability of the guided wave system in monitoring corrosion is established. These signals are further analysed for quantifying the rate of corrosion.

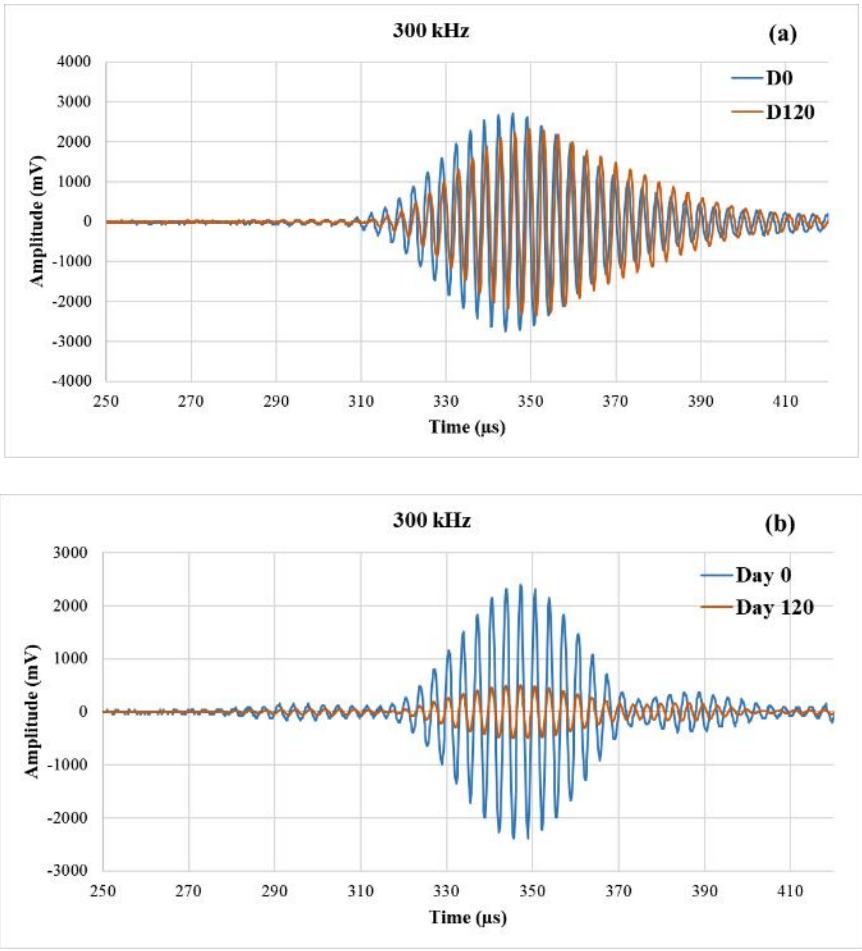

Figure 6.7. Time domain signals for (a) UD and (b) D specimens for day 0 and day 120.

One of the straightforward measures for monitoring the condition of the waveguide is the energy of the transmitted wave. The magnitude of the transmitted energy can be greatly influenced by the deterioration of the steel-concrete interface bond as well as the distortion of the reinforcing bar due to corrosion. As the specimens are exposed to corrosion, the norm of the transmitted energy is determined by recording the transmitted time signals sequentially. Fast Fourier Transform is applied on the time signals as:

$$A(F_I) = \mathrm{FFT}(f(x)) \tag{6.3}$$

Where $A(F_i)$ is the Fast Fourier Transform of the i^{th} time signal $f(t)_i$

The norm of energy is computed over a frequency window ω ± B/2.

$$E_i = \sum_{\omega-B/2}^{\omega+B/2} A(F_i) \quad (6.4)$$

Where ω is the excitation frequency and B is the bandwidth

The transmission index is calculated as 1's complement of the ratio of the ith energy norm (E_i) and the initial energy norm E_0.

$$TI(i) = 1 - \frac{E_i}{E_0} \quad (6.5)$$

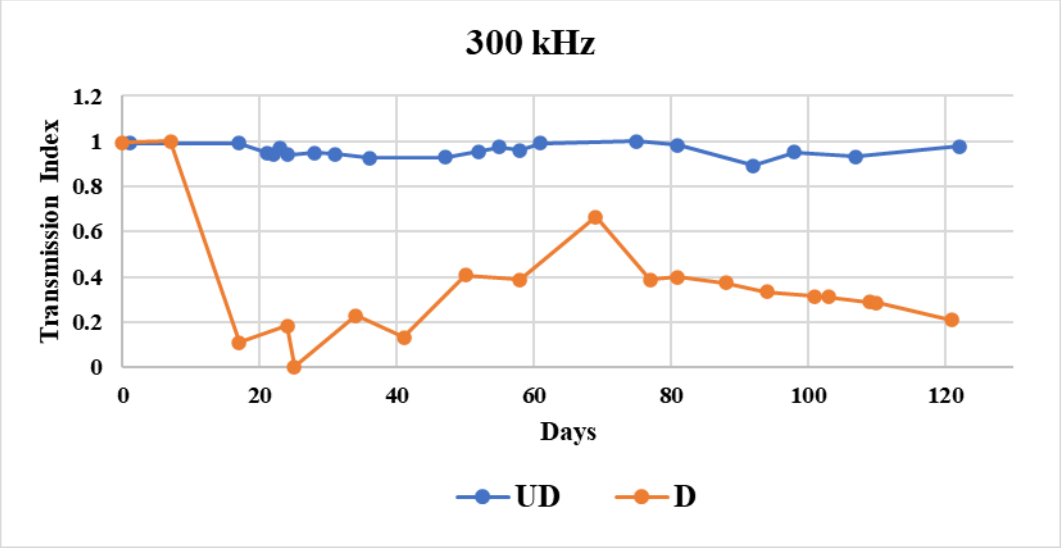

Figure 6.8. Transmission index for UD & D specimens

Figure 6.8 presents TI for the UD and D specimens with time of exposure to corrosion. The UD specimen has a TI close to 1 indicating no corrosion throughout the exposure. The TI of the D specimen, on the other hand, was widely varying. It had a sudden drop at about the 10th and the 14th day. It may be recalled that the electrochemical methods too detected a sharp increase in corrosion activity in the D specimen during this period. However, the TI went up considerably since then until the 75th day. This phenomenon has been reported by Sharma and Mukherjee (Sharma and Mukherjee 2010, Sharma

and Mukherjee 2011). Unlike the electrochemical systems that indirectly determine the rate of corrosion by the electrical activity, the guided wave system examines the physical condition of the bar. At the initial stage of corrosion only the surface of the bar experiences corrosion. The corrosion product has a higher volume than steel. Thus, it applies out an outward pressure on the concrete. As a result, a contact pressure is generated between the bar and the surrounding concrete that lets more wave energy to leak into concrete. Thus, less energy is transmitted to the receiving end. This is the initial phase of corrosion. As corrosion progresses, more corrosion products accumulate. Eventually, the corrosion products breakdown due to the excessive contact pressure. As a result, the leakage into concrete goes down and TI goes up again. At the 70^{th} day, the bar enters the third phase of corrosion, when there is metal loss that distorts the waveguide. As a result, the wave energy scatters from those locations and the TI goes down once again. From that point onwards the TI goes down continuously. It is at the third phase of the corrosion the bar strength gets affected. Clearly, the guided wave system is able to generate a more nuanced information about the state of corrosion than the electrochemical method. As it examines the physical state of the bar, it is unlikely to be misled by the presence of the healing fluid.

Figure 6.9 shows the TI for the two healed specimens. The TI for these specimens was between the UD and the D specimens. However, these specimens did not exhibit the wide fluctuations in TI as in the D specimen. The TI went down at a slower rate than the D specimen. The reduction in the TI indicates that there is some distortion in the bar due to corrosion; however, it is likely to remain restricted in a small area.

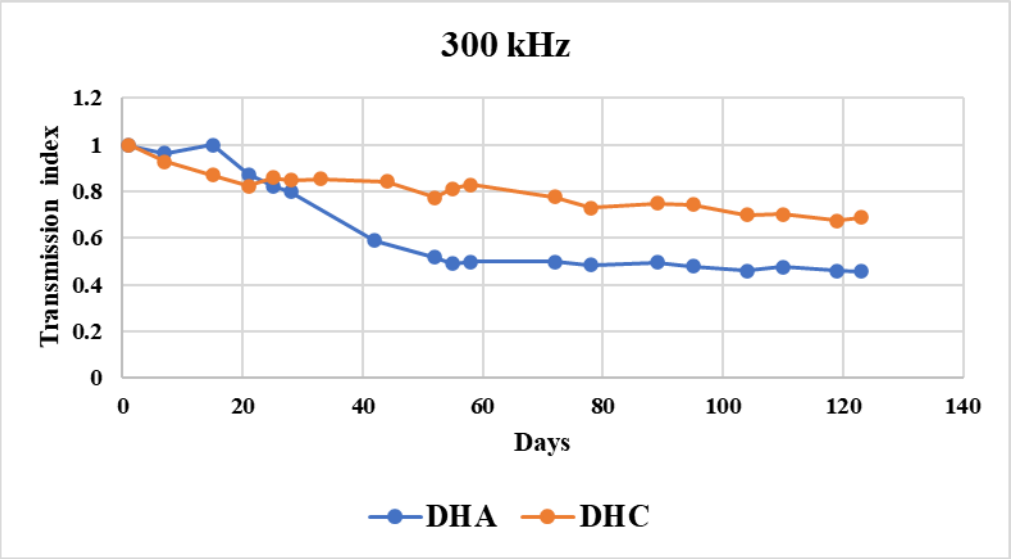

Figure 6.9. Transmission index the healed DHC and DHA specimens

A measure of the rate of corrosion in the bars can be obtained from the recorded TIs at the third phase of corrosion, between days 80 and 120. Table 1 presents the rates. The UD sample shows no reduction in TI. In case of the D specimen, the reduction is TI is about 5×10^{-3}/day. Although the healed samples exhibit a reduction in TI, but at a considerably slower rate. The DHA and DHC specimens show only 10% and 20% rate of reduction in TI in comparison to D. This indicates that there is a considerably slower rate of corrosion in the healed samples. This is further examined through destructive tests at the completion of the corrosion exposure.

Table 1. Rate of TI with corrosion exposure

Sample	TI		Rate per day
	Day 80	Day 120	
UD	0.995	0.995	0
D	0.4	0.2	-5×10^{-3}
DHA	0.44	0.42	-0.5×10^{-3}
DHC	0.78	0.74	-1.0×10^{-3}

3.4 Mass loss and tensile strength of rebars

The rebars were dug out, cleaned, and visually examined after the completion of the experiment. Figure 6.10 shows the condition of rebar after 120 days. The rebar for UD specimen showed no visible corrosion, while clear signs of corrosion was visible in the D specimen in the zone of the crack. The DHC and DHA specimens also showed some corrosion albeit restricted to a smaller area than the D specimen.

Figure 6.10. Visual inspection of rebar

The mass loss was calculated for all specimens after extracting the rebar. The UD specimen did not show any mass loss. D specimen exhibited a mass loss of 0.37%. The mass loss for DHC and DHA specimens was 0.29% and 0.25% respectively.

The specimens were subjected to uniaxial tensile test in a universal testing machine.

The specimens were placed between the two jaws (140 mm) and clamped firmly to perform the tension test. The jaws are pulled apart to apply tension on the sample. The loading speed was 5mm/minute. The tension was applied to the sample until it reached the fracture point. The fracture pattern is shown in Figure 6.11 for all specimens. The UD specimen showed a typical symmetric cup and cone failure pattern. The D sample failed at a location of corrosion and the symmetry in the fracture plane was lost. This is because of the eccentricity in loading created due to uneven corrosion in the bar. The healed sample too showed a failure pattern similar to that of D specimen. Thus, the healed samples too had developed some eccentricity due to corrosion.

Figure 6.11. Fracture morphology for all specimens after tensile testing

The stress-strain curves are presented in Figure 6.12. The UD sample exhibited the stress-strain behaviour close to that of a fresh bar. The D sample too had a similar stress-strain behaviour until the load reached close to the point of failure. However, the strain at failure was significantly reduced from 0.26 to 0.18. Thus, as a result of corrosion, the bar has lost ductility. The healed bars too had a strain at failure that is lower than that of the UD specimen but higher than that of the D specimen. The loss in ductility in the DHC specimen was higher than that in the DHA specimen.

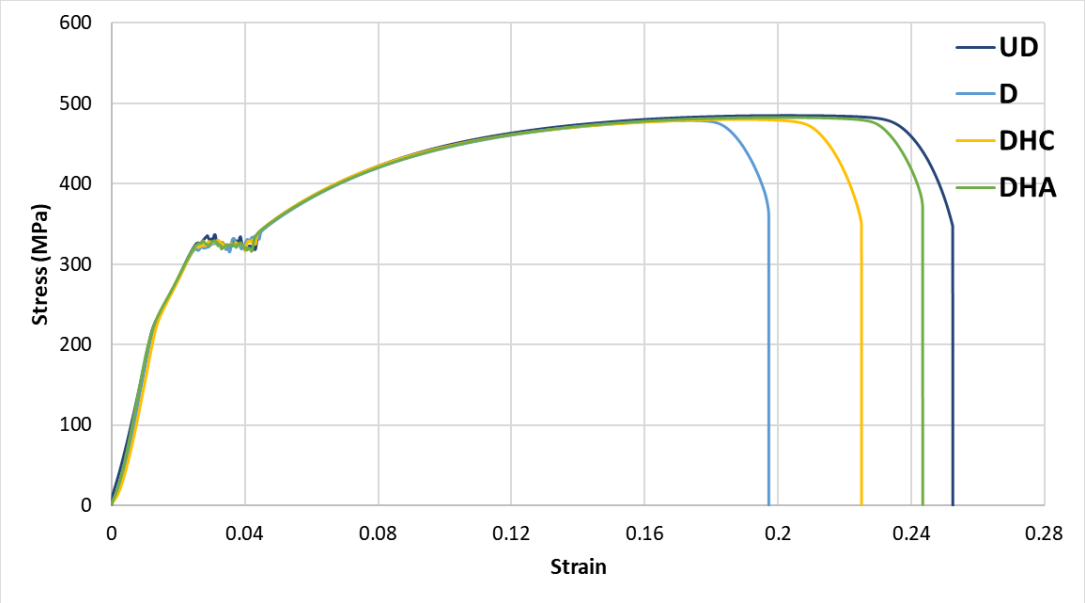

Figure 6.12. Stress-strain curves of the bars

Conclusions

This paper demonstrates the performance of bacterially healed specimens in impeding reinforcement corrosion. The specimens were cracked and healed with two different sources of calcium. They were subjected to natural corrosive environment for continuous 120 days. Electrochemical tests, ultrasonic tests and visual inspection of the specimens was conducted throughout the period of exposure. At the end of the exposure period, the bars were dugout and destructive tests were conducted.

It was observed that the electrochemical techniques are suitable in discerning the onset of corrosion. They are suitable for the specimens without the healing fluid. However, their results were somewhat misleading for the healed samples. The presence of electrolytes within the healing fluid means that these methods indicate the likelihood of corrosion due to the presence of the healing fluid.

The guided wave ultrasonic technique is suitable for monitoring corrosion in the healed samples. This technique examines the physical condition of the corroding bar rather than the electrochemical activity. Thus, a nuanced information about the state of corrosion can be obtained through this technique. A transmission index through the bar is developed that can be calibrated with the rate of corrosion. It is noted that the undamaged sample suffered little corrosion. The rate of corrosion in the cracked sample was significantly higher. Healing of the crack has dramatically reduced the rate of corrosion. With calcium acetate it was 10% and with calcium chloride 20% of that of the unrepaired sample. Thus, healing of cracks is very effective in impeding corrosion.

The destructive tests revealed that cracking in concrete significantly accelerates the rate of corrosion. Healing of the crack considerably impedes the corrosion although it does not eliminate it. Within the period of exposure, the corrosion did not cause any loss of strength. The ductility, however, was significantly affected by corrosion. Healing treatment could reduce the loss of mass and ductility of the bar.

This investigation demonstrates that healing of cracks in concrete slows down the rate of corrosion. There is a marginal effect of the choice of healing agent. Healing with calcium acetate showed a lower rate of corrosion than the calcium chloride. However, calcium chloride results in faster healing. Thus, there is a trade-off in the choice of

healing agent. In all the samples there was no perceptible loss in strength of the bars due to corrosion. This is because the limited corrosion exposure to the bars. A longer-term corrosion exposure of the healed samples would be necessary for enumeration of the rate of loss of strength and the effect of healing thereof.

Data Availability Statement

Some or all data, models, or code generated or used during the study are available from the corresponding author by request.

Acknowledgements

The authors would like to acknowledge the contribution of Australian Government Research Training Program Scholarship in supporting this research. This research is supported by the Australia Research Council Linkage grant LP180100132 in partnership with industry partners ConBioCrete, Mainroads Western Australia and Structural Specialities and Projects.

References

Achal, V., A. Mukherjee, D. Kumari and Q. Zhang (2015). "Biomineralization for sustainable construction–A review of processes and applications." Earth-science reviews **148**: 1-17.

Aggelis, D. and T. Shiotani (2007). "Repair evaluation of concrete cracks using surface and through-transmission wave measurements." Cement and Concrete Composites **29**(9): 700-711.

Anagnostopoulos, C. A. (2014). "Effect of different superplasticisers on the physical and mechanical properties of cement grouts." Construction and Building Materials **50**: 162-168.

Assouli, B., G. Ballivy and P. Rivard (2008). "Influence of environmental parameters on application of standard ASTM C876-91: half cell potential measurements." Corrosion Engineering, Science and Technology **43**(1): 93-96.

Broomfield, J. (2003). Corrosion of steel in concrete: understanding, investigation and repair, CRC Press.

De Belie, N. and J. Wang (2016). "Bacteria-based repair and self-healing of concrete." Journal of Sustainable Cement-Based Materials **5**(1-2): 35-56.

De Muynck, W., D. Debrouwer, N. De Belie and W. Verstraete (2008). "Bacterial carbonate precipitation improves the durability of cementitious materials." Cement and concrete Research **38**(7): 1005-1014.

Dhami, N. K., M. S. Reddy and A. Mukherjee (2013). "Biomineralization of calcium carbonates and their engineered applications: a review." Frontiers in microbiology **4**.

Dhami, N. K., S. M. Reddy and A. Mukherjee (2012). Biofilm and microbial applications in biomineralized concrete. Advanced topics in Biomineralization, InTech.

Dubey, A. A., R. Murugan, K. Ravi, A. Mukherjee and N. K. Dhami (2022). "Investigation on the Impact of Cementation Media Concentration on Properties of Biocement under Stimulation and Augmentation Approaches." Journal of Hazardous, Toxic, and Radioactive Waste **26**(1): 04021050.

Ducasse-Lapeyrusse, J., R. Gagné, C. Lors and D. Damidot (2017). "Effect of calcium gluconate, calcium lactate, and urea on the kinetics of self-healing in mortars." Construction and Building Materials **157**: 489-497.

Elsener, B. (2002). "Macrocell corrosion of steel in concrete–implications for corrosion monitoring." Cement and concrete composites **24**(1): 65-72.

Erşan, Y. Ç., E. Hernandez-Sanabria, N. Boon and N. De Belie (2016). "Enhanced crack closure performance of microbial mortar through nitrate reduction." Cement and concrete composites **70**: 159-170.

Erşan, Y. Ç., H. Verbruggen, I. De Graeve, W. Verstraete, N. De Belie and N. Boon (2016). "Nitrate reducing CaCO3 precipitating bacteria survive in mortar and inhibit steel corrosion." Cement and Concrete Research **83**: 19-30.

Farrugia, C., R. P. Borg, L. Ferrara and J. Buhagiar (2019). "The application of Lysinibacillus sphaericus for surface treatment and crack healing in mortar." Frontiers in Built Environment **5**: 62.

Jonkers, H. M., A. Thijssen, G. Muyzer, O. Copuroglu and E. Schlangen (2010). "Application of bacteria as self-healing agent for the development of sustainable concrete." Ecological engineering **36**(2): 230-235.

Kaur, N. P., S. Majhi, N. K. Dhami and A. Mukherjee (2020). "Healing fine cracks in concrete with bacterial cement for an advanced non-destructive monitoring." Construction and Building Materials **242**: 118151.

Kaur, N. P., J. K. Shah, S. Majhi and A. Mukherjee (2018). "Healing and Simultaneous Ultrasonic Monitoring of Cracks in Concrete." Materials Today Communications.

Ling, H. and C. Qian (2017). "Effects of self-healing cracks in bacterial concrete on the transmission of chloride during electromigration." Construction and Building Materials **144**: 406-411.

Lu, Y., J. Li, L. Ye and D. Wang (2013). "Guided waves for damage detection in rebar-reinforced concrete beams." Construction and Building Materials **47**: 370-378.

Majhi, S., A. Mukherjee, N. V. George, V. Karaganov and B. Uy (2021). "Corrosion monitoring in steel bars using laser ultrasonic guided waves and advanced signal processing." Mechanical Systems and Signal Processing **149**: 107176.

Montemor, M., A. Simoes and M. Ferreira (2003). "Chloride-induced corrosion on reinforcing steel: from the fundamentals to the monitoring techniques." Cement and concrete composites **25**(4-5): 491-502.

Neville, A. M. (1995). Properties of concrete, Longman London.

Panasyuk, V., V. Marukha and V. Sylovanyuk (2014). Injection Technologies for the Repair of Damaged Concrete Structures, Springer Netherlands.

Popovics, S., J. L. Rose and J. S. Popovics (1990). "The behaviour of ultrasonic pulses in concrete." Cement and Concrete Research **20**(2): 259-270.

Poursaee, A. (2016). Corrosion of steel in concrete structures. Corrosion of steel in concrete structures, Elsevier**:** 19-33.

Qian, C., H. Chen, L. Ren and M. Luo (2015). "Self-healing of early age cracks in cement-based materials by mineralization of carbonic anhydrase microorganism." Frontiers in microbiology **6**: 1225.

Rodrigues, R., S. Gaboreau, J. Gance, I. Ignatiadis and S. Betelu (2020). "Reinforced concrete structures: A review of corrosion mechanisms and advances in electrical methods for corrosion monitoring." Construction and Building Materials: 121240.

Shao-feng, Z., L. Chun-hua and L. Rong-gui (2011). "Experimental determination of chloride penetration in cracked concrete beams." Procedia Engineering **24**: 380-384.

Sharma, A., S. Sharma, S. Sharma and A. Mukherjee (2015). "Ultrasonic guided waves for monitoring corrosion of FRP wrapped concrete structures." Construction and Building Materials **96**: 690-702.

Sharma, S. and A. Mukherjee (2010). "Longitudinal guided waves for monitoring chloride corrosion in reinforcing bars in concrete." Structural Health Monitoring **9**(6): 555-567.

Sharma, S. and A. Mukherjee (2011). "Monitoring corrosion in oxide and chloride environments using ultrasonic guided waves." Journal of Materials in Civil Engineering **23**(2): 207-211.

Sharma, S. and A. Mukherjee (2013). "Nondestructive evaluation of corrosion in varying environments using guided waves." Research in Nondestructive Evaluation **24**(2): 63-88.

Sharma, S. and A. Mukherjee (2014). "Ultrasonic guided waves for monitoring the setting process of concretes with varying workabilities." Construction and Building Materials **72**(Supplement C): 358-366.

Sharma, S. and A. Mukherjee (2015). "Ultrasonic guided waves for monitoring corrosion in submerged plates." Structural Control and Health Monitoring **22**(1): 19-35.

Shiotani, T. and D. G. Aggelis (2009). "Wave propagation in cementitious material containing artificial distributed damage." Materials and Structures **42**(3): 377-384.

Song, H.-W. and V. Saraswathy (2007). "Corrosion monitoring of reinforced concrete structures-A." Int. J. Electrochem. Sci **2**(1): 1-28.

Stocks-Fischer, S., J. K. Galinat and S. S. Bang (1999). "Microbiological precipitation of CaCO3." Soil Biology and Biochemistry **31**(11): 1563-1571.

Stratfull, R. (1968). "How chlorides affect concrete used with reinforcing steel." Materials Protection.

Trtnik, G. and M. Gams (2014). "Recent advances of ultrasonic testing of cement based materials at early ages." Ultrasonics **54**(1): 66-75.

Vijay, K. and M. Murmu (2019). "Effect of calcium lactate on compressive strength and self-healing of cracks in microbial concrete." Frontiers of Structural and Civil Engineering **13**(3): 515-525.

Wang, J., Y. C. Ersan, N. Boon and N. De Belie (2016). "Application of microorganisms in concrete: a promising sustainable strategy to improve concrete durability." Applied microbiology and biotechnology **100**(7): 2993-3007.

Wang, J., H. Soens, W. Verstraete and N. De Belie (2014). "Self-healing concrete by use of microencapsulated bacterial spores." Cement and concrete research **56**: 139-152.

Xu, J., Y. Du, Z. Jiang and A. She (2015). "Effects of Calcium Source on Biochemical Properties of Microbial CaCO3 Precipitation." Frontiers in microbiology **6**.

Yeih, W. and R. Huang (1998). "Detection of the corrosion damage in reinforced concrete members by ultrasonic testing." Cement and Concrete Research **28**(7): 1071-1083.

Zheng, T., C. Qian and Y. Su (2020). "Influences of different calcium sources on the early age cracks of self-healing cementitious mortar." Biochemical Engineering Journal: 107849.

Chapter 7 Conclusions and recommendations

One of the major concerns in Civil infrastructure, especially for reinforced concrete structure is its vulnerability to cracking. Durability and service life of concrete structures is greatly affected by cracking of concrete, resulting in premature deterioration of concrete and reinforcement corrosion. It is therefore imperative to heal these cracks. A significant number of healing technologies have been developed by the researchers in recent years such as cementitious grout, epoxy, resins or bacterial based. Several investigations recently have focused on the use of bacteria based self-healing techniques for reinforced concrete structures [1]. However, to determine the efficacy of healing, it is important to realistically assess the state of corrosion over the period of exposure. The main focus of this study was to monitor the efficacy of bacterial healing for remediation of cracks in concrete over a period of 120 continuous days. For the first time, this thesis will report long term monitoring of bacterial healing subjected to natural corrosion.

The key objectives of the research were as follows:

- To investigate the efficacy of conventional healing techniques for concrete cracks and potential of ultrasonic monitoring techniques
- To investigate the efficacy of bacterial healing technique with simultaneous monitoring
- To investigate the impact of different calcium sources in bacterial induced carbonate precipitation and crack healing
- Long term monitoring of efficacy of bacterial healing in impeding reinforcement corrosion

These objectives have been achieved and the findings along with key conclusions have been reported in Chapters 3 to Chapter 6 and summarised below.

Chapter 3: is a published work in the journal as *'Kaur, et al., Healing and Simultaneous Ultrasonic Monitoring of Cracks in Concrete. Material Today Communications, 2018'* https://doi.org/10.1016/j.mtcomm.2018.10.022. This chapter investigates the healing of cracks of different widths in concrete and illustrates the ability of the ultrasonic techniques to monitor the progression of healing. A numerical technique based on two-dimensional finite difference time domain (FDTD) has also been used to determine the potential of the ultrasonic stress waves in monitoring healing. It has been reported that the ultrasonic technique is able to discern the progressive healing process. Signal attenuation was found to be most suitable for monitoring healing.

Chapter 4 is a published work in the journal as *'Kaur, et al., Healing Fine Cracks in Concrete with Bacterial Cement for an Advanced Non-destructive Monitoring. Construction and Building Materials, 2020'* https://doi.org/10.1016/j.conbuildmat.2020.118151. This chapter investigates the healing of fine cracks using the bacterial based healing technique. The evidence and efficiency of bacterial healing is investigated using advanced monitoring techniques. The ultrasonic signal has been processed further using an advanced STFT technique to obtain a nuanced observation of the crack healing process. The evidence of bacterial healing was confirmed through visual inspection, scanning electron microscopy and X-ray dispersion spectrum and water tightness tests.

Chapter 5 reports the efficacy of using various calcium sources for bacterially induced carbonate precipitation and crack healing of concrete. The evidence of healing is investigated using advanced monitoring techniques. Simultaneously, an attempt has been made to monitor the rebar through electrochemical measurements and guided wave technique to study the efficacy of healing in impeding corrosion.

Chapter 6 reports the long-term performance of healed samples subjected to chloride induced reinforcement corrosion. The healed samples were subjected to salt water ponding for 120 days. They were monitored through various electrochemical and ultrasonic guided wave techniques. After ponding, the samples were broken to visually examine the rebar condition. Mass loss and tensile tests were carried out to get insights of rebar condition.

7.1 Recommendations for future research

- Although small amount of bacterial fluid is utilized for crack healing applications, production of ammonia during hydrolysis of urea poses environmental concerns. Further investigation is required to overcome this problem.
- In the construction sector, any new idea or improvement to an existing methodology necessitates extensive practical investigation. Bacterial based healing technology appears to be the most promising solution for long-lasting constructions. Although, lot of research has been conducted at laboratory scale, very few projects have been carried out in real life concrete applications to test this new technology's appropriateness at a large scale [2-5]. However, its long-term impact needs to be explored.

- The bacterial healing needs further investigation and design of appropriate monitoring methods to evaluate its effect on reinforcement corrosion.
- Further investigations on the depth of chloride penetration needs to be done.

References

1. De Muynck, W., N. De Belie, and W. Verstraete, *Microbial carbonate precipitation in construction materials: A review.* Ecological Engineering, 2010. **36**(2): p. 118-136.
2. Mors, R. and H.M. Jonkers, *Bacteria-based self-healing concrete: evaluation of full-scale demonstrator projects.* RILEM Technical Letters, 2019. **4**: p. 138-144.
3. Zhang, X. and C. Qian, *WITHDRAWN: Engineering Application of Microbial Self-healing Concrete in Lock Channel Wall*. 2020, Elsevier.
4. Wiktor, V. and H. Jonkers, *Field performance of bacteria-based repair system: Pilot study in a parking garage.* Case Studies in Construction Materials, 2015. **2**: p. 11-17.
5. Van Mullem, T., et al., *First Large-Scale Application with Self-Healing Concrete in Belgium: Analysis of the Laboratory Control Tests.* Materials, 2020. **13**(4): p. 997.